Summer 2019

Biochemical Investigations of Proteins Associated with Iron Homeostasis in *Escherichia coli*

Matthew Ryan Blahut

Biochemical investigations of proteins associated with iron homeostasis in *Escherichia coli*

by

Matthew Ryan Blahut

Bachelor of Arts
Case Western Reserve University, 2010

Submitted in Partial Fulfillment of the Requirements

For the Degree of Doctor of Philosophy in

Chemistry

College of Arts and Sciences

University of South Carolina

2019

Accepted by:

Franklin W. Outten, Major Professor

Maksymilian Chruszcz, Committee Member

Hui Wang, Committee Member

Michael Wyatt, Committee Member

Cheryl L. Addy, Vice Provost and Dean of the Graduate School

DEDICATION

This work is dedicated to the loving memory of my Grandmothers, my Uncle Mark, and our beloved cat Hank who were all inspirational in my academic career. Additionally, I dedicate this work to my family, my fiancé Courtney, her family, and our sweet cats Adama and Oliver.

ACKNOWLEDGEMENTS

I would first like to thank Dr. Wayne Outten for admitting me into his lab to work on metal homeostasis in addition to allowing me to take over the work on the SufS project granting me the opportunity to grow as a researcher. While my projects did not always go smoothly, I acquired a critical understanding of the significance of troubleshooting experiments along with the persistence necessary to tackle more difficult projects. Thank you for permitting me the chance to utilize most of the experiments I felt necessary to resolve issues in research while also learning new techniques. I just wish Game of Thrones was not such a letdown in that last few seasons, but Barry seems extremely promising.

I would also like to acknowledge our collaborators who aided us in techniques with which we lacked the means to perform on our own. Specifically, I want to thank Dr. Thomas Makris for promoting my understanding of transient kinetics and allowing me to use both the stopped-flow and your UV-visible spectrometer as both were crucial to my work. Also, I thoroughly enjoyed joking about the inability of southerners to handle snow as well as our discussions on the 90s and hockey.

For the labmates with whom I worked, I also want to show my appreciation as well. Specifically, I want to thank Dr. Khaleh Thomas and Dr. Yuyuan Dai for taking time to help make sure I understood how to use the equipment in our lab and learned how to fix broken equipment. The two of them ensured that I would not make agarose gels with water instead of TAE buffer.

Personally, I want to thank my parents and brother who were with me from the start of all this as well as my sweet Panda Buffalo Dr. Courtney Wise. Without her support every day in addition to her advice with respect to projects, I would never have successfully obtained two first author publications. Along with her, I must thank my beloved cats Adama, Oliver, and Hank. We unfortunately had to say goodbye to our perfect boy Hank this past July. These boys, no matter how stressful the lab may be, made everything better after arriving home.

ABSTRACT

The regulation of transition metals within living organisms is essential to the persistence of life. Of particular interest to our lab is iron due to the prevalence of this metal within the cell in addition to the numerous functions it performs. Fe-S cofactors are a significant prosthetic group consisting of iron that are necessary for the function of various metalloproteins. Generation of Fe-S clusters depends on several biosynthesis pathways varying between organisms with Isc and Suf both utilized in *E. coli*. While Isc controls Fe-S manufacturing under normal conditions, Suf assumes control when the cell is exposed to iron deplete conditions or oxidative stress. Consisting of six proteins, cluster synthesis cannot begin without the sulfur obtained from free cellular cysteine via a cysteine desulfurase reaction. As one of the six proteins coded for by *suf*, the PLP-bound SufS protein operates as a type II cysteine desulfurase capable of interacting with cysteine to produce alanine and persulfide. This process, however, requires a sulfur shuttle in the form of SufE capable of increasing desulfurase activity up to 50-fold when added to SufS. While the steady state kinetics of this mechanism have been investigated, the exact pre-steady state kinetics as well as the intermediates involved offer critical targets for analysis due to the lack of the Suf pathway in humans. In this dissertation, we investigated the mechanism by which *E. coli* SufS performs the cysteine desulfurase process alone successfully assigning several intermediates while determining the pre-steady state kinetics. Furthermore, the addition of SufE reveals a novel effector role beyond the ability to solely remove sulfur from SufS and instead alter the reaction mechanism. Other studies have

hinted at this allosteric enhancement, but this is the first instance in which the cysteine desulfurase process shows this impact. Finally, we also investigate two other proteins associated with iron regulation through regulation of iron reduction (YqjI), which revealed a link between iron regulation and nickel levels, and potential iron storage (FtnB). The combined importance of iron and Suf in pathogenic bacteria along with the absence of Suf in humans offer optimal therapeutic drug targets.

TABLE OF CONTENTS

LIST OF TABLES

LIST OF FIGURES

List of Abbreviations

AA ..... Atomic Absorption

Ala ..... Alanine

Amp ..... Ampicillin

ATP ..... Adenosine Triphosphate

βME ..... β-mercaptoethanol

Cys ..... Cysteine

DTNB ..... 5,5'-dithiobis(2-nitro-benzoic acid)

DTT ..... Dithiothreitol

EHS ..... 1-ethyl-3-(3-dimethylaminopropyl)carbodiimide hydrochloride

EXAFS ..... Extended X-ray Absorption Fine Structure

FAD ..... Flavin Adenine Dinucleotide

Fe-S ..... Iron-Sulfur

FF ..... Fast-Flow

FPLC ..... Fast Protein Liquid Chromatography

Fur ..... Ferric Uptake Regulator

H_2O_2 ..... Hydrogen Peroxide

HEPES ..... 4-(2-hydroxyethyl)-1-piperazineethanesulfonic acid

IAEDANS ..... 5-((((2-Iodoacetyl)amino)ethyl)amino)Naphthalene-1-Sulfonic Acid

ICP-MS ..... Inductively-coupled plasma mass spectrometry

IPTG ..... Isopropyl-B-thiogalactopyranoside

Isc ..... Iron Sulfur Cluster

ITC ..... Isothermal Titration Calorimetry

kDa ..... kiloDalton

Kn ..... Kanamycin

MF2 ..... Mag-fura-2

NADH ..... Nicotinamide Adenine Dinucleotide

NADPH ..... Nicotinamide Adenine Dinucleotide Phosphate

nfeF ..... Ni-responsive Fe-uptake Flavoprotein

nfeR ..... Ni-responsive Fe-uptake Regulator

NHS ..... N-hydroxysuccinimide

Nif ..... Nitrogen Fixation

NMR ..... Nuclear Magnetic Resonance

NNDP ..... *N*,*N*-dimethyl-*p*-phenylenediamine sulfate

NSLS ..... National Synchrotron Light Source

ONPG ..... o-nitrophenyl-β-D-galactopyranoside

PAR ..... 4-(2-pyridylazo)-resorcinol

PDA ..... Photodiode Array

PDB ..... Protein Data Bank

PLP ..... Pyridoxal-5'-Phosphate

PMT ..... Photomultiplier tube

ROS ..... Reactive Oxygen Species

Sc ..... Scale Factors

Suf ..... Sulfur formation

TCEP ..... tris(2-carboxyethyl)phosphine

UV ..... Ultraviolet

WT ..... Wildtype

XANES ..... X-ray Absorption Near Edge Structure

XAS ..... X-ray Absorption Spectroscopy

CHAPTER 1

INTRODUCTION

Iron

Transition metal bioavailability has incurred substantial variation over the course of geographic and evolutionary history while substantially impacting metabolic strategies and biological evolution.[1-3] One of the metals that shaped the ecologic development of earth is iron, the fourth most abundant element in the crust of planet earth. The two most abundant physiological forms of iron are Fe^{3+} (ferric) and Fe^{2+} (ferrous), but the potential for many other oxidation states exists. Fe^{3+} is the more frequent and less harmful of the two but lacks solubility under aerobic conditions, resulting in the need for iron-containing and iron-storage proteins, like ferritin.[4] Fe^{2+}, however, has increased solubility but a prevalence to generate harmful reactive oxygen species (ROS) such as hydroxyl radicals via a Fenton reaction.[5, 6]

$$Fe^{2+} + H_2O_2 \longrightarrow Fe^{3+} + {}^{-}OH + {}^{\bullet}OH$$

Hydroxyl radicals for which the cell lacks any detoxification method potentially induce DNA mutations, lipid peroxidation, or amino acid conversions among other harmful effects detrimental to organisms. These potential issues demand proper regulation as iron is integrated into proteins as mono- or di-nuclear species, heme centers, or iron-sulfur (Fe-S) clusters to function in nitrogen fixation, photosynthesis, and respiration.[7]

Sulfur

Within the human body, sulfur is the eighth most abundant element by weight while serving as a vital nonmetallic element essential to life. Sulfur plays numerous roles through the biosynthesis of many essential compounds including vitamins (thiamine and biotin), amino acids (cysteine and methionine), and prosthetic groups (Fe-S clusters) in all organisms. In humans, methionine serves as a source of sulfur via ingestion, due to being an essential amino acid, followed by synthesis into cysteine or other sulfur containing compounds. The principal method by which sulfur incorporation occurs in most organisms, however, is through assimilation of sulfate followed by cysteine biosynthesis.[8] This usable sulfur is obtained by means of various enzymes classified as cysteine desulfurases. When paired with iron, this sulfur operates as a source for the construction of the essential cofactors, Fe-S clusters.[9]

Iron-Sulfur Clusters and their Functions

Fe-S clusters likely comprised one of the earliest biomolecular catalysts consisting of functionally adaptable and highly pervasive prosthetic groups.[10, 11] With their early foundation in evolution, they are currently observed in over 120 distinct types of proteins and enzymes.[12-14] The base structure of Fe-S clusters involves the binding of free sulfide to iron. This iron is held in place via the thiolate sulfur from cysteine residues, with a tetrahedral S coordination at each iron site, although alternative amino acids such as serine, histidine, and aspartate also can bind the iron. Multiple types of Fe-S clusters exist with the two most prevalent being the rhombic [2Fe-2S] and the cubic [4Fe-4S], which is generated via assembly of two [2Fe-2S] clusters. Other detected forms

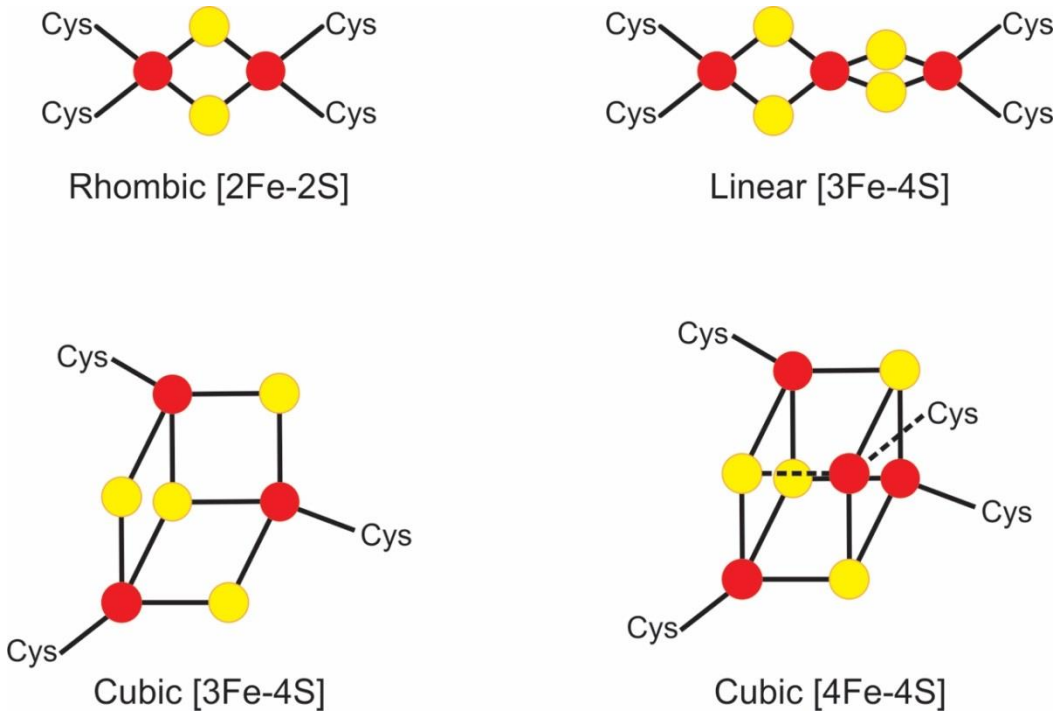

Figure 1.1. Various types of Fe-S clusters. Yellow circles represent S atoms while red circles represent iron atoms. Iron atoms are ligated to the sulfurs of the labeled cysteine residues.

constructed from [4Fe-4S] clusters include the linear or cubic [3Fe-4S], resulting from loss of one Fe, and [8Fe-7S], generated by cluster fusion (Figure 1.1).[12] The existence of multiple cluster types permits the numerous functions exhibited by these clusters.

The responsibilities for these Fe-S prosthetic groups include, but are not limited to, biological electron transport, substrate binding, and transcription/translational regulation. Fe-S clusters are optimal for involvement in electron transfer pathways associated with crucial processes such as photosynthesis and redox chemistry with their ability to delocalize electron density over both S and Fe atoms.[14-16] Fe-S clusters can also sense distinct environmental stimuli, and using different sensing schemes, regulate gene transcription and translation in bacteria, as shown by SoxR.[17, 18] Aside from the previously mentioned functions, clusters are heavily involved in enzyme activity regulation, protein structure, and disulfide reduction, as well as be utilized by proteins in substrate binding and activation, among other roles.

Iron-Sulfur Cluster Biogenesis Pathways

With organismal survival dependent on controlled generation of Fe-S clusters, three major biosynthesis pathways are observed in prokaryotes, although their presence or absence varies among species with conservation in some eukaryotes.[19] The three are the nitrogen fixation (Nif) system, the iron-sulfur cluster (Isc) system, and the mobilization of sulfur (Suf) system. Initially discovered in azototrophic bacteria, the Nif pathway operates in association with the maturation of Fe-S containing nitrogenase enzymes (Figure 1.2).[20, 21] Due to the focus of our lab on *E. coli* however, we are more focused on Isc and Suf pathways in *E. coli*. Under normal cellular conditions, Isc serves

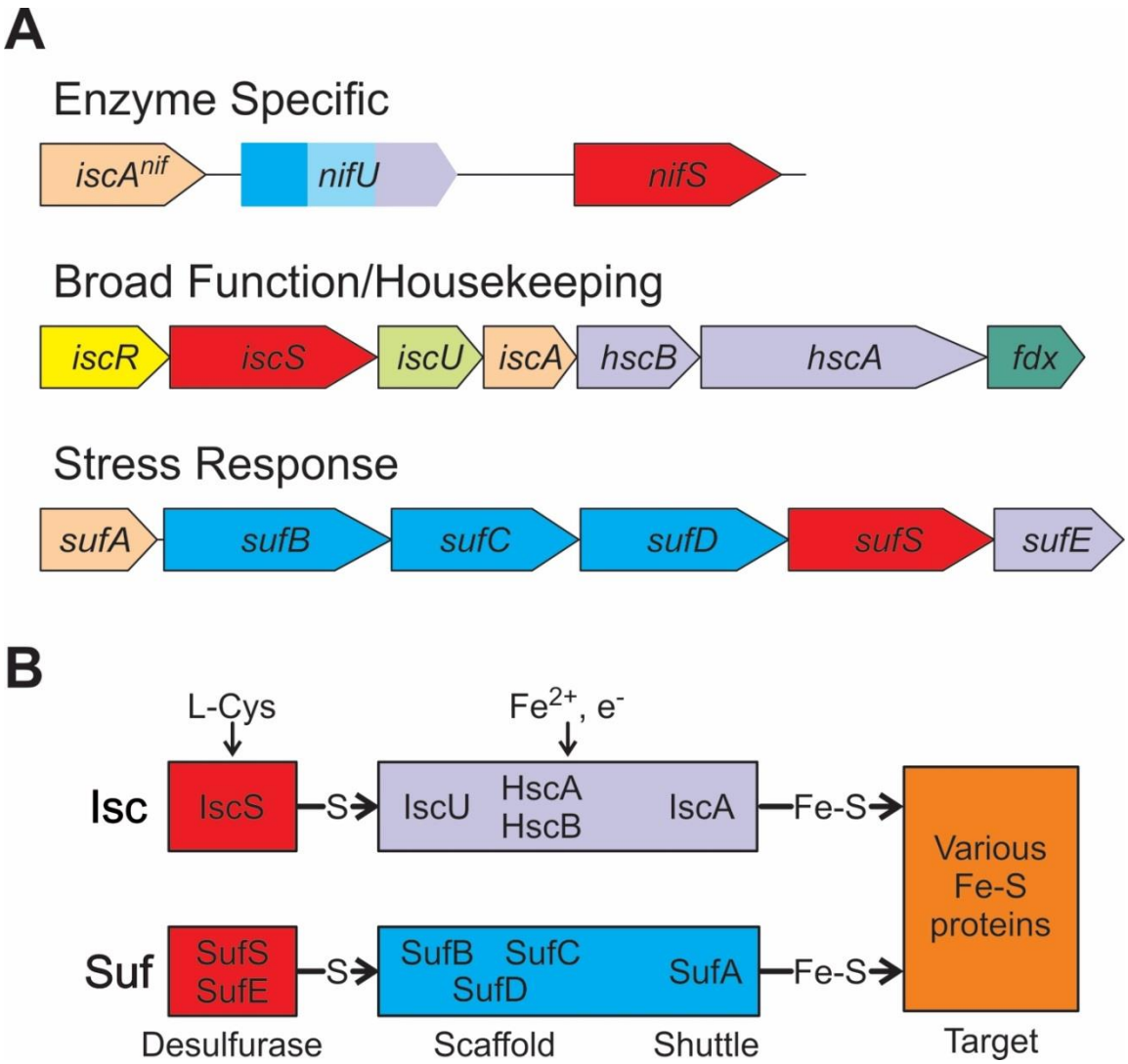

Figure 1.2. A. Operons for Fe-S cluster biogenesis. **B**. Pathways used for biogenesis of Fe-S clusters.

as the primary Fe-S "housekeeping" pathway, while Suf performs this responsibility in environments of iron starvation and oxidative stress.[22, 23]

The Isc Pathway

The Isc system consists of three critical proteins (IscS, IscU, and IscA) responsible for the synthesis of Fe-S clusters in *E. coli*, while also being partially conserved in eukaryotic mitochondria. With a currently undetermined iron source, the pathway initiates when IscS, which contains the pyridoxal-5'-phosphate (PLP) cofactor, performs cysteine desulfurase activity on free L-cysteine. This results in the generation of persulfide and alanine. From there, IscS transfers the available sulfur to IscU for the assembly of either [2Fe-2S] or [4Fe-4S].[24, 25] These clusters can be transferred to acceptor proteins, with IscA being capable of receiving the clusters as a member of the A-type carrier protein family responsible for Fe-S cluster shuttling.[26-28] An A-type carrier protein along with a PLP-dependent cysteine desulfurase observed in Isc are two protein types also observed in the Suf systems. [29]

The Suf Pathway and Regulation

The Suf pathway is present in archaea, parasites, numerous forms of bacteria (aside from *E. coli*), as well as other organisms including partial conservation in plant chloroplasts of some photosynthetic eukaryotes.[30] As previously discussed, Suf controls Fe-S biogenesis in *E. coli* in situations of oxidative stress or diminished iron levels, which is further exemplified by the regulation of the *suf* genes.

Transcriptional regulation of *suf* genes stems from the ferric uptake regulator (Fur), IscR, an Fe-S transcription factor, and OxyR, which senses hydrogen peroxide (H_2O_2). Fur

regulates over 100 genes associated with iron usage, homeostasis, and other yet to be elucidated functions [31]. It is allosterically up-regulated by the binding of Fe^{2+} to the N-terminus increasing the affinity of Fur to its DNA-binding sequence permitting repression of transcription for genes involved in iron uptake. Basal *suf* transcripts remain at low levels under iron-replete and normal cellular conditions due to repression by Fe^{2+}-Fur bound at the *suf* promoter (Figure 1.3). Fur demetallation when iron is limited induces a reduction in Fur binding permitting increased *suf* transcription.[32] The second pathway regulator involves presence or absence of an Fe-S cluster on IscR. When iron homeostasis is altered by a decrease in available iron, Fur repression fades resulting in increased production of apo-IscR. This apo form activates both *suf* and *isc*, but the *isc* activation is offset by the generation of the small RNA ryhB, which degrades *isc* mRNA, leaving an upregulated *suf* to generate clusters.[33] Finally, OxyR induces *suf* expression when treated with H_2O_2 via oxidation of disulfide bond formation.[34] All the previously mentioned transcriptional regulators correspond to the conditions under which Suf operates in *E. coli* providing for enhanced functional ability when necessary.[35] Additionally, Suf can maintain Fe-S biogenesis when the Isc pathway is deleted, illustrating the potential of Suf to serve as the primary cluster biogenesis pathway. The genes for *E. coli suf* are all transcribed from a single unit recognized as the *sufABCDSE* operon responsible for the six Suf proteins, SufA, SufB, SufC, SufD, SufS, and SufE. The six proteins that constitute the Suf pathway all have specific functions instrumental in the generation of Fe-S clusters. The PLP-bound SufS initiates Suf by acquiring sulfur from free cysteine using a cysteine desulfurase mechanism and generating a transportable persulfide. Following persulfide formation, SufE procures and shuttles the persulfide to SufB.[36-39] SufB generally assembles a [4Fe-

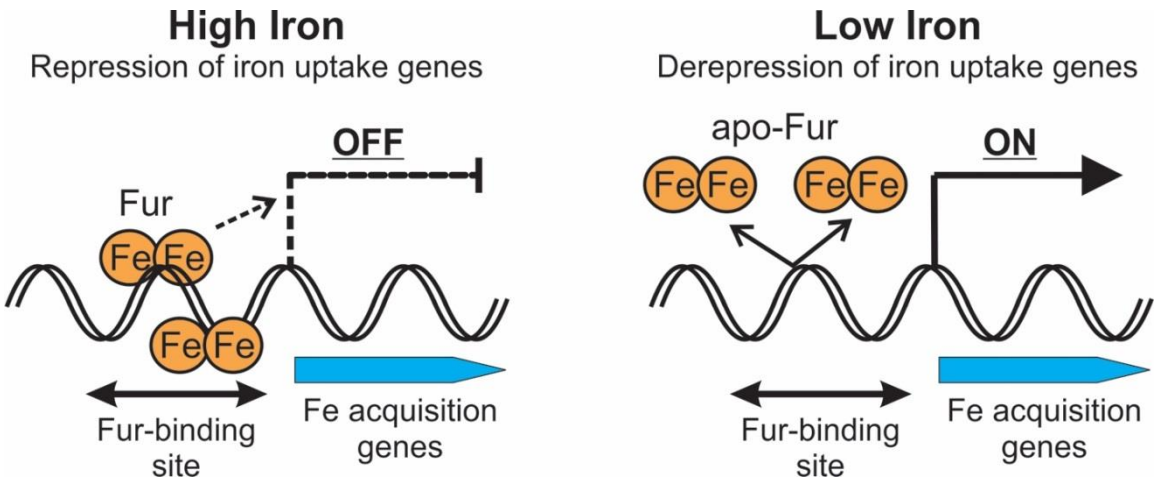

Figure 1.3. Regulation of transcription of genes involved in iron uptake by the ferric uptake regulator (Fur) regulon. The ability of Fur to inhibit transcription is shown under iron replete (left) and iron limiting conditions (right).

4S] cluster, although [2Fe-2S] is also possible, under anoxic conditions using the persulfide in combination with iron obtained from a currently unknown source.[40-42] Partially homologous to SufB, the exact function of SufD remains undetermined, although the inability of SufB to incorporate iron in the absence of SufD indicates a potential involvement in iron trafficking.[43] Both SufB and SufD, together with the ATPase protein SufC, combine to form the $SufBC_2D$ complex capable of producing a [4Fe-4S] cluster. Although SufB manages this individually, the $SufBC_2D$ complex exhibits enhanced interaction with SufE when obtaining persulfide as well as SufA, which acts as an Fe-S A-type carrier protein.[44-46]

SufS, PLP, and Cysteine Desulfurases

The need for sulfur in all Fe-S biogenesis pathways requires a protein responsible for cysteine desulfurase activity. NifS and IscS perform this function in the Nif and Isc systems, respectively, while SufS requisitions sulfur as part of the Suf pathway.[19, 29, 47, 48] All three of these cysteine desulfurase proteins depend on the cofactor PLP to properly function. The enzyme mechanism for this interaction, common in PLP-containing cysteine desulfurases, initiates when Schiff base forms between the cysteine α-amino group and PLP during the binding of PLP and cysteine. Then, to generate the desired persulfide, a catalytic cysteine residue of the enzyme functions as a nucleophile and attacks the sulfhydryl group of the cysteine bound to PLP. This makes the persulfide available to any biosynthetic pathways involving sulfur-containing molecules, like Fe-S clusters.[9, 49] Although the cysteine desulfurase mechanism is similar among PLP-containing enzymes, key distinguishing factors segregate them into two separate classifications.

PLP-containing cysteine desulfurases are grouped as either type I or type II desulfurases.[50, 51] Despite shared homology as well as similarities in function, fold, and quaternary structure, subtle structural and sequential differences identify SufS as a type II desulfurase, while NifS and IscS are type I.[9] Type I cysteine desulfurases are marked by the active site cysteine being located on a long, structurally disordered loop. With the persulfide present on this loop, type I desulfurases can interact with an assortment of sulfur acceptor molecules. Classified as type I, the aforementioned IscS protein is instrumental in the generation of most *E. coli* thio cofactors through interactions with numerous sulfur acceptor molecules [52]. Further distinguishing type I from type II desulfurases, the activity of IscS is not significantly impacted by the presence or absence of the sulfur acceptors.[38, 53] Additionally, this protein can interact directly with the IscU protein that serves as an assembly and delivery platform for Fe-S cofactors without the presence of a sulfur shuttling protein.[52] This independent nature of IscS corresponds to another major distinction between type I and type II desulfurases, despite the similarities to SufS.

Members of the type II cysteine desulfurase family possess an active site cysteine located on a short, structurally defined loop.[9, 54] Additionally, this class of desulfurases requires another protein operating as the sole sulfur acceptor from the desulfurase critical for their cellular function. In the case of SufS, SufE performs this duty by binding to SufS and enhancing the desulfurase activity by up to 50-fold.[37, 38] For this effect to occur, the acquired persulfide on SufS reaches cysteine-364, at which point SufE will retrieve the persulfide using its own cysteine-51, under reducing conditions, and transport the sulfur to awaiting proteins, such as $SufBC_2D$, involved in the production of sulfur-containing cofactors. [55]

SufS-SufE complex

From a functional perspective, SufS alone in the presence of 2 mM DTT and 2 mM L-cysteine fails to perform its responsibility as a cysteine desulfurase with paltry activity levels of 2.6 nmol of S^{2-} min^{-1} mg^{-1} in comparison to IscS (51.7 nmol of S^{2-} min^{-1} mg^{-1}).[38] However, as a type 2 cysteine desulfurase family member, the presence of the sulfur shuttling SufE protein amplified the activity to 41 nmol of S^{2-} min^{-1} mg^{-1}, which is comparable to IscS. The SufS-SufE activity can be further enhanced approximately 4-fold with the addition of $SufBC_2D$.[38] Along with analogous desulfuration to IscS, the SufS-SufE combination illustrated minimal inhibition when mixed with H_2O_2, while IscS revealed notable reduction in enzyme function, further illustrating the role of Suf in oxidative stress conditions.[38] The enzymatic capabilities of the SufS-SufE complex were then determined by Selbach et al. to be further improved by substituting DTT with TCEP due to TCEP being a stronger reductant better capable of removing sulfur from SufE, allowing maximum SufS-SufE turnover in the absence of $SufBC_2D$.[36]

SufS Structure, Amino Acids, and Mechanism

Despite thorough steady-state analysis and structure of SufS persulfide production from *E. coli*, limited investigation into the structure, mechanism, key amino acids of the process has been performed. With regards to structure, SufS is a homodimeric protein with one PLP bound to each monomer at lysine-226.[56] The PLP initially adopts an internal aldimine conformation absorbing at 420 nm prior to cysteine interaction and is obligatory to SufS folding as the absence of PLP results in misfolded and completely insoluble SufS, making analysis of the protein without this cofactor impossible. Upon forming a Schiff

base with cysteine, the PLP transforms through multiple intermediates as the persulfide is formed on cysteine-364.[57] From here, in the presence of both SufE and reductant, the persulfide is abstracted before the SufS can turnover and again perform the cysteine desulfurase activity.

Initially characterized by Zheng et al., the general mechanism by which PLP-dependent cysteine desulfurase enzymes operate begins with the PLP in a resting internal aldimine conformation as previously mentioned.[58, 59] From here, addition of free cysteine induces a conformation shift beginning with formation of a gem-diol and resulting in the formation of an external (Cys-) aldimine. With various uncharacterized proton transfers and the use of a cysteine residue in the active site, Cys-quinonoid followed by Cys-ketimine intermediates arise.[54, 58, 60] After ketimine formation, the generation of many other conformations occurs prior the return of the enzyme to the initial internal aldimine state with the assistance of the sulfur shuttling protein. Our work in SufS and SufE is focused on isolating and evaluating the amino acids vital to this process in addition to evaluating the kinetics as conformational shifts result for PLP.

The overall mechanism by which the SufS-SufE complex abstracts sulfur from cysteine appears to result via a two-step ping-pong process in which the first stage is a desulfurase reaction followed by a transpersulfurase reaction.[39, 61] The desulfurase stage revolves around the conformational changes experienced by PLP upon cysteine interaction prior to C364 removing sulfur and releasing alanine (the cysteine from which sulfur was abstracted). The transpersulfuration stage focuses on the movement of the persulfide from SufS C364 to SufE C51 before SufE further shuttles the sulfur to the final target (Figure 1.4).[61] Structural and hydrogen-deuterium exchange analysis combined to demonstrate that

the SufS-SufE desulfurase process likely results using a two-site model with one of the SufS monomers performing the activity while bound to SufE with interactions at the dimeric interface regulating this process.[61, 62] Whether the second monomer remains inactive or alternates functionality with the active SufS monomer remains unknown with the specifics of the SufS-SufE structure currently not elucidated.

Aside from SufS and IscS, a third protein exists in *E. coli* capable of cysteine desulfurase activity. The PLP-dependent CsdA shares ~43% sequence homology to SufS and is also categorized in the type II family of cysteine desulfurases. CsdA can weakly generate sulfur for Fe-S clusters if it is overexpressed. Additionally, the sulfur acceptor protein CsdE is ~35% homologous to SufE, suggesting potential structural similarities in the complexes formed between these cysteine desulfurases and their sulfur acceptors. Structurally, SufS and CsdA were shown to be very similar with the minor exceptions being a kink in H4 (helix-4) of CsdA and a shorter H2-H3 loop.[59, 63] In 2013, solution of the CsdA-CsdE complex demonstrated the presence of a CsdA dimer along with two CsdEs, each interacting with a different CsdA. This interaction was observed to alter the active site around PLP, but more pronounced modifications were revealed involving the CsdE structure.[64] The most significant observed alteration involves an ~11Å shift in position of the active site cysteine-61 along with the loop on which it is located after binding. This cysteine responsible for obtaining the sulfur from CsdA moves from a low access hydrophobic cavity of the loop potentially permitting easier accessibility to the cysteine during the transpersulfuration reaction. Structurally, the active site cysteine of SufE is in a similar hydrophobic cavity.[64-66] Due to the homology CsdA-CsdE shares with SufS-SufE,

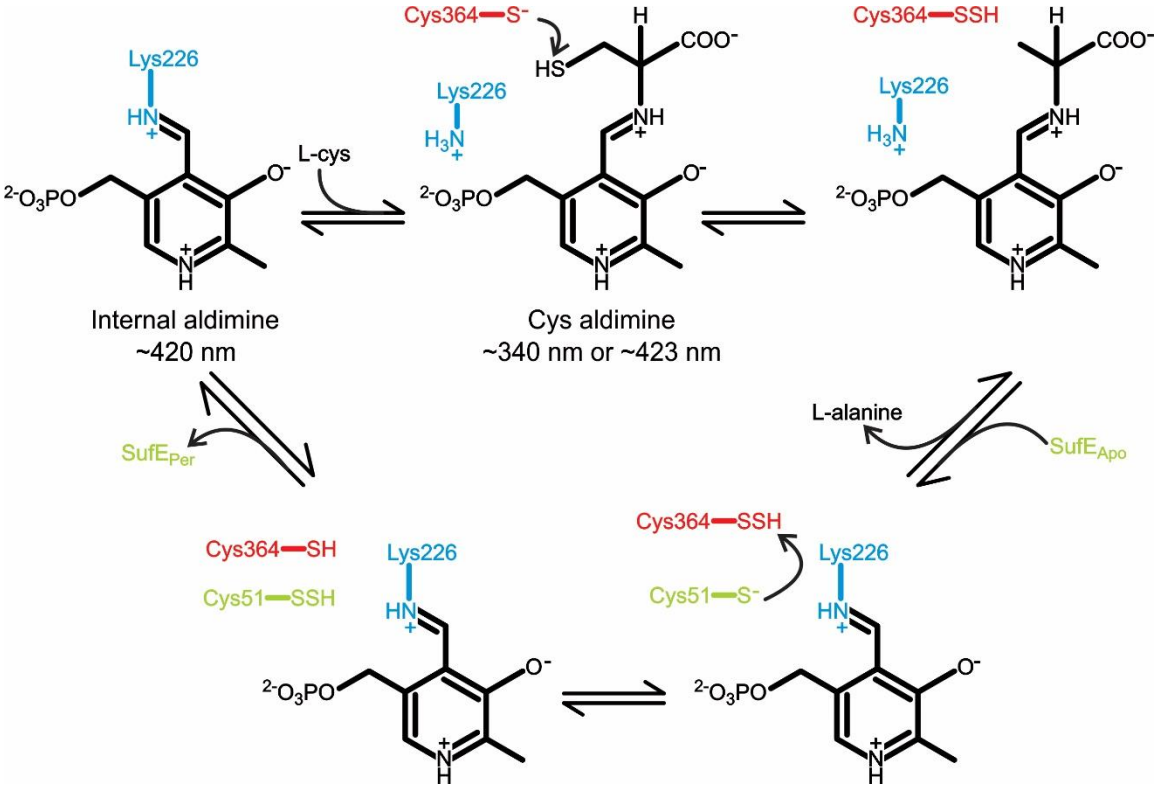

Figure 1.4 Early proposed mechanism by which the SufS-SufE complex functions together in the removing sulfur from cysteine. Key structural intermediates of the PLP cofactor are illustrated as well as important amino acids such as SufS L226 (blue), SufS C364 (red), and SufE C51 (green), although our current work has identified other key amino acids as well as their function.[62]

it was suggested that the interaction of SufS and SufE results in similar alterations, although current studies are underway in our lab to evaluate the validity of this statement.

Iron Storage with Ferritin

While the iron source from which the Suf pathway acquires iron remains a mystery, the major foundation of safe iron storage within the cell exists in the form of ferritin. As previously described, iron storage in the Fe^{3+} form is required in organisms ranging from humans to *E. coli* to prevent hydroxyl radical formation that potentially leads to numerous issues. A group of proteins utilized to perpetuate cell survival at variable iron levels is the ferritin family. In *E. coli*, the four known ferritin-like proteins are Ferritin A (FtnA), Bacterioferritin (Bfr), DNA-Binding protein of starved cells (Dps) and FtnB.[67-69] Both FtnA and Bfr function as 24 subunit proteins consisting of 24 monomers with each ~20 kDa in size in four-helical bundle motifs. These monomers form a spherical protein capable of storing ferric iron in the interior. FtnA operates as the primary iron-storage protein within the cell capable of accruing up to 4,500 iron atoms and serves a major role in iron storage during the stationary phase of cell growth. Circumstances of iron starvation result in the release of iron during conditions of iron from FtnA. Bfr is also capable of storing 4,500 iron atoms, but the current role in *E. coli* is uncertain despite implications having been made that Bfr acts as the primary iron storage protein in other microorganisms. Unlike FtnA and Bfr, Dps consists of only 12 monomers with the potential to sequester up to 500 iron atoms.[68] This ferritin forms a stable complex with DNA while performing as a guardian against oxidative damage through iron sequestration.

These three *E. coli* ferritins, like ferritins observed in other organisms including humans, rely on a conserved ferroxidase center capable of oxidizing ferrous iron into the more stable ferric form for sequestration. The amino acids that sculpt this center form a di-iron site consisting of a combination of conserved histidine and glutamate residues with various potential arrangements depending on the organism.[70-72] From here, molecular O_2 (or H_2O_2 for Dps) oxidizes the ferrous iron to ferric iron to store the mineral form of iron within ferritin. Figure 1.5 illustrates the overall structure of FtnA as well as the architecture of the ferroxidase center within *E. coli* FtnA, which contains three iron-binding sites, although sites A and B are primarily used for di-iron oxidation with no major known function for site C.[73] The question to then ask is what happens if a ferritin-like protein lacks the conserved amino acids of the ferroxidase center, such as FtnB.

FtnB

E. coli FtnB shares 36% identical and 56% similar amino acids to FtnA, designating the protein as a fourth potential member of the ferritin protein family in *E. coli*. However, the key amino acids this protein lacks make up the ferroxidase center conserved in other ferritin proteins. The conserved amino acids E49 and E129 of iron-binding site C become serine and histidine respectively in FtnB, with the histidine still capable of binding iron at the site. The presence of the serine, however, fails as a ligand for ferrous iron likely resulting in an inability of site C to bind iron. Additionally, H53 of site A becomes glutamine in FtnB, which is only capable of binding ferric iron, and E50, which links the irons of site A and B, is an asparagine incapable of bridging the di-iron. Despite lacking the conserved ferroxidase center, the importance of FtnB has been observed via gene

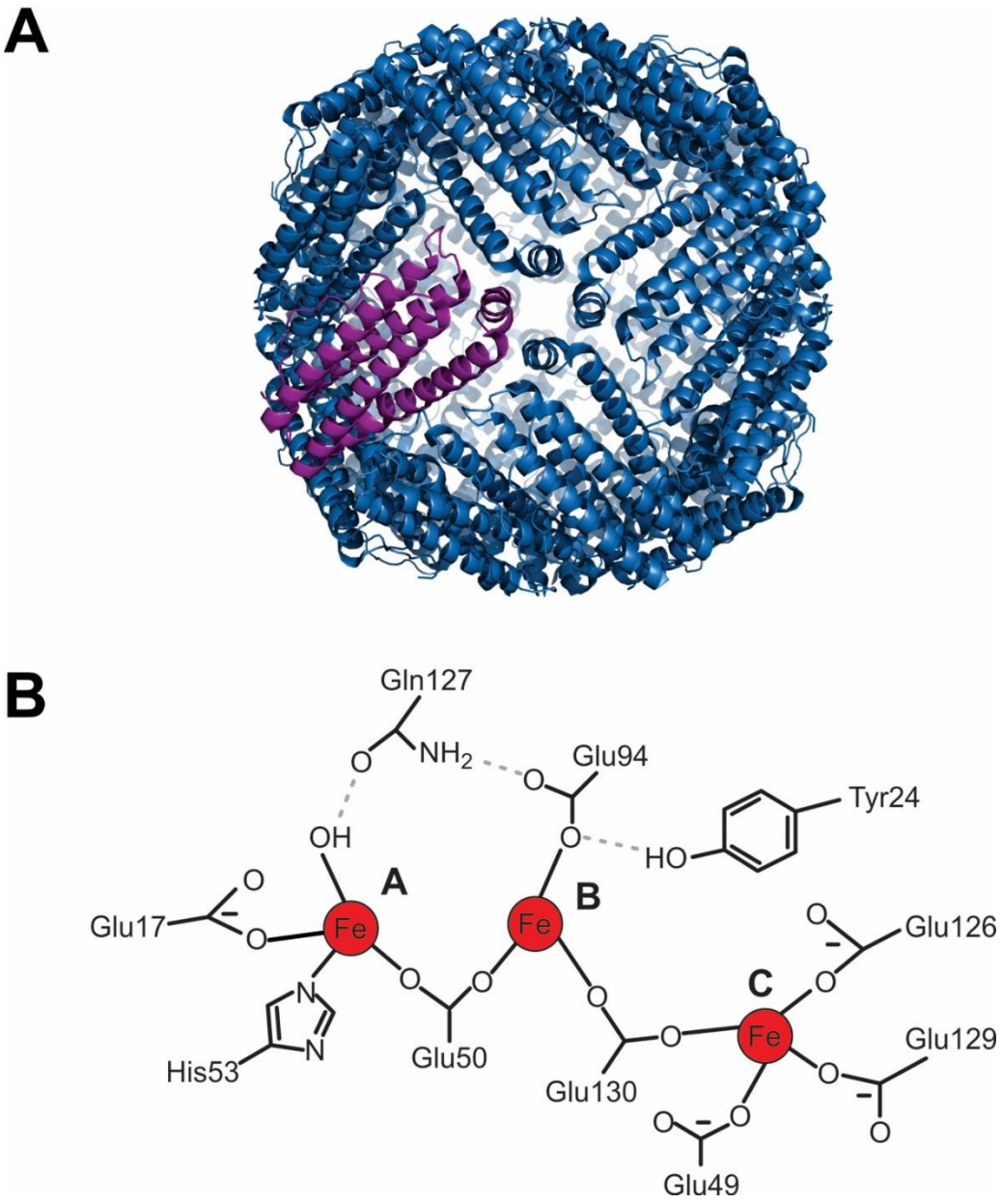

Figure 1.5 Structure of the iron storage protein FtnA from *E. coli*. **A**. Crystal structure of the FtnA 24-mer consisting of 24 monomers (one shown in purple) within which iron is stored. **B**. FtnA ferroxidase center capable of oxidizing two Fe^{2+} atoms simultaneously prior to storing them as Fe^{3+} in the interior of the oligomer.[73]

deletion. In *Salmonella enterica*, *ftnB* deletion results in a defect in Fe-S repair when cells are exposed to H_2O_2.[74] Additionally, deletion of *ftnB* in *Salmonella typhiumurium* demonstrates the requirement of *ftnB* for the organism to maintain normal levels of virulence.[75] Aside from roles in virulence and Fe-S repair, multiple proteins are involved in the transcriptional regulation of *ftnB*.

There are three known transcriptional regulators with respect to *ftnB*, potentially indicative of the significance. First, Fur seemingly upregulates expression of *ftnB* resulting in enhanced FtnB production in situations of elevated iron levels, potentially demonstrating the prospective function of iron storage or controlling cellular iron levels.[76] The second transcriptional controller of *ftnB* is another regulon referred to as Cpx, which operates in controlling transcription based off a variety of cell enveloped disturbances including pH, envelope protein expression, and copper.[74, 77] In the case of *ftnB*, the toxic levels of copper result in increased *ftnB* induction in a Cpx-dependent manner, potentially to store iron and reduce the risk of damage from oxygen radicals [78]. Finally, the last known regulator of *ftnB* transcription is CsrA, a key component of the carbon storage regulator system that serves heavily in carbon motility and bacterial pathogen virulence.[79, 80] This protein inhibits transcription of *ftnB*, although whether this is direct or indirect regulation and the exact reasoning are not yet understood.

Regulatory Proteins Involving Other Metals

Besides storage, regulatory cellular maintenance of iron levels, in addition to other metals like zinc and nickel, results via the use of metal chaperones, metal chelators, importers/exporters, and metalloregulators. The restrictive nature of the bacterial cell

membrane necessitates the assistance of active transporters capable of aiding the passage of metal ions through the lipid bilayer, which requires importers and exporters to assist the metal. This is the case with the water insoluble ferric iron interacting with a siderophore to chelate thus iron and import it from the environment. Chaperones deter metal toxicity by complexing with the metal and transporting it to the intended target protein. Furthermore, with the desired homeostatic balance of metals in the cell, metalloregulatory proteins responsible for the sensing of metal levels operate through the regulation of transcriptional expression of metal utilizing proteins and metal homeostasis while responding to changes in cellular metal levels. One of these regulators that was previously discussed is the Fur regulon.

As was previously discussed, Fe-S clusters are one of the iron-containing cofactors required by some proteins. The other three are mono- or di-iron centers and heme. These functional cofactors perform essential roles involving enzymes, structure, signaling, and transcriptional regulation, among other functions. The numerous services of iron combined with potential for toxicity if left unregulated demands a governing system responsible for global iron regulation found in the Fur regulon.

One family of enzymes associated with Fur involves bacterial ferric reductases responsible for reducing chelated Fe^{3+} to soluble Fe^{2+} for use by iron metalloproteins. In order to keep pace with the requirement of the cell for reduced iron, ferric reductases speed up cytosolic iron reduction. This function is performed either by assimilatory iron reduction, in which Fe^{3+} is catalyzed to generate Fe^{2+}, or disassimilatory iron reduction where the ferric reductase facilitates the action of Fe^{3+} as an electron acceptor for respiratory reactions.[81] Assimilatory reductases also behave as flavin reductases in which

Fe^{3+} reduction is coupled to the oxidation of NAD(P)H flavin oxidoreductases (flavin for short).[82] NADH or NADPH act as the electron source transferring e^- to Fe^{3+} with the assistance of flavins like FAD, FMN, or riboflavin. Despite the presence of many flavin reductases, none were known to specifically be ferric-siderophore reductases, until the study of *yqjH*.

YqjH and YqjI

The *yqjH* gene of *E. coli* codes for the flavin adenine dinucleotide (FAD)-bound, NADPH-dependent ferric reductase YqjH capable of reducing ferric siderophores such as enterobactin in preparation for in vivo iron utilization. The mechanism resulting in iron reduction occurs via a single-electron transfer via a double-displacement reaction driven by NADPH as the electron source with various Fe^{3+} sources capable of being reduced (Figure 1.6).[83] Regulation of yqjH stems from multiple sources with the first being the previously mentioned Fur. Just upstream of the transcriptional start site for *yqjH* is the DNA-binding region known as the Fur box to which Fur can bind and inhibit transcription of *yqjH*.[84] As part of the Fur regulon, YqjH operates as a protein involved in iron homeostasis.[31]

In addition to Fur, *yqjH* is also regulated by the protein YqjI. Upstream of *yqjH* is a separate gene transcribed in the opposite direction known as *yqjI*. These genes are separated by a 287 bp region containing consisting of separate sequences involved in transcriptional regulation of the two genes, including binding sites for YqjI. The YqjI protein exists in both oligomeric and monomeric forms with the oligomer capable of inhibiting transcription of both itself and *yqjH*. YqjI inhibits these two genes by interacting

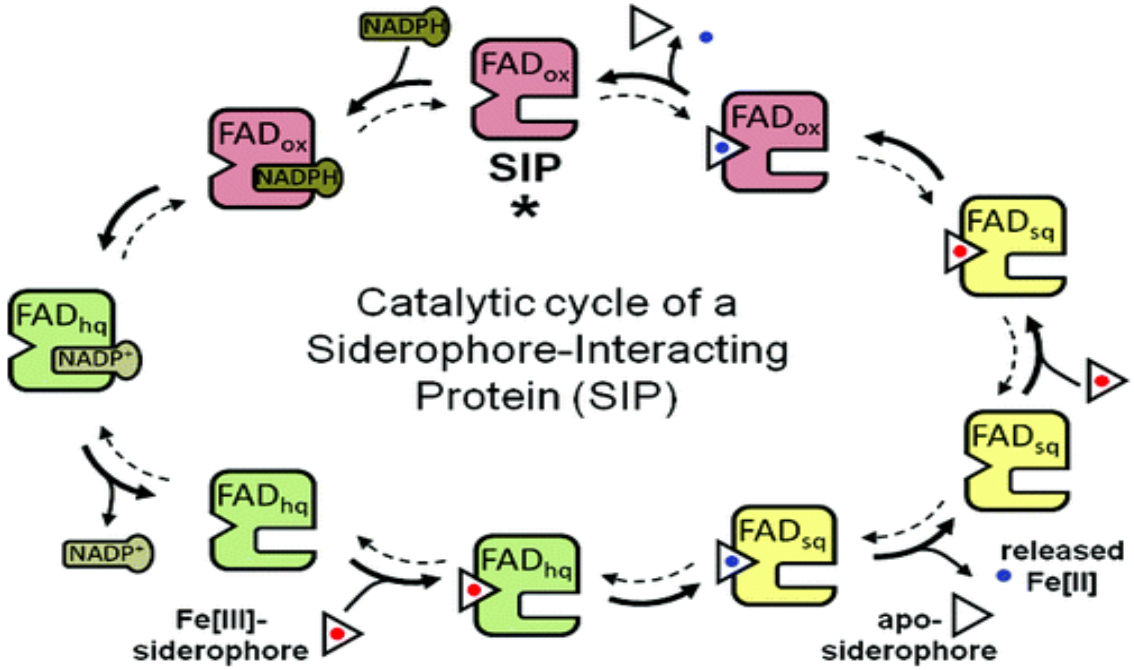

Figure 1.6 Mechanism by which the FAD-bound siderophores interacting protein YqjH reduces Fe^{3+} with assistance from NADPH as an electron source.[83]

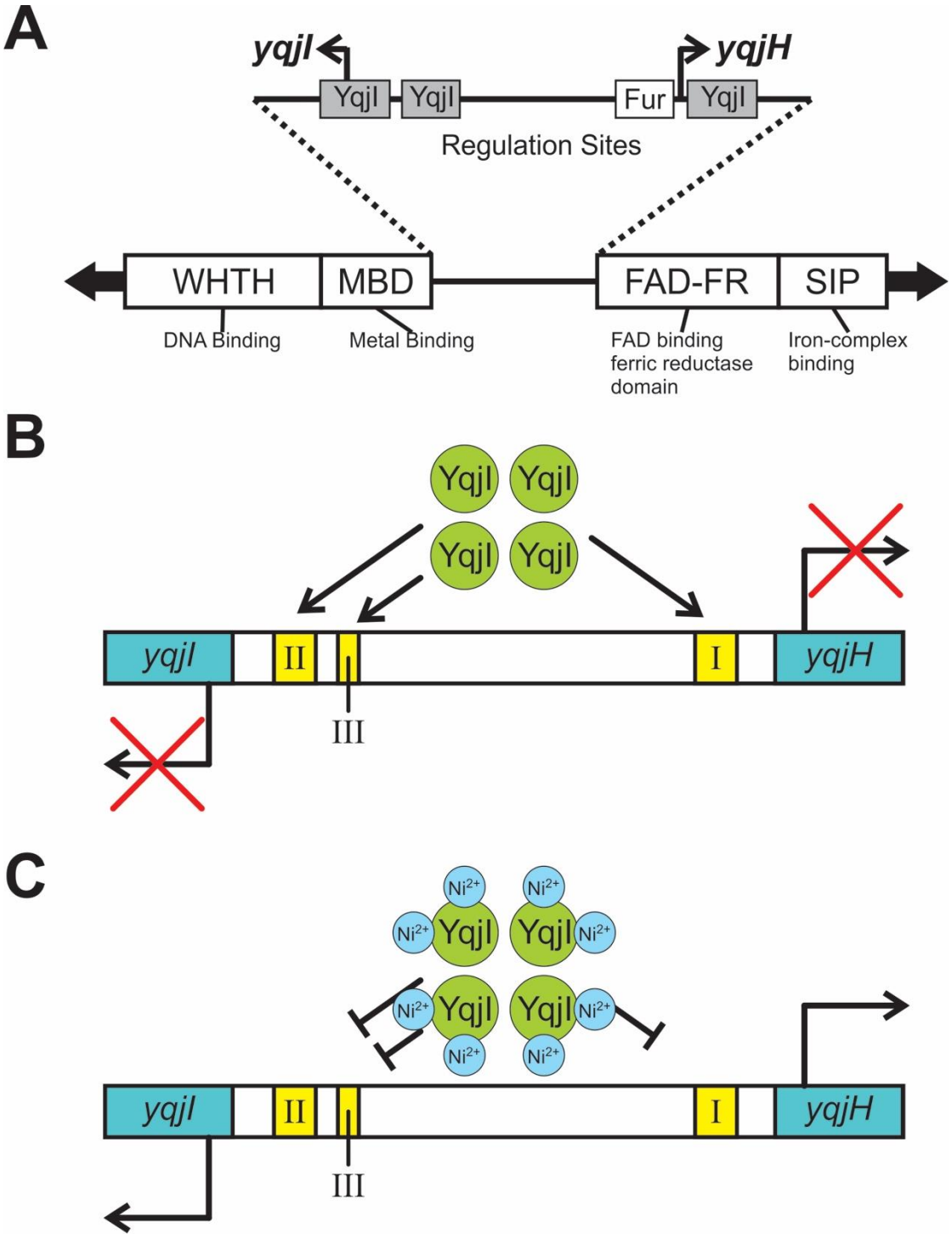

Figure 1.7 The *yqjH-yqjI* intergenic region used by YqjI to inhibit transcription of both genes. **A**. Key coding region for both genes as well as the three intergenic binding sites of YqjI in addition to the Fur site used for regulating *yqjH*.[85] **B**. YqjI inhibits both genes under normal conditions. **C**. When nickel is present, the nickel binds to YqjI and inhibits YqjI binding ability.

with three similar DNA sites with the first upstream of *yqjH* and the third upstream of *yqjI*.[84] This regulation occurs in a cooperative manner requiring further detail to understand the exact mechanism from which it stems.[86] Control of YqjI regulation involves nickel capable of inhibiting YqjI binding and increasing transcription of the two genes (Figure 1.7). This creates a cross-regulation between nickel and iron homeostasis potentially linked to the NiFe hydrogenase family of enzymes. We sought to determine the method through which nickel both associated with and regulated YqjI.

Biomedical Relevance

Numerous pathogenic bacteria including *Mycobacterium tuberculosis* depend upon iron as well as the incorporation of Fe-S clusters in metalloproteins to persist and remain harmful to humans. Due to the importance of this metal, humans and pathogens must ensure regulatory homeostasis for survival to prevent potential generation of harmful ROS. Identification of new methods to disrupt iron regulation in harmful pathogens while avoiding harmful side effects drives much of our work.

The significance of investigating the specific intermediates of the cysteine desulfurase mechanism for the Suf pathway stems from the prominence of Suf in various bacterial genomes associated with human medical diseases. While one of two Fe-S biogenesis pathways in *E. coli*, the Suf system is the sole pathway in *M. tuberculosis*, which shares 70% genetic conservation with the *E. coli* form.[87] With the arrival of antibiotic resistant strains of this bacteria resulting in an increased susceptibility of people to untreatable forms of the disease tuberculosis, new antibiotics must be developed. The isolation of key structural features of these mechanistic intermediates offers the potential

for new antibiotic design. Additionally, Suf functions in other harmful organisms like *Shigella*, responsible for bacillary dysentery. The importance of Suf under disruption of iron homeostasis and the lack of known Suf pathway homologues in humans make this pathway optimal for drug design. Besides Suf, FtnB studies offer further insight and potential drug treatment options with diseases and disorders corresponding to iron such as Friedrich's ataxia or anemia. Additionally, with the necessity of FtnB in the virulence typhoid fever as well as the presence of the gene in dysentery, this protein offers a major potential drug target [74]. Finally, YqjI introduces an indirect link between nickel and iron with implications in cellular toxicity with further investigation into the significance required before the true biomedical relevance can be elucidated.

Overall Aims

The overall focus of my work while in the laboratory of Dr. F. Wayne Outten has been the in vivo and in vitro characterization of various proteins involved bacterial metal homeostasis. With respect to the Suf pathway, my initial aim was the characterization of mechanistic intermediates, both kinetically and structurally, exhibited by treating SufS with L-cysteine as well as the identification for the amino acids vital for this process to occur. After intermediate assignment with SufS alone, the next goal was the determination of the additional processive stages experienced by introducing the sulfur-shuttling SufE protein as well as the strong reductant TCEP. When working with YqjI, we elucidated the in vivo and in vitro method by which nickel inhibited the proteins ability to regulate transcription while also further characterizing the nickel binding site. Finally, the primary

goal involving the characterization of FtnB ended up revolving around purification of the protein in its native state, something that has proven extremely difficult to do.

References

1. Anbar, A. D., Oceans. Elements and evolution. *Science* **2008,** *322* (5907), 1481-3.

2. Anbar, A. D.; Duan, Y.; Lyons, T. W.; Arnold, G. L.; Kendall, B.; Creaser, R. A.; Kaufman, A. J.; Gordon, G. W.; Scott, C.; Garvin, J.; Buick, R., A whiff of oxygen before the great oxidation event? *Science* **2007,** *317* (5846), 1903-6.

3. Konhauser, K. O.; Pecoits, E.; Lalonde, S. V.; Papineau, D.; Nisbet, E. G.; Barley, M. E.; Arndt, N. T.; Zahnle, K.; Kamber, B. S., Oceanic nickel depletion and a methanogen famine before the Great Oxidation Event. *Nature* **2009,** *458* (7239), 750-3.

4. Andrews, S. C.; Robinson, A. K.; Rodriguez-Quinones, F., Bacterial iron homeostasis. *FEMS Microbiol Rev* **2003,** *27* (2-3), 215-37.

5. Touati, D., Iron and oxidative stress in bacteria. *Arch Biochem Biophys* **2000,** *373* (1), 1-6.

6. Winterbourn, C. C., Toxicity of iron and hydrogen peroxide: the Fenton reaction. *Toxicol Lett* **1995,** *82-83*, 969-74.

7. Ratledge, C.; Dover, L. G., Iron metabolism in pathogenic bacteria. *Annu Rev Microbiol* **2000,** *54*, 881-941.

8. Wirtz, M.; Droux, M., Synthesis of the sulfur amino acids: cysteine and methionine. *Photosynth Res* **2005,** *86* (3), 345-62.

9. Mihara, H.; Esaki, N., Bacterial cysteine desulfurases: their function and mechanisms. *Appl Microbiol Biotechnol* **2002,** *60* (1-2), 12-23.

10. Huber, C.; Eisenreich, W.; Hecht, S.; Wachtershauser, G., A possible primordial peptide cycle. *Science* **2003,** *301* (5635), 938-40.

11. Wachtershauser, G., On the chemistry and evolution of the pioneer organism. *Chem Biodivers* **2007,** *4* (4), 584-602.

12. Beinert, H.; Holm, R. H.; Munck, E., Iron-sulfur clusters: nature's modular, multipurpose structures. *Science* **1997,** *277* (5326), 653-9.

13. Beinert, H., Iron-sulfur proteins: ancient structures, still full of surprises. *J Biol Inorg Chem* **2000,** *5* (1), 2-15.

14. Johnson, M. K., Iron-sulfur proteins. In *Encyclopedia of inorganic chemistry*, King, R. B., Ed. John Wiley & Sons: Chichester, 1994; Vol. 1, pp 1896-1915.

15. Glaser, T.; Hedman, B.; Hodgson, K. O.; Solomon, E. I., Ligand K-edge X-ray absorption spectroscopy: a direct probe of ligand-metal covalency. *Acc Chem Res* **2000,** *33* (12), 859-68.

16. Noodleman, L.; Case, D. A., Density-Functional Theory of Spin Polarization and Spin Coupling in Iron-Sulfur Clusters. *Adv Inorg Chem* **1992,** *38*, 423-+.

17. Kiley, P. J.; Beinert, H., The role of Fe-S proteins in sensing and regulation in bacteria. *Curr Opin Microbiol* **2003,** *6* (2), 181-5.

18. Demple, B.; Ding, H.; Jorgensen, M., Escherichia coli SoxR protein: sensor/transducer of oxidative stress and nitric oxide. *Methods Enzymol* **2002,** *348*, 355-64.

19. Ayala-Castro, C.; Saini, A.; Outten, F. W., Fe-S cluster assembly pathways in bacteria. *Microbiol Mol Biol Rev* **2008,** *72* (1), 110-25, table of contents.

20. Jacobson, M. R.; Brigle, K. E.; Bennett, L. T.; Setterquist, R. A.; Wilson, M. S.; Cash, V. L.; Beynon, J.; Newton, W. E.; Dean, D. R., Physical and genetic map of the major nif gene cluster from Azotobacter vinelandii. *J Bacteriol* **1989,** *171* (2), 1017-27.

21. Jacobson, M. R.; Cash, V. L.; Weiss, M. C.; Laird, N. F.; Newton, W. E.; Dean, D. R., Biochemical and genetic analysis of the nifUSVWZM cluster from Azotobacter vinelandii. *Mol Gen Genet* **1989,** *219* (1-2), 49-57.

22. Nachin, L.; Loiseau, L.; Expert, D.; Barras, F., SufC: an unorthodox cytoplasmic ABC/ATPase required for [Fe-S] biogenesis under oxidative stress. *EMBO J* **2003,** *22* (3), 427-37.

23. Outten, F. W.; Djaman, O.; Storz, G., A suf operon requirement for Fe-S cluster assembly during iron starvation in Escherichia coli. *Mol Microbiol* **2004,** *52* (3), 861-72.

24. Agar, J. N.; Krebs, C.; Frazzon, J.; Huynh, B. H.; Dean, D. R.; Johnson, M. K., IscU as a scaffold for iron-sulfur cluster biosynthesis: sequential assembly of [2Fe-2S] and [4Fe-4S] clusters in IscU. *Biochemistry* **2000,** *39* (27), 7856-62.

25. Agar, J. N.; Zheng, L. M.; Cash, V. L.; Dean, D. R.; Johnson, M. K., Role of the IscU protein in iron-sulfur cluster biosynthesis: IscS-mediated assembly of a [Fe2S2] cluster in IscU. *J Am Chem Soc* **2000,** *122* (9), 2136-2137.

26. Ollagnier-de-Choudens, S.; Sanakis, Y.; Fontecave, M., SufA/IscA: reactivity studies of a class of scaffold proteins involved in [Fe-S] cluster assembly. *J Biol Inorg Chem* **2004,** *9* (7), 828-38.

27. Vinella, D.; Brochier-Armanet, C.; Loiseau, L.; Talla, E.; Barras, F., Iron-sulfur (Fe/S) protein biogenesis: phylogenomic and genetic studies of A-type carriers. *PLoS Genet* **2009,** *5* (5), e1000497.

28. Vinella, D.; Loiseau, L.; Ollagnier de Choudens, S.; Fontecave, M.; Barras, F., In vivo [Fe-S] cluster acquisition by IscR and NsrR, two stress regulators in Escherichia coli. *Mol Microbiol* **2013,** *87* (3), 493-508.

29. Johnson, D. C.; Dean, D. R.; Smith, A. D.; Johnson, M. K., Structure, function, and formation of biological iron-sulfur clusters. *Annu Rev Biochem* **2005,** *74*, 247-81.

30. Takahashi, Y.; Tokumoto, U., A third bacterial system for the assembly of iron-sulfur clusters with homologs in archaea and plastids. *J Biol Chem* **2002,** *277* (32), 28380-3.

31. McHugh, J. P.; Rodriguez-Quinones, F.; Abdul-Tehrani, H.; Svistunenko, D. A.; Poole, R. K.; Cooper, C. E.; Andrews, S. C., Global iron-dependent gene regulation in Escherichia coli. A new mechanism for iron homeostasis. *J Biol Chem* **2003,** *278* (32), 29478-86.

32. Nachin, L.; El Hassouni, M.; Loiseau, L.; Expert, D.; Barras, F., SoxR-dependent response to oxidative stress and virulence of Erwinia chrysanthemi: the key role of SufC, an orphan ABC ATPase. *Mol Microbiol* **2001,** *39* (4), 960-72.

33. Beauchene, N. A.; Myers, K. S.; Chung, D.; Park, D. M.; Weisnicht, A. M.; Keles, S.; Kiley, P. J., Impact of Anaerobiosis on Expression of the Iron-Responsive Fur and RyhB Regulons. *MBio* **2015,** *6* (6), e01947-15.

34. Zheng, M.; Wang, X.; Templeton, L. J.; Smulski, D. R.; LaRossa, R. A.; Storz, G., DNA microarray-mediated transcriptional profiling of the Escherichia coli response to hydrogen peroxide. *J Bacteriol* **2001,** *183* (15), 4562-70.

35. Zheng, M.; Aslund, F.; Storz, G., Activation of the OxyR transcription factor by reversible disulfide bond formation. *Science* **1998,** *279* (5357), 1718-21.

36. Selbach, B. P.; Pradhan, P. K.; Dos Santos, P. C., Protected sulfur transfer reactions by the Escherichia coli Suf system. *Biochemistry* **2013,** *52* (23), 4089-96.

37. Loiseau, L.; Ollagnier-de-Choudens, S.; Nachin, L.; Fontecave, M.; Barras, F., Biogenesis of Fe-S cluster by the bacterial Suf system: SufS and SufE form a new type of cysteine desulfurase. *J Biol Chem* **2003,** *278* (40), 38352-9.

38. Dai, Y.; Outten, F. W., The E. coli SufS-SufE sulfur transfer system is more resistant to oxidative stress than IscS-IscU. *FEBS Lett* **2012,** *586* (22), 4016-22.

39. Selbach, B.; Earles, E.; Dos Santos, P. C., Kinetic analysis of the bisubstrate cysteine desulfurase SufS from Bacillus subtilis. *Biochemistry* **2010,** *49* (40), 8794-802.

40. Layer, G.; Gaddam, S. A.; Ayala-Castro, C. N.; Ollagnier-de Choudens, S.; Lascoux, D.; Fontecave, M.; Outten, F. W., SufE transfers sulfur from SufS to SufB for iron-sulfur cluster assembly. *J Biol Chem* **2007,** *282* (18), 13342-50.

41. Wollers, S.; Layer, G.; Garcia-Serres, R.; Signor, L.; Clemancey, M.; Latour, J. M.; Fontecave, M.; Ollagnier de Choudens, S., Iron-sulfur (Fe-S) cluster assembly: the SufBCD complex is a new type of Fe-S scaffold with a flavin redox cofactor. *J Biol Chem* **2010,** *285* (30), 23331-41.

42. Blanc, B.; Clemancey, M.; Latour, J. M.; Fontecave, M.; Ollagnier de Choudens, S., Molecular investigation of iron-sulfur cluster assembly scaffolds under stress. *Biochemistry* **2014,** *53* (50), 7867-9.

43. Saini, A.; Mapolelo, D. T.; Chahal, H. K.; Johnson, M. K.; Outten, F. W., SufD and SufC ATPase activity are required for iron acquisition during in vivo Fe-S cluster formation on SufB. *Biochemistry* **2010,** *49* (43), 9402-12.

44. Chahal, H. K.; Dai, Y.; Saini, A.; Ayala-Castro, C.; Outten, F. W., The SufBCD Fe-S scaffold complex interacts with SufA for Fe-S cluster transfer. *Biochemistry* **2009,** *48* (44), 10644-53.

45. Chahal, H. K.; Outten, F. W., Separate FeS scaffold and carrier functions for SufB(2)C(2) and SufA during in vitro maturation of [2Fe2S] Fdx. *J Inorg Biochem* **2012,** *116*, 126-34.

46. Gupta, V.; Sendra, M.; Naik, S. G.; Chahal, H. K.; Huynh, B. H.; Outten, F. W.; Fontecave, M.; Ollagnier de Choudens, S., Native Escherichia coli SufA, coexpressed with SufBCDSE, purifies as a [2Fe-2S] protein and acts as an Fe-S transporter to Fe-S target enzymes. *J Am Chem Soc* **2009,** *131* (17), 6149-53.

47. Fontecave, M.; Ollagnier-de-Choudens, S., Iron-sulfur cluster biosynthesis in bacteria: Mechanisms of cluster assembly and transfer. *Arch Biochem Biophys* **2008,** *474* (2), 226-37.

48. Roche, B.; Aussel, L.; Ezraty, B.; Mandin, P.; Py, B.; Barras, F., Iron/sulfur proteins biogenesis in prokaryotes: formation, regulation and diversity. *Biochim Biophys Acta* **2013,** *1827* (3), 455-69.

49. Zheng, L.; Dean, D. R., Catalytic formation of a nitrogenase iron-sulfur cluster. *J Biol Chem* **1994,** *269* (29), 18723-6.

50. Black, K. A.; Dos Santos, P. C., Shared-intermediates in the biosynthesis of thio-cofactors: Mechanism and functions of cysteine desulfurases and sulfur acceptors. *Biochim Biophys Acta* **2015,** *1853* (6), 1470-80.

51. Mihara, H.; Fujii, T.; Kato, S.; Kurihara, T.; Hata, Y.; Esaki, N., Structure of external aldimine of Escherichia coli CsdB, an IscS/NifS homolog: implications for its specificity toward selenocysteine. *J Biochem* **2002,** *131* (5), 679-85.

52. Py, B.; Barras, F., Building Fe-S proteins: bacterial strategies. *Nat Rev Microbiol* **2010,** *8* (6), 436-46.

53. Kato, S.; Mihara, H.; Kurihara, T.; Takahashi, Y.; Tokumoto, U.; Yoshimura, T.; Esaki, N., Cys-328 of IscS and Cys-63 of IscU are the sites of disulfide bridge formation in a covalently bound IscS/IscU complex: implications for the mechanism of iron-sulfur cluster assembly. *Proc Natl Acad Sci U S A* **2002,** *99* (9), 5948-52.

54. Tirupati, B.; Vey, J. L.; Drennan, C. L.; Bollinger, J. M., Jr., Kinetic and structural characterization of Slr0077/SufS, the essential cysteine desulfurase from Synechocystis sp. PCC 6803. *Biochemistry* **2004,** *43* (38), 12210-9.

55. Sendra, M.; Ollagnier de Choudens, S.; Lascoux, D.; Sanakis, Y.; Fontecave, M., The SUF iron-sulfur cluster biosynthetic machinery: sulfur transfer from the SUFS-SUFE complex to SUFA. *FEBS Lett* **2007,** *581* (7), 1362-8.

56. Mihara, H.; Maeda, M.; Fujii, T.; Kurihara, T.; Hata, Y.; Esaki, N., A nifS-like gene, csdB, encodes an Escherichia coli counterpart of mammalian selenocysteine lyase. Gene cloning, purification, characterization and preliminary x-ray crystallographic studies. *J Biol Chem* **1999,** *274* (21), 14768-72.

57. Fontecave, M.; Choudens, S. O.; Py, B.; Barras, F., Mechanisms of iron-sulfur cluster assembly: the SUF machinery. *J Biol Inorg Chem* **2005,** *10* (7), 713-21.

58. Zheng, L.; White, R. H.; Cash, V. L.; Dean, D. R., Mechanism for the desulfurization of L-cysteine catalyzed by the nifS gene product. *Biochemistry* **1994,** *33* (15), 4714-20.

59. Lima, C. D., Analysis of the E. coli NifS CsdB protein at 2.0 A reveals the structural basis for perselenide and persulfide intermediate formation. *J Mol Biol* **2002,** *315* (5), 1199-208.

60. Behshad, E.; Bollinger, J. M., Jr., Kinetic analysis of cysteine desulfurase CD0387 from Synechocystis sp. PCC 6803: formation of the persulfide intermediate. *Biochemistry* **2009,** *48* (50), 12014-23.

61. Kim, D.; Singh, H.; Dai, Y.; Dong, G.; Busenlehner, L. S.; Outten, F. W.; Frantom, P. A., Changes in Protein Dynamics in Escherichia coli SufS Reveal a Possible Conserved Regulatory Mechanism in Type II Cysteine Desulfurase Systems. *Biochemistry* **2018,** *57* (35), 5210-5217.

62. Singh, H.; Dai, Y.; Outten, F. W.; Busenlehner, L. S., Escherichia coli SufE sulfur transfer protein modulates the SufS cysteine desulfurase through allosteric conformational dynamics. *J Biol Chem* **2013,** *288* (51), 36189-200.

63. Fujii, T.; Maeda, M.; Mihara, H.; Kurihara, T.; Esaki, N.; Hata, Y., Structure of a NifS homologue: X-ray structure analysis of CsdB, an Escherichia coli counterpart of mammalian selenocysteine lyase. *Biochemistry* **2000,** *39* (6), 1263-73.

64. Kim, S.; Park, S., Structural changes during cysteine desulfurase CsdA and sulfur acceptor CsdE interactions provide insight into the trans-persulfuration. *J Biol Chem* **2013,** *288* (38), 27172-80.

65. Liu, G.; Li, Z.; Chiang, Y.; Acton, T.; Montelione, G. T.; Murray, D.; Szyperski, T., High-quality homology models derived from NMR and X-ray structures of E. coli proteins YgdK and Suf E suggest that all members of the YgdK/Suf E protein family are enhancers of cysteine desulfurases. *Protein Sci* **2005,** *14* (6), 1597-608.

66. Goldsmith-Fischman, S.; Kuzin, A.; Edstrom, W. C.; Benach, J.; Shastry, R.; Xiao, R.; Acton, T. B.; Honig, B.; Montelione, G. T.; Hunt, J. F., The SufE sulfur-acceptor protein contains a conserved core structure that mediates interdomain interactions in a variety of redox protein complexes. *J Mol Biol* **2004,** *344* (2), 549-65.

67. Hudson, A. J.; Andrews, S. C.; Hawkins, C.; Williams, J. M.; Izuhara, M.; Meldrum, F. C.; Mann, S.; Harrison, P. M.; Guest, J. R., Overproduction, purification and characterization of the Escherichia coli ferritin. *Eur J Biochem* **1993,** *218* (3), 985-95.

68. Abdul-Tehrani, H.; Hudson, A. J.; Chang, Y. S.; Timms, A. R.; Hawkins, C.; Williams, J. M.; Harrison, P. M.; Guest, J. R.; Andrews, S. C., Ferritin mutants of Escherichia coli are iron deficient and growth impaired, and fur mutants are iron deficient. *J Bacteriol* **1999,** *181* (5), 1415-28.

69. Smith, J. L., The physiological role of ferritin-like compounds in bacteria. *Crit Rev Microbiol* **2004,** *30* (3), 173-85.

70. Jameson, G. N.; Jin, W.; Krebs, C.; Perreira, A. S.; Tavares, P.; Liu, X.; Theil, E. C.; Huynh, B. H., Stoichiometric production of hydrogen peroxide and parallel formation of ferric multimers through decay of the diferric-peroxo complex, the first detectable intermediate in ferritin mineralization. *Biochemistry* **2002,** *41* (45), 13435-43.

71. Hwang, J.; Krebs, C.; Huynh, B. H.; Edmondson, D. E.; Theil, E. C.; Penner-Hahn, J. E., A short Fe-Fe distance in peroxodiferric ferritin: control of Fe substrate versus cofactor decay? *Science* **2000,** *287* (5450), 122-5.

72. Moenne-Loccoz, P.; Krebs, C.; Herlihy, K.; Edmondson, D. E.; Theil, E. C.; Huynh, B. H.; Loehr, T. M., The ferroxidase reaction of ferritin reveals a diferric mu-1,2 bridging peroxide intermediate in common with other O2-activating non-heme diiron proteins. *Biochemistry* **1999,** *38* (17), 5290-5.

73. Bou-Abdallah, F.; Yang, H.; Awomolo, A.; Cooper, B.; Woodhall, M. R.; Andrews, S. C.; Chasteen, N. D., Functionality of the three-site ferroxidase center of Escherichia coli bacterial ferritin (EcFtnA). *Biochemistry* **2014,** *53* (3), 483-95.

74. Velayudhan, J.; Castor, M.; Richardson, A.; Main-Hester, K. L.; Fang, F. C., The role of ferritins in the physiology of Salmonella enterica sv. Typhimurium: a unique role for ferritin B in iron-sulphur cluster repair and virulence. *Mol Microbiol* **2007,** *63* (5), 1495-507.

75. Potts, A. H.; Guo, Y.; Ahmer, B. M. M.; Romeo, T., Role of CsrA in stress responses and metabolism important for Salmonella virulence revealed by integrated transcriptomics. *PloS one* **2019,** *14* (1), e0211430.

76. Troxell, B.; Fink, R. C.; Porwollik, S.; McClelland, M.; Hassan, H. M., The Fur regulon in anaerobically grown Salmonella enterica sv. Typhimurium: identification of new Fur targets. *BMC Microbiol* **2011,** *11*, 236.

77. Raivio, T. L.; Silhavy, T. J., Periplasmic stress and ECF sigma factors. *Annu Rev Microbiol* **2001,** *55*, 591-624.

78. Price, N. L.; Raivio, T. L., Characterization of the Cpx regulon in Escherichia coli strain MC4100. *J Bacteriol* **2009,** *191* (6), 1798-815.

79. Zere, T. R.; Vakulskas, C. A.; Leng, Y.; Pannuri, A.; Potts, A. H.; Dias, R.; Tang, D.; Kolaczkowski, B.; Georgellis, D.; Ahmer, B. M.; Romeo, T., Genomic Targets and Features of BarA-UvrY (-SirA) Signal Transduction Systems. *PloS one* **2015,** *10* (12), e0145035.

80. Rivera-Chavez, F.; Baumler, A. J., The Pyromaniac Inside You: Salmonella Metabolism in the Host Gut. *Annu Rev Microbiol* **2015,** *69*, 31-48.

81. Schroder, I.; Johnson, E.; de Vries, S., Microbial ferric iron reductases. *FEMS Microbiol Rev* **2003,** *27* (2-3), 427-47.

82. Fontecave, M.; Coves, J.; Pierre, J. L., Ferric reductases or flavin reductases? *Biometals* **1994,** *7* (1), 3-8.

83. Miethke, M.; Hou, J.; Marahiel, M. A., The siderophore-interacting protein YqjH acts as a ferric reductase in different iron assimilation pathways of Escherichia coli. *Biochemistry* **2011,** *50* (50), 10951-64.

84. Wang, S.; Wu, Y.; Outten, F. W., Fur and the novel regulator YqjI control transcription of the ferric reductase gene yqjH in Escherichia coli. *J Bacteriol* **2011,** *193* (2), 563-74.

85. Blahut, M.; Dzul, S.; Wang, S.; Kandegedara, A.; Grossoehme, N. E.; Stemmler, T.; Outten, F. W., Conserved cysteine residues are necessary for nickel-induced allosteric regulation of the metalloregulatory protein YqjI (NfeR) in E. coli. *J Inorg Biochem* **2018,** *184*, 123-133.

86. Wang, S.; Blahut, M.; Wu, Y.; Philipkosky, K. E.; Outten, F. W., Communication between binding sites is required for YqjI regulation of target promoters within the yqjH-yqjI intergenic region. *J Bacteriol* **2014,** *196* (17), 3199-207.

87. Huet, G.; Castaing, J. P.; Fournier, D.; Daffe, M.; Saves, I., Protein splicing of SufB is crucial for the functionality of the Mycobacterium tuberculosis SUF machinery. *J Bacteriol* **2006,** *188* (9), 3412-4.

CHAPTER 2

DIRECT OBSERVATION OF INTERMEDIATES IN THE SUFS CYSTEINE DESULFURASE REACTION REVEALS FUNCTIONAL ROLES OF CONSERVED ACTIVE-SITE RESIDUES[1]

[1] This research was originally published in the Journal of Biological Chemistry. Blahut, M., Wise, C. E.; Dong, G.; Bruno, M.; Makris, T.; Frantom, P.; Dunkle, J.; Outten, F.W., Direct observation of intermediates in the SufS cysteine desulfurase reaction reveals functional roles of conserved active-site residues. *J Biol Chem* **2019,** *In press.*

Abstract

Iron–sulfur (Fe-S) clusters are necessary for the proper functioning of numerous metalloproteins. Fe-S cluster (Isc) and sulfur utilization factor (Suf) pathways are the key biosynthetic routes responsible for generating these Fe-S cluster prosthetic groups in *Escherichia coli*. Whereas Isc dominates under normal conditions, Suf takes over during periods of iron depletion and oxidative stress. Sulfur acquisition via these systems relies on the ability to remove sulfur from free cysteine using a cysteine desulfurase mechanism. In the Suf pathway, the dimeric SufS protein uses the cofactor pyridoxal-5'-phosphate (PLP) to abstract sulfur from free cysteine, resulting in the production of alanine and persulfide. Despite much progress, the stepwise mechanism by which this PLP-dependent enzyme operates remains unclear. Here, using rapid-mixing kinetics in conjunction with X-ray crystallography, we analyzed the pre-steady state kinetics of this process while assigning early intermediates of the mechanism. We employed H123A and C364A SufS variants to trap Cys-aldimine and Cys-ketimine intermediates of the cysteine desulfurase reaction, enabling direct observations of these intermediates and associated conformational changes of the SufS active site. Of note, we propose that Cys-364 is essential for positioning the Cys-aldimine for Cα deprotonation, His-123 acts to protonate the Ala-eneamine intermediate, and Arg-56 facilitates catalysis by hydrogen bonding with the sulfhydryl of Cys-aldimine. Our results, along with previous SufS structural findings, suggest a detailed model of the SufS-catalyzed reaction from Cys binding to C–S bond formation and indicate that Arg-56, His-123, and Cys-364 are critical SufS residues in this C–S bond cleavage pathway.

Introduction

Iron-sulfur (Fe-S) clusters perform vital functions in a myriad of reactions including electron transfer, amino acid biosynthesis, and central carbon metabolism.[2, 3] Despite their significance, a number of questions still remain regarding the mechanism through which Fe-S clusters are generated. To avoid the inherent toxicity of sulfide and labile iron, most organisms use a carefully orchestrated in vivo Fe-S cluster biogenesis pathway controlled by protein-protein interactions. Production of these important clusters in *Escherichia coli* occurs via two major pathways, Isc and Suf.[4] While Isc directs Fe-S generation under normal conditions, Suf dominates in environments of oxidative stress and iron starvation.[5-8]

Encoded by the *suf* operon, the Suf system in *E. coli* consists of six proteins responsible for the biogenesis and transfer of Fe-S clusters to the apo form of target Fe-S metalloproteins. The pyridoxal 5'-phosphate (PLP)-dependent homodimeric SufS enzyme provides the sulfide component of the Fe-S cluster.[9] SufS belongs to a family of cysteine desulfurases responsible for liberating sulfur from free cysteine resulting in an enzyme-bound S-sulfanylcysteine species (often referred to as a persulfide). The desulfurase activity is usually coupled via a ping-pong mechanism to a second transpersulfuration step where the persulfide species is transferred from the active site cysteine residue to acceptor proteins or metabolites.[10, 11]

The cysteine desulfurase enzymes are divided into two separate groups depending on their structures and reactivity.[12] Type I desulfurases have high basal activity and an extended and flexible active site loop. Type II desulfurase family members conversely have diminished basal activity along with a shortened active site anchor that limits

structural flexibility and solvent access to the persulfide intermediate after the desulfurase reaction.[13, 14] Type II enzymes often interact with a partner protein that enhances their activity by specifically accepting the persulfide from the enzyme in a transpersulfuration reaction that completes the entire ping-pong reaction.[15] For example, the *E. coli* type II enzyme SufS requires acceptor protein SufE to remove the persulfide from SufS active site Cys-364 to allow turnover.[16, 17] Transpersulfuration from SufS Cys-364 to SufE Cys-51 is carried out via a thiol exchange mechanism when the two proteins interact. SufE, carrying the S-sulfanylcysteine species, will then transfer the persulfide to the $SufBC_2D$ scaffold complex to be reduced to sulfide and incorporated into nascent Fe-S cluster.[18]

A proposed chemical mechanism for SufS, based on other characterized cysteine desulfurase enzymes, is shown in Scheme 2.1.[19-21] Resting SufS contains PLP bound to Lys-226 in an internal aldimine (Schiff base) conformation (**1**).[11] As shown in Scheme 2.1, upon L-cysteine substrate binding, a *gem*-diamine intermediate is formed (**2**) followed by formation of the Cys-aldimine (**3**) (sometimes referred to as the external aldimine). The Cys-aldimine converts to a short-lived Cys-quinonoid intermediate (**4**) followed by a Cys-ketimine (**5**). The desulfurase step occurs as Cys-364 carries out a nucleophilic attack on the substrate sulfur, converting the Cys-ketimine into the Ala-eneamine and forming a persulfide on Cys-364 (**6**). Mutation of active site Cys-364 to alanine results in the elimination of cysteine desulfurase activity.[22] The alanine product is ultimately released and the internal aldimine regenerated between PLP and Lys-226 (**6-10**). As the detailed mechanism demonstrates, there are several important acid-base catalysis steps involved in the desulfurase reaction, including the deprotonation of C_α on the cysteine substrate, deprotonation of Cys-364 to generate the nucleophilic thiolate

Scheme 2.1.

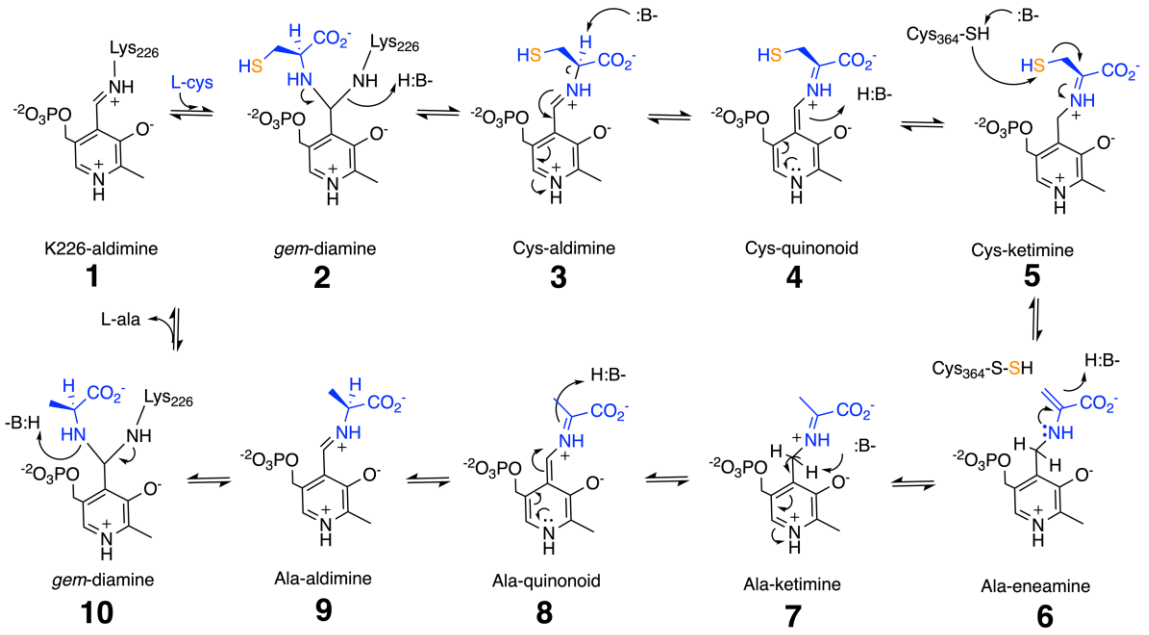

Scheme 2.1. General cysteine desulfurase reaction scheme for SufS prior to this study. L-cysteine substrate is shown in blue (C, H, O, N) and orange (S). PLP and SufS active site residues are in black.

anion, protonation of the Cys-quinonoid C4' to facilitate formation of the Cys-ketimine, and protonation of the Ala-eneamine following C-S bond breakage (Scheme 2.1).

The exact active site residues that carry out these acid-base catalyst steps are presently unknown. Multiple sequence aligments indicate His-123 is a highly conserved residue in the active site that could potentially be involved in proton transfer during SufS cysteine desulfurase activity (Figure 2.1A). Wild-type (WT) SufS crystal structures indicate His-123 forms a π-π stacking interaction with the PLP aromatic group and is optimally located to function as a acid-base catalyst during the desulfurase reaction (Figure 2.1B).[23] Based on the these observations, it was previously proposed to play such a role.[19]

Recent structural characterization by Dunkle et al. focused on conformational changes thought to be associated with transpersulfuration.[24] The new structures reported here investigate the mechanism of the desulfurase reaction. Here, we have mutated His-123 and Cys-364 to alanine and performed a detailed analysis of WT, C364A, and H123A SufS enzymes using UV-visible absorption spectroscopy, transient kinetics via stopped-flow spectroscopy, and X-ray crystallography. The two active site mutants assisted in trapping Cys-aldimine and Cys-ketimine intermediates of the cysteine desulfurase reaction. As a result, the mutants facilitated the direct structural observation of these two reaction intermediates and associated conformational changes to the SufS active site. Emerging from the analysis is a rich picture of the functional roles of several amino acids conserved across the SufS family including the unanticipated, essential role of Cys-364 in positioning the Cys-aldimine for C_α deprotonation, and the essential role of His-123 in protonating the ala-eneamine intermediate.

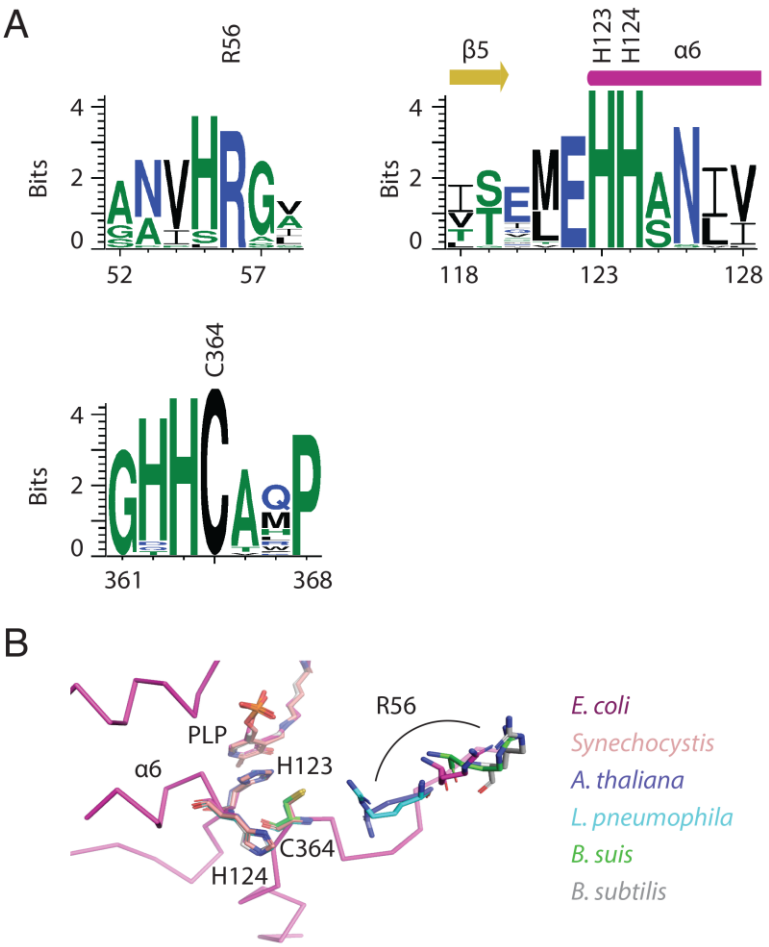

Figure 2.1. (A) A sequence logo indicates active site residues of interest that are highly conserved across SufS proteins. The sequence alignment was made from 29 members of the InterPro SufS family (IPR010970) chosen from distinct nodes of a sequence similarity network to model sequence diversity in the family. (B) A structural superposition of six SufS family members from the PDB reveals that several residues, such as His-123 and His-124, adopt an identical position in all structures, while the location of Arg-56 (indicated by an arc) varies.

Materials and Methods

Strains and plasmid preparation

SufS, SufS mutants, and SufE were all expressed using the pET21a vector (Novagen) as previously described.[10] SufS H123A and SufS C364A mutations were constructed following the QuikChange II site-directed mutagenesis protocol (Agilent) with mutations confirmed via sequencing. Each plasmid was transformed into BL21(DE3) *E. coli* cells for expression and purification. All primers and strains are defined in Tables 2.1 and 2.2 respectively.

Protein expression and purification

SufS, SufS mutant derivatives, and SufE were expressed in the pET21a vector using BL21(DE3) *E. coli*cells. Cells grown overnight in LB with 100 µg/ml ampicillin at 37 ˚C were diluted by 1:100 into fresh LB with ampicillin and incubated with shaking at 200 rpm to reach an OD_{600} of 0.5 – 0.7. For SufS expression, cells were induced with 500 µM isopropyl β-D-1-thiogalactopyranoside (IPTG) at 18 ˚C for 24 hours with shaking at 200 rpm. Cells were harvested via centrifugation at 7460 xg for 10 min at 4 ˚C and stored at -80 ˚C until use. These cells were then resuspended in the Q-Sepharose loading buffer consisting of 25 mM Tris-HCl, pH 8.0, 10 mM β-mercaptoethanol (βME), and 1 mM phenylmethylsulfonyl flouride. For lysis, two 2-min cycles of sonication at 50% amplitude of 1 s on and 2 s off were performed using a Branson digital sonifier 450. 1% streptomycin sulfate was then added to the lysed cells followed by centrifugation at 31000 xg for 35min. SufS and SufS mutants were purified with anion exchange (Q-Sepharose), hydrophobic interaction (Phenyl FF) and gel filtration (Superdex 200) (GE

Table 2.1. Primer sequences for plasmid construction of *pET21a_sufS* and *pET21a_sufE* and for site-directed mutagenesis[2] to construct *pET21a_SufS H123A* and *pET21a_SufS C364A*.

Protein	Primer Sequence
SufS	5'-GAGGGGATCCATGATTTTTTCCGTCGACAA-3' 5'-TGCCCTCGAGTTATCCCAGCAAACGGTGAA-3'
SufE	5'-AGGCCATATGGCTTTATTGCCGGATAA-3' 5'-TCCTGGATCCTTAGCTAAGTGCAGCGGCTT-3'
SufS H123A	5'-CATCAGTCAGATGGAGGCCCACGCTAACATTGTTC-3' 5'-GAACAATGTTAGCGTGGGCCTCCATCTGACTGATG-3'
SufS C364A	5'-CGTACCGGACATCACGCCGCAATGCCATTGATG-3' 5'-CATCAATGGCATTGCGGCGTGATGTCCGGTACG-3'

[2] codons mutated from WT sequence are underlined in the table

Table 2.2. Strains used in this study for storage and expression of proteins[3]

Strain Name	Genotype/characteristics	Source or Reference
BL21(DE3)	*ompT gal dcm lon hsdS$_B$*($r_B^- m_B^-$) λ(DE3 [*lacI lacUV5-T7p07 ind1 sam7 nin5*]) [*malB*$^+$]$_{K\text{-}12}$(λ^S)	Laboratory Strain
DH5α	*endA1 glnV44 thi-1 recA1 relA1 gyrA96 deoR nupG purB20* φ80d*lacZ*ΔM15 Δ(*lacZYA-argF*)U169, hsdR17($r_K^- m_K^+$), λ$^-$	Laboratory Strain
MB153	DH5α pET21a_sufS Amp^R	37
MB154	DH5α pET21a_sufS(H123A) Amp^R	This Study
MB155	DH5α pET21a_sufS(C364A) Amp^R	This Study
MB156	DH5α pET21a_sufE Amp^R	37
MB157	BL21(DE3) pET21a_sufS Amp^R	37
MB158	BL21(DE3) pET21a_sufS(H123A) Amp^R	This Study
MB159	BL21(DE3) pET21a_sufS(C364A) Amp^R	This Study
MB160	BL21(DE3) pET21a_sufE Amp^R	37

[3] Ampicillin resistance (Amp^R)

Healthcare) chromatography resins in sequence. The Q-sepharose column used a linear gradient from 25 mM Tris-HCl, pH 8.0, 10 mM βME to 25 mM Tris-HCl, pH 8.0, 1 M NaCl, 10 mM βME. For the phenyl FF column, SufS was eluted using a linear gradient from 25 mM Tris-HCl, pH 8.0, 100 mM NaCl, 1 M ammonium sulfate, 10 mM βME to 25 mM Tris-HCl, pH 8.0, 10 mM βME. The Superdex200 column was run with 25 mM Tris-HCl, pH 8.0, 150 mM NaCl, 10 mM βME. Final protein purity was evaluated using SDS-PAGE and the protein was concentrated via a 10 kDa molecular weight Amicon Ultra concentration filter (Millipore). Purified SufS was frozen in liquid nitrogen and stored at – 80 ˚C until further use.

SufE expression was performed using a similar protocol as SufS with a few modifications. For SufE, cells were induced with 500 µM IPTG at 37 ˚C for 3 hours with shaking at 200 rpm. SufE purification used anion exchange and gel filtration chromatography for purification. The buffers were the same as those used for SufS purification.

PLP quantification

In order to determine PLP content of SufS, SufS was diluted to ~1.5 mg/ml as part of an 800 µl sample using 10 mM Tris, pH = 8.0 buffer. 200 µl of 5 M NaOH was added to the protein and incubated for 10 min at 75 ˚C. 85 µl of 12 M HCl was then added to the sample. Denatured SufS protein was removed by centrifugation at 16000 xg for 2 min. The supernatant containing released PLP was transferred to a cuvette. The absorbance at 390 nm was measured with the resulting value compared to a free PLP

quantification standard line to determine the amount of PLP present. PLP occupancy per monomer of SufS was then calculated based on molar ratios of PLP:SufS monomer.

Cysteine desulfurase activity assay

SufS cysteine desulfurase activity was determined by following the protocol used by Dai *et al*.[10] For reactions involving SufS and SufE, concentrations of 0.5 μM and 2.0 μM were used respectively. With SufS or SufS mutants alone, the selected concentration was either 0.5 μM or 20 μM. The reaction was performed at room temperature for 10 min.

UV-visible absorption spectroscopy

Using an Agilent 8453 UV-Visible absorption spectrophotometer, both spectra and kinetics were monitored for extended time periods. 30 μM of WT, H123A, or C364A SufS was treated with 500 μM cysteine in the presence of 2 mM TCEP in buffer (25 mM Tris, 150 mM NaCl, pH = 7.4). Initial scans were measured 10 s after mixing with final scans occurring at 150 min.

Stopped-flow absorption spectroscopic analysis

Stopped-flow absorption experiments were performed at 4 °C on an Applied Photophysics Ltd. SX20 stopped-flow spectrophotometer equipped with an anaerobic accessory using either a PDA or PMT. L-cysteine was prepared anaerobically in anoxic 25 mM Tris, 150 mM NaCl at pH 8.0 (at 4 ˚C) within a crimped vial to remain anaerobic. WT-SufS (or variant) was diluted at 4 °C to 75 μM using 25 mM Tris, 150 mM NaCl, pH

= 8.0. Concentrations of cysteine ranging from 800 µM to 3 mM (pre-mix) were mixed 1:1 with 75 µM SufS for a post-mix SufS concentration of 37.5 µM. Full spectral (PDA) or single wavelength (PMT) data was collected out to 5 to 20 s, depending on cysteine concentration. Data was then fit to a double exponential model using Pro Data Viewer version 4.2.18 (APP). (Figures 2.2-2.4).

Global analysis and singular value decomposition

PDA data was analyzed using SVD with Pro-KIV global analysis software (APP). SVD fitting for H123A showed two nonzero singular values corresponding to two transitions between three spectrally distinct species. In order to process the data, the following model was used in which k_1' characterizes a pseudo-first-order rate constant during which L-cysteine concentrations are in large excess compared to the enzyme.

$$\text{SufS-PLP} + \text{L-Cys} \xrightarrow{k'_1} \text{Int-1} \xrightarrow{k_2} \text{Int-2}$$

For the above model, initial rates for input were determined via single-wavelength kinetics using the PMT. The final rate constants calculated by global analysis demonstrated favorable agreement with these PMT values.

X-ray crystallography

Crystallization of SufS wild-type was performed by mixing 1 µl protein at ~ 10 mg/ml with 2 µL of 4.3 M NaCl and 0.1 M MES pH 6.5 followed by incubation at 20 °C in sitting drop vapor diffusion trays.[25] Crystallization of SufS H123A was performed by mixing 1 µl protein at 12 mg/ml with 2 µl 4.3 M NaCl and 0.1 M MES pH 6.5 (PLP bound structure) or 2 µL 4.0 M NaCl and 0.1 M MES pH 6.5 (Cys-ketimine structure). In

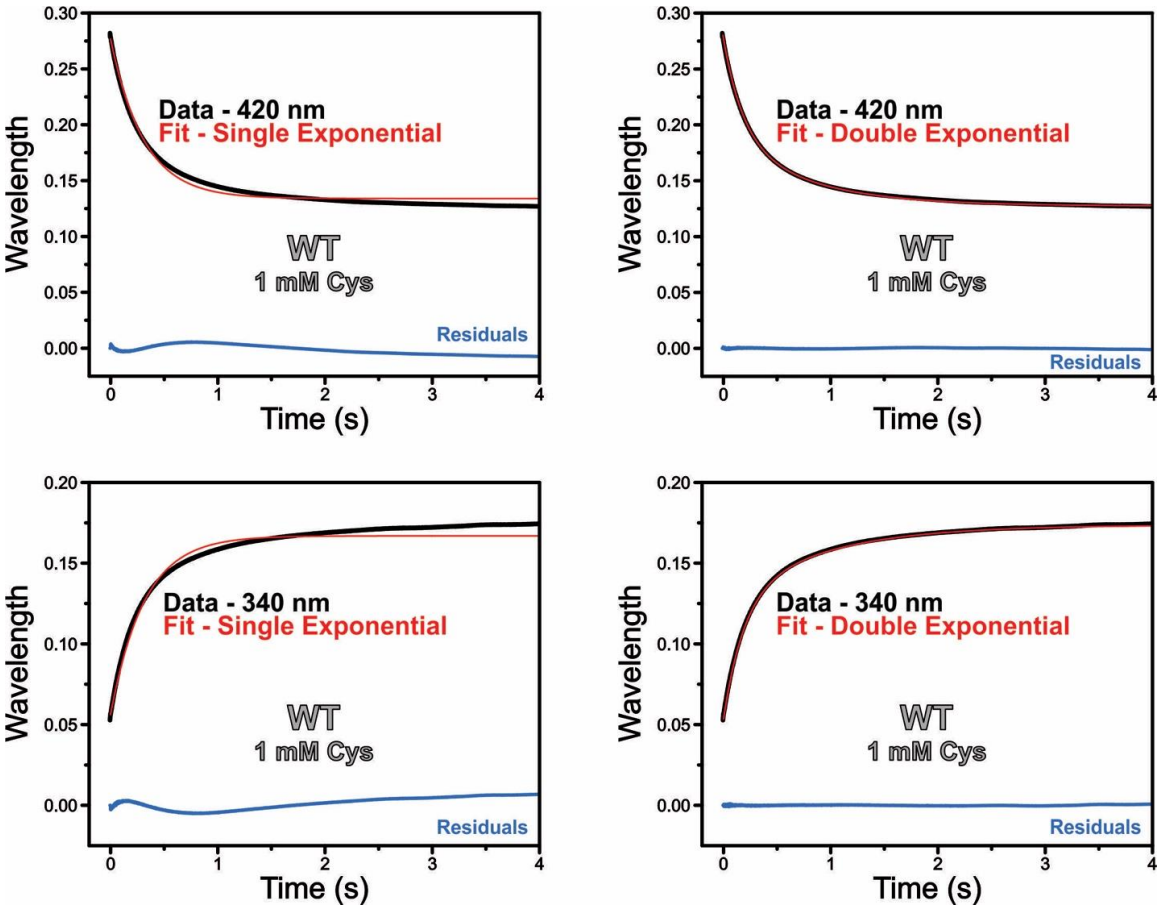

Figure 2.2. Residuals and fits of UV-visible absorption data collected by PMT from 37.5 μM WT SufS (post-mix) mixed with 1 mM of L-cysteine at 4 °C using single or double exponential functions. Black line is the raw data, red line is the fit for one of the models, and blue line shows the residuals for each fit.

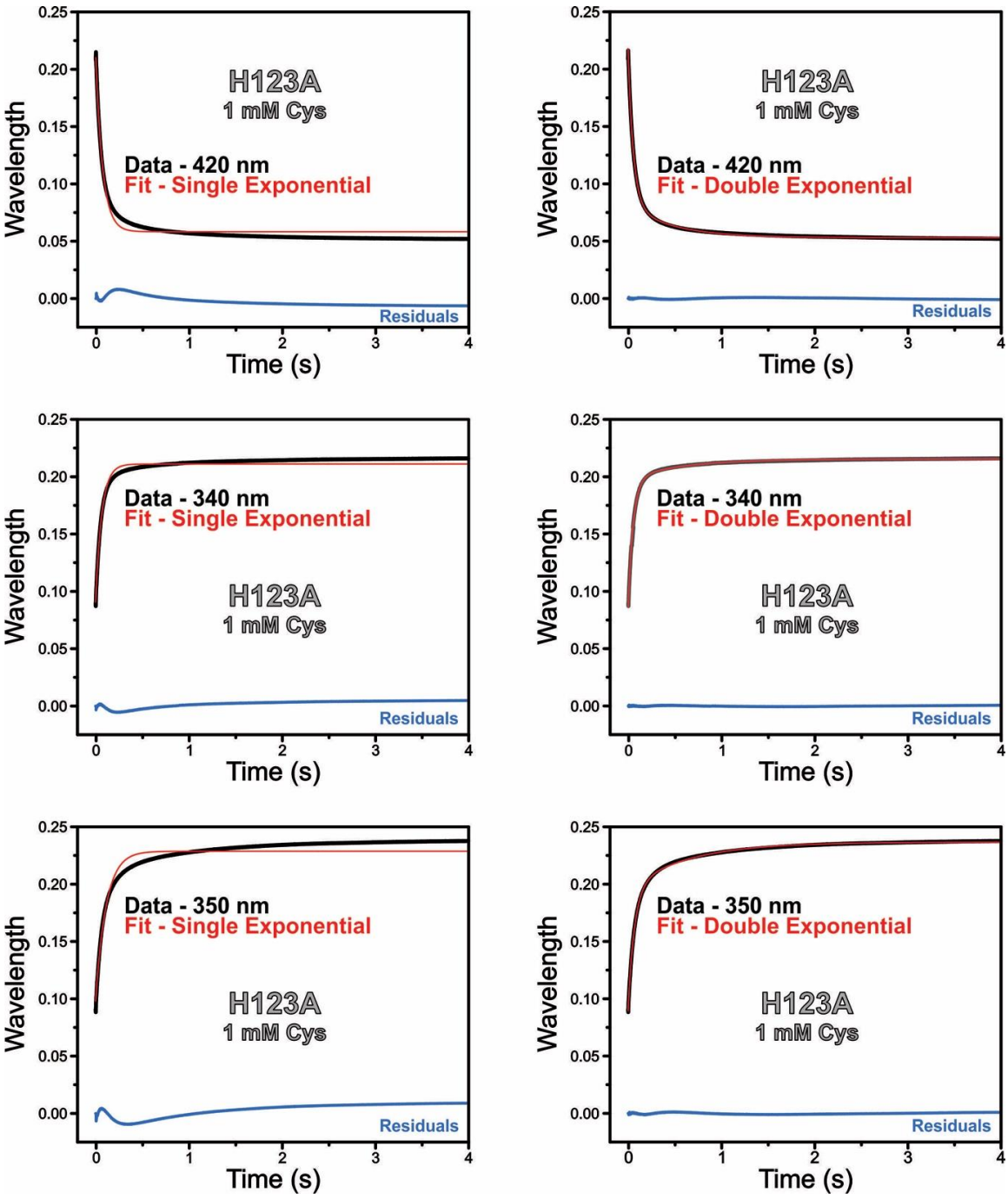

Figure 2.3. Residuals and fits of UV-visible absorption data collected by PMT from 37.5 μM H123A SufS (post-mix) mixed with 1 mM of L-cysteine at 4 °C using single or double exponential functions. Black line is the raw data, red line is the fit for one of the models, and blue line shows the residuals for each fit.

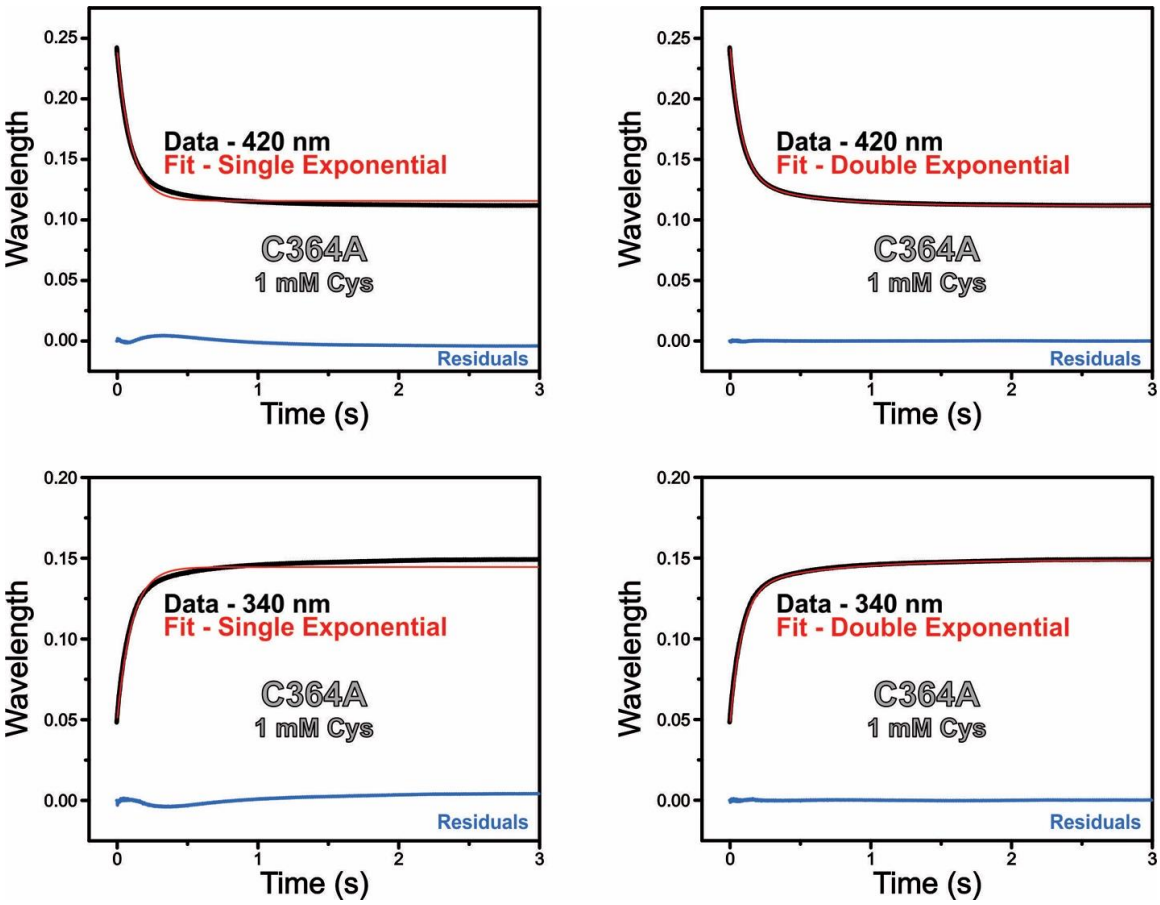

Figure 2.4. Residuals and fits of UV-visible absorption data collected by PMT from 37.5 μM WT SufS (post-mix) mixed with 1 mM of L-cysteine at 4 °C using single or double exponential functions. Black line is the raw data, red line is the fit for one of the models, and blue line shows the residuals for each fit.

both cases incubation at 20 °C in sitting drop vapor diffusion trays occurred. Crystals typically formed in less than 7 days. To obtain the structure of SufS H123A in the absence of substrate, H123A crystals were incubated in mother liquor diluted 1:1 with 100% v/v glycerol followed by plunge freezing in liquid N_2. To obtain the structures of SufS wild-type and SufS His-123 following L-cysteine addition, crystals were incubated in mother liquor plus 10 mM L-cysteine diluted 1:1 with 100% v/v glycerol. The crystals were plunge frozen in liquid N_2 following 5-30 min incubation with L-cysteine.

Crystallization of SufS C364A was performed by mixing 1 µl of 14 mg/ml protein with 2 µL of crystallization conditions (20 – 30 % w/v PEG 3350, 0.1 M Tris-HCl pH 7, 0.2 M $MgCl_2$) followed by incubation at 20 °C in sitting drop vapor diffusion trays. Addition of L-cysteine to SufS C364A was accomplished by incubating the crystals in mother liquor plus 50 mM L-cysteine diluted 1:1 with 100 % v/v glycerol. The crystals were incubated -20 °C for 30 min, warmed to 37 °C for 30 min then allowed to return to room temperature before plunge freezing in liquid N_2. Structures were solved using crystals with and without the temperature cycling step revealing it is not required to obtain the Cys-aldimine intermediate, but the best diffracting crystals underwent temperature cycling.

Native X-ray diffraction data was collected at the Advanced Photon Source beamline 22-ID, outfitted with an Eiger 16M detector, using 0.5° oscillations and a 1.000 Å wavelength. Anomalous X-ray diffraction data was collected at 22-ID using 1.74 Å wavelength X-rays.

Reflections were integrated and merged using X-ray Detector Software (XDS). Structure solution was carried out by molecular replacement in the PHENIX software

suite using 1jf9 with all heteroatoms removed as the search model.[25] Phenix.refine was used to improve the initial structure solutions and generate the unbiased $F_o - F_c$ maps indicating ligand electron density. Initial coordinates and refinement restraints for PLP linked to Cys-aldimine or Cys-ketimine were generated by phenix.elbow and the models were improved by iterative cycles of manual modeling in Coot coupled with phenix.refine. Occupancy refinement of PLP Cys-aldimine and PLP Cys-ketimine was performed once the final model was obtained and atomic displacement parameters (B-factors) refinement had converged. Anomalous maps were calculated using phenix.maps with phases derived from coordinates without ligands.

Figures were generated with Pymol. Superpositions were performed by aligning one SufS monomer to the SufS variant monomer with the Pymol align command. Data collection and refinement statistics can be found in Table 2.3.

Sequence conservation analysis

A sequence similarity network was constructed from 18,567 sequences of the SufS Interpro family IPR010970 as previously described.[24] Briefly, sequences with an alignment score of 45 or better were binned to create 1011 nodes. Of these nodes, 29 composed of > 100 sequences were chosen for further analysis. One representative sequence was chosen from the 29 nodes with preference given to Swiss-Prot reviewed entries.

The representative sequences were aligned with MUltiple Sequence Comparison by Log-Expectation (MUSCLE) and the resulting alignment was used to estimate the conservation of SufS residues.[26]

Table 2.3. Data collection and refinement statistics.

	WT Cys soak	C364A Cys-ald		H123A	H123A Cys-ket	
	6O10	**6O11**		**6O12**	**6O13**	
	Native	Native	Anomalous	Native	Native	Anomalous
Data collection	APS 22-ID	APS 22-ID	APS 22-ID	APS 22-ID	APS 22-ID	APS 22-ID
Space group	$P4_32_12$	$P4_22_12$	$P4_22_12$	$P4_32_12$	$P4_32_12$	$P4_32_12$
Cell dimensions						
a, *b*, *c* (Å)	126.40, 126.40, 133.68	126.42, 126.42, 67.08	126.58, 126.58, 67.12	127.28, 127.28, 134.16	126.01, 126.01, 137.21	126.02, 126.02, 137.00
α, β, γ (°)	90, 90, 90	90, 90, 90	90, 90, 90	90, 90, 90	90, 90, 90	90, 90, 90
Wavelength	1.000	1.000	1.740	1.000	1.000	1.740
Resolution (Å)[a]	44.69-2.00 (2.07-2.00)	35.69-1.84 (1.90-1.84)	89.50-3.90 (4.00-3.90)	43.40-2.05 (2.12-2.05)	44.55-2.20 (2.28-2.20)	92.75-3.20 (3.28-3.20)
R_{meas} (%)	11.3(421.1)	8.5(200.0)	5.1(6.6)	17.5(282.2)	11.7(211.9)	13.3(41.0)
I/σI	17.26(0.84)	15.51(0.76)	43.68(36.39)	15.92(0.68)	12.71(1.14)	16.33(7.21)
Completeness (%)	99.9(99.8)	97.9(83.8)	99.9(100.0)	99.2(95.0)	99.9(99.5)	100.0(100.0)
Redundancy	26.7 (24.9)	11.8 (6.7)	12.2 (12.6)	6.7 (6.0)	14.8 (15.0)	13.8(15.4)
$CC_{1/2}$ (%)	99.9 (36.7)	99.9 (49.6)	99.9 (99.9)	99.1(45.7)	99.8(61.0)	99.7(97.7)
Refinement						
Resolution (Å)	44.69 - 2.00 (2.07 - 2.00)	35.69 - 1.84 (1.90 - 1.84)		43.40 - 2.05 (2.12 - 2.05)	44.55 - 2.20 (2.28 - 2.20)	
No. reflections	73439 (7236)	46697 (3927)		68944 (6521)	56320 (5508)	
R_{work}/R_{free} (%)	18.24(31.42)/ 20.39(35.81)	18.38(34.21)/ 21.62(36.07)		19.45(35.09)/ 21.59(37.08)	18.73(35.23)/ 19.86(36.14)	
No. atoms	3308	3245		3216	3234	
Protein	3119	3126		3114	3122	
Ligand	16	23		16	23	
Water	173	96		86	89	
B factors						
Protein	53.66	48.81		39.56	65.59	
Ligand	45.88	40.21		42.20	62.66	
Water	58.38	49.43		39.52	67.26	
R.m.s deviations						
Bond lengths (Å)	0.007	0.006		0.008	0.007	
Bond angles (°)	0.92	0.81		0.85	0.92	

Results

A metastable substrate-PLP intermediate in the reaction of SufS H123A with cysteine.

During and after purification of WT and C364A SufS, a PLP absorption feature at ~422 nm is observed (Figure 2.5A and data not shown). The 422 nm feature is assigned as the Lys-226-PLP internal aldimine. In contrast, after the first anion exchange step of purification, the SufS H123A fractions showed a more complex spectrum consisting of two absorption maxima at 418 nm and 350 nm (Figure 2.5A). As the purification proceeds through additional chromatographic steps, the 350 nm absorption feature in SufS H123A is gradually lost (Figure 2.5B). This feature at 350 nm will be further elaborated on below. The final PLP absorbance after purification of SufS H123A shows a slight decrease in extinction coefficient along with a subtle blue shift to around 418 nm, compared to 422 nm observed in WT SufS. WT and the mutant forms of SufS were all confirmed to have greater than 95% PLP occupancy following purification (see Materials and Methods for details).

To test if the H123A mutation alters the ability of the mutant SufS to complete the first half of the ping-pong reaction, persulfide production by WT, C364A, and H123A enzymes was measured (Table 2.4). Due to the lack of the active site thiolate anion, the C364A mutant of SufS should not be able to form persulfide. The results in Table 2.4 show that both the H123A and C364A mutations abolish the ability of SufS to generate persulfide from L-cysteine. The addition of the SufE partner protein had no effect on the activity of either mutant SufS protein (Table 2.4). In contrast, WT SufS, in the absence of SufE, carries out a single turnover reaction producing one equivalent of persulfide. Under

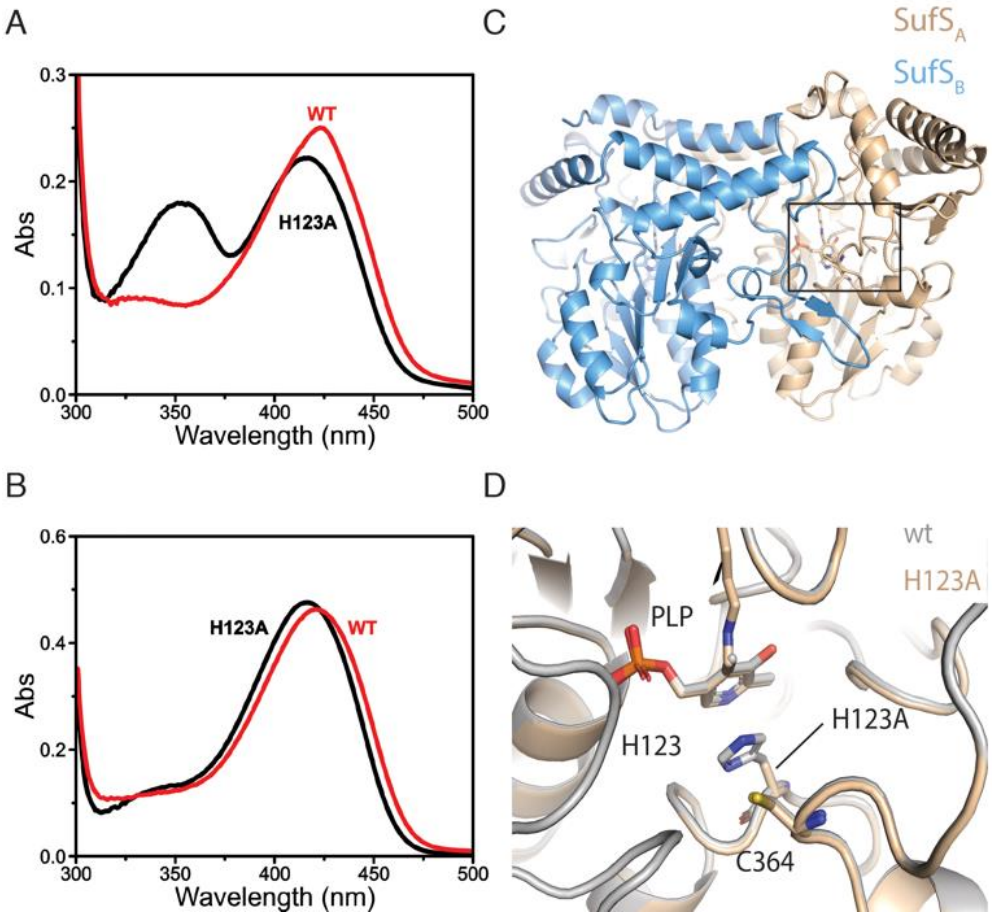

Figure 2.5. (A) UV-visible absorption spectra for fractions containing WT or H123A SufS from initial purification step using an anion exchange column. (B) UV-visible absorption spectra for fractions containing WT or H123A SufS from second purification step using a hydrophobic interaction column. Presence of SufS was confirmed in all fractions by SDS-PAGE. (C) An image of the SufS homodimer including a box denoting the active site region shown below. (D) A superposition of WT SufS and SufS H123A reveals that the mutation does not affect the position of other critical active site components such as PLP or Cys-364.

Table 2.4: Cysteine desulfurase activity for SufS and its mutant derivatives[1]

SufS	μM Persulfide generated per μM SufS	μM Persulfide generated per μM SufS + SufE[2]
WT	1.10 ± 0.06	16.1 ± 1.2
H123A	0.09 ± 0.01	0
C364A	0.07 ± 0.02	0

[1] Desulfurase assays were performed in triplicate. Error shown (±) indicates one standard deviation above and below the average.
[2] 1 μM of SufS with 4 μM of SufE

these conditions, using DTT as the reductant, SufS stops upon completion of the first half of the ping-pong reaction because the persulfide species is resistant to reduction by DTT. When SufE is added to WT SufS, it removes the SufS persulfide as part of the transpersulfuration reaction. The SufE persulfide is accessible to DTT and is reduced to sulfide under these conditions, allowing SufE to perform additional cycles of transpersulfuration.[11] These results suggest the substrate-PLP intermediate trapped in the SufS H123A mutant has not yet been desulfurated.

The crystal structure was solved for SufS H123A and the resulting $F_o - F_c$ difference electron density maps indicated the presence of PLP in agreement with the chemical analysis. A superposition of the mutant homodimer with the WT SufS homodimer revealed that the two structures were near identical with an RMSD of 0.159 Å (Figure 2.5C,D). This result suggests that the unusual spectral characteristics of PLP within SufS H123A observed during purification were due to the loss of the π-π stacking or H-bonding interactions from His-123 rather than long-range structural changes in or around the active site.

It was previously shown that upon binding to L-cysteine, the PLP absorption spectrum in WT SufS shows a decrease in the 422 nm signal and the appearance of a feature at 340 nm.[14] In order to better define the altered optical features noted during purification of the SufS H123A variant, UV-visible absorption spectra were taken before and after the addition of varying concentrations of the L-cysteine substrate (Figures 2.6 and 2.7). Immediately after the addition of 500 μM cysteine to WT SufS, decrease of the internal aldimine peak at 422 nm was observed along with a subtle red shift of that feature to 424 nm (Figure 2.7A). These changes coincided with a concomitant increase

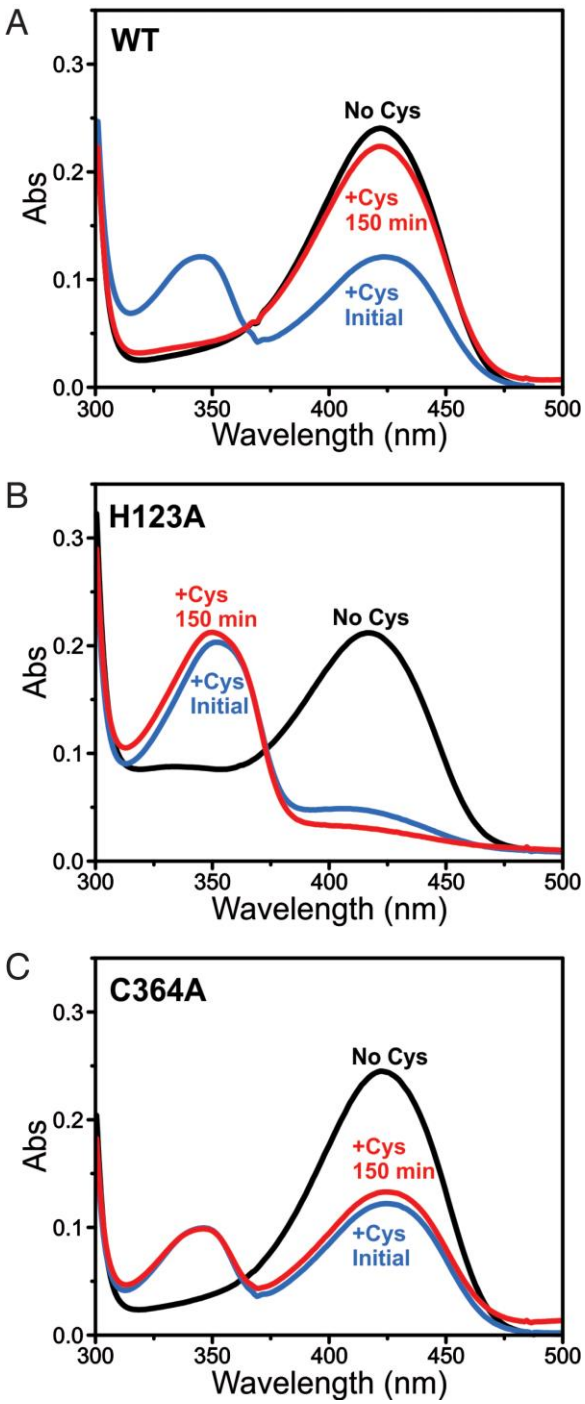

Figure 2.6. UV-visible absorption spectra during 150-min treatment with 500 µM L-cysteine for (A) WT, (B) H123A, and (C) C364A SufS.

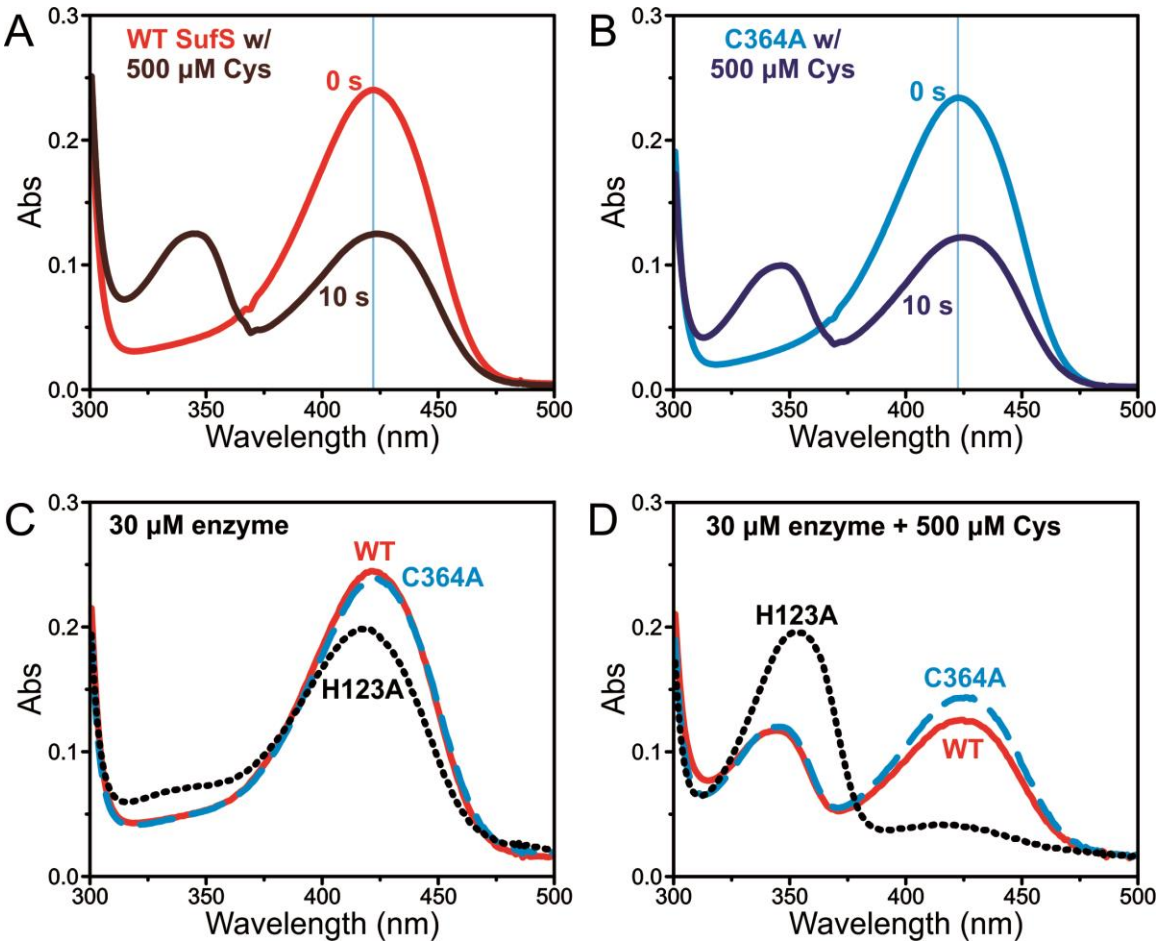

Figure 2.7. UV-visible absorption spectra for purified (A) wild-type SufS and (B) C364A SufS before and approximately 10 seconds after the addition of 500 µM L-cysteine in the presence of 2 mM TCEP. Additionally, UV-visible absorption spectra comparing purified (C) wild-type, H123A, and C364A SufS in the absence of cysteine or (D) after the addition of 500 µM cysteine. Blue line shows the initial absorption maxima at 422 nm prior to L-cysteine addition in (A) and (B).

of the feature at 343 nm (Figure 2.6A). Following the completion of the desulfurase reaction after the consumption of cysteine (~150 min after 500 μM cysteine is added), the internal aldimine at 422 nm is restored (Figure 2.6A).

The optical changes observed in steady-state reactions of the SufS mutants were distinctly altered from WT SufS. As noted above, prior to L-cysteine addition, the spectrum of purified H123A SufS is characterized by a single major absorption feature at 418 nm. Upon the addition of excess cysteine, H123A shows a greater accumulation of a species at the same 350 nm feature that is observed during purification (Figures 2.5A and 2.6B). In contrast to WT or C364A SufS, relatively little signal is observed in the 420 nm region. Based on the observation that the addition of L-cysteine can reproduce the 350 nm species, we tentatively assign this feature to a substrate-PLP intermediate that is captured by the H123A mutation. This 350 nm species is stable as it is still present 150 min after L-cysteine addition (Figure 2.6B), which is in agreement with the results presented in Figure 2.5. Kinetic monitoring of the peak at 350 nm over time did not show any reversibility of this feature over the 150 min (data not shown).

Upon the addition of excess L-cysteine to C364A SufS, the resting state 422 nm peak is partially converted to a species with absorbances at 343 nm and 424 nm similar to the spectrum obtained for WT SufS (Figure 2.7B and Figure 2.6C). However, unlike WT SufS, C364A did not revert back to the resting state at 422 nm, even out to 150 min. These results suggest that the H123A and C364A mutations can trap different PLP-substrate intermediates.

Pre-steady state stopped-flow kinetic analysis of WT and mutant SufS reaction intermediates.

Standard cysteine desulfurase assays measure the persulfide or alanine products of the first half of the ping-pong reaction and neither approach can be used to analyze individual reaction steps prior to L-cysteine desulfuration. Therefore, stopped-flow UV-visible absorption spectroscopy in both photodiode array (PDA) and photomultiplier tube (PMT) modes was used to analyze the progression of reaction intermediates upon mixing of L-cysteine with SufS and its mutants. WT, H123A, or C364A SufS was rapidly mixed with varying concentrations of anoxic L-cysteine at 4 °C. Initial examination of the WT SufS reaction via stopped-flow absorption spectroscopy using the PDA detector revealed a concerted shift from 422 nm to the 343 and 424 nm species with a clear isosbestic point for the transitions (Figure 2.8A). Fitting the changes in 343 nm and 422 nm absorbances over time measured by the PMT detector required a two-summed exponential equation for each wavelength, representing two kinetically distinguishable steps involved in formation of the 343 nm species (see Experimental Procedures). (Figure 2.8B, Table 2.5). The two phases are split between an initial, cysteine dependent fast phase and a cysteine independent slow phase. A zero-intercept for the former fast phase suggests an essentially irreversible binding of cysteine to the PLP cofactor (k_1 = 5.1 mM^{-1} s^{-1}) followed by a slower step (k_2 = 1.4 s^{-1}) (Figure 2.8C, Table 2.5).

The general absorption changes of the C364A SufS mutant (transition from 422 to 343 and 424 nm with a clear isosbestic point) are highly similar to those observed in WT SufS (Figures 2.8A and 2.9). The derived kinetic rate constants (k_1 = 11 mM^{-1} s^{-1}, k_2 = 1.6 s^{-1}) also are similar to that of the WT enzyme (Table 2.5). These similarities indicate

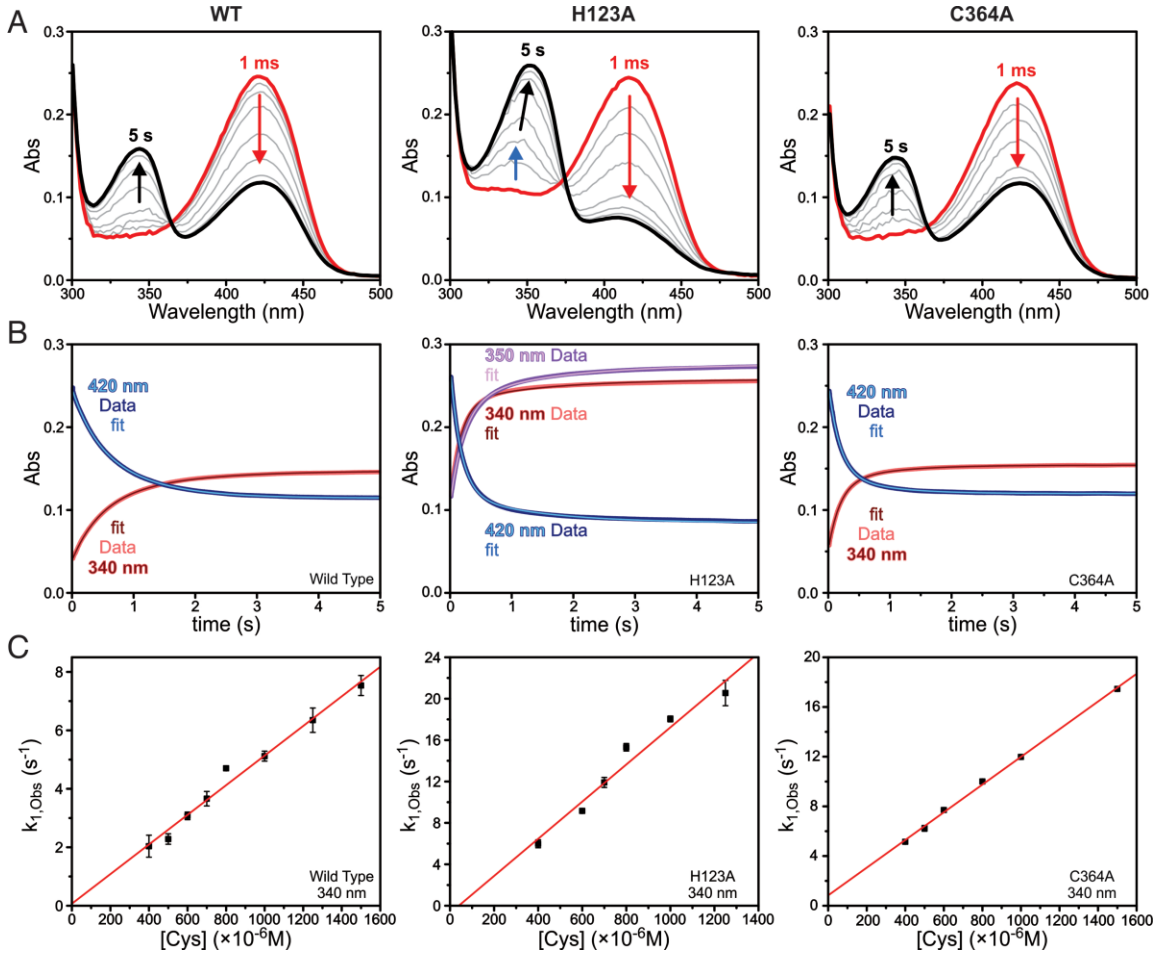

Figure 2.8. Stopped flow analysis of 37.5 μM (post-mix) WT (*left*), H123A (*center*), and C364A SufS (*right*) with with various cysteine concentrations. (A) Absorbance spectrum at various time points for the reaction of 400 μM cysteine with SufS. (B) Absorbance versus time traces monitored at 340 nm and 420 nm for 400 μM cysteine mixed with SufS. (C) Fast phase ($1/\tau_1$) at different cysteine concentrations monitored at 340 nm (in which $1/\tau_1$ is the reciprocal relaxation time).

Table 2.5: Comparison of SufS stopped-flow data collected in PMT mode at indicated wavelengths.

Protein and phase	Wavelength	
	340 nm	**350 nm (for H123A only)**
WT SufS k_{fast} ($M^{-1}s^{-1}$)	5.1 (±0.3)x10^3	–
H123A SufS k_{fast} ($M^{-1}s^{-1}$)	1.8 (±0.2)x10^4	1.3 (±0.1)x10^4
C364A SufS k_{fast} ($M^{-1}s^{-1}$)	1.1 (±0.1)x10^4	–
WT SufS k_{slow} (s^{-1})	1.4 ±0.3	–
H123A SufS k_{slow} (s^{-1})	1.3 ±0.1	1.3 ±0.1
C364A SufS k_{slow} (s^{-1})	1.6 ±0.1	–

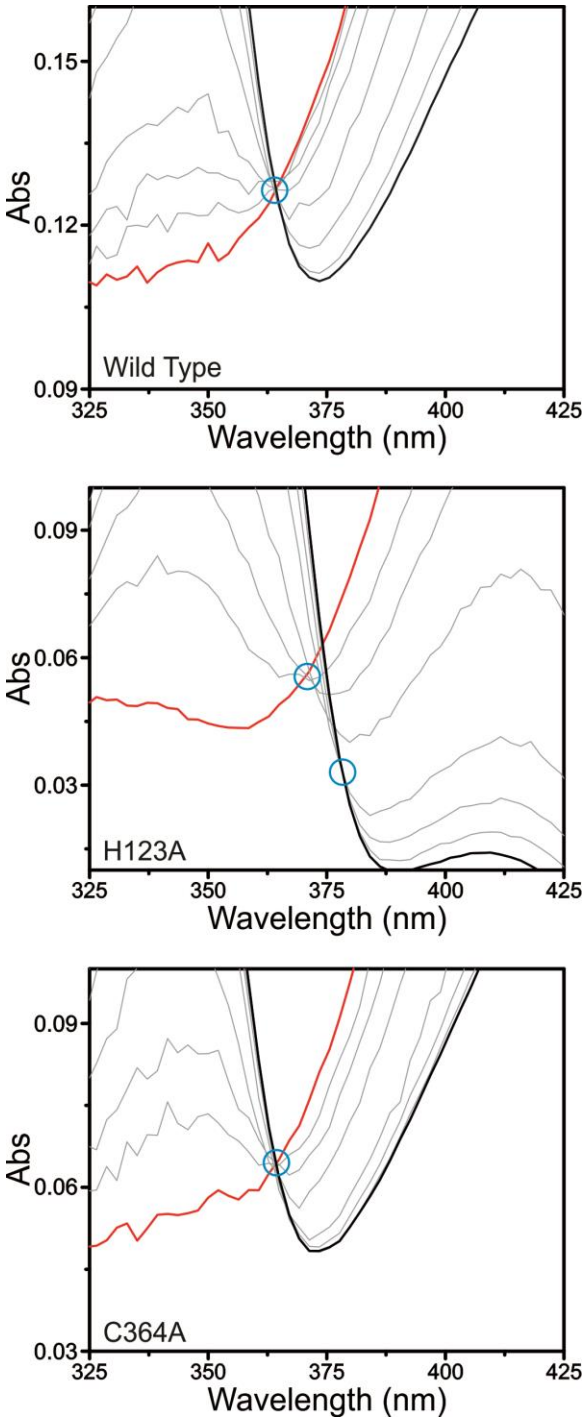

Figure 2.9. Magnified view of isosbestic points (blue circle) for stopped-flow analysis of 37.5 μM (post-mix) WT (*top*), H123A (*middle*), and C364A SufS (*bottom*) with absorbance spectrum at various time points for the reaction of 400 μM cysteine with SufS.

that the steps being monitored at 340 and 420 nm likely correspond to early stages in the ping-pong mechanism prior to L-cysteine desulfuration.

In contrast to WT and C364A SufS, the reaction of L-cysteine with the H123A mutant exhibits a more complex kinetic process. The blue-shifted internal aldimine at 418 nm is consumed without a concomitant appearance of the 424 nm species, regardless of the L-cysteine concentration. These results closely match the effects noted in steady-state experiments (Figure 2.5A and 2.6B). The complexity of this process is evidenced by a clear lack of isosbestic points during the transitions (Figures 2.8A and 2.9). An initial intermediate with a λ_{max} ~345 nm is quickly formed within ~300 ms followed by a much slower shift to a species at ~350 nm over the following 4.7 s (Figure 2.8A and Figure 2.10). The latter absorption feature at 350 nm is identical to that observed in the steady-state reactions described above (Figure 2.6B). Global analysis by singular value decomposition (SVD) was used to analyze the PDA data in order to further establish that two distinct intermediates are formed in the reaction of H123A SufS with L-cysteine. The evolution of PDA spectra could not be adequately fit with a single kinetic process, but minimally required two steps and the inclusion of a spectroscopically distinguishable intermediate at 345 nm (Figure 2.11). Like C364A, the derived kinetic rate constants for H123A (k_1 = 18 mM^{-1} s^{-1}, k_2 = 1.3 s^{-1}) are similar to those for the WT enzyme (Table 2.5).

The X-ray crystal structure of a SufS Cys-aldimine

The intermediates formed upon incubation of SufS mutants with L-cysteine were structurally characterized. First, the diffraction data was measured on a WT SufS crystal

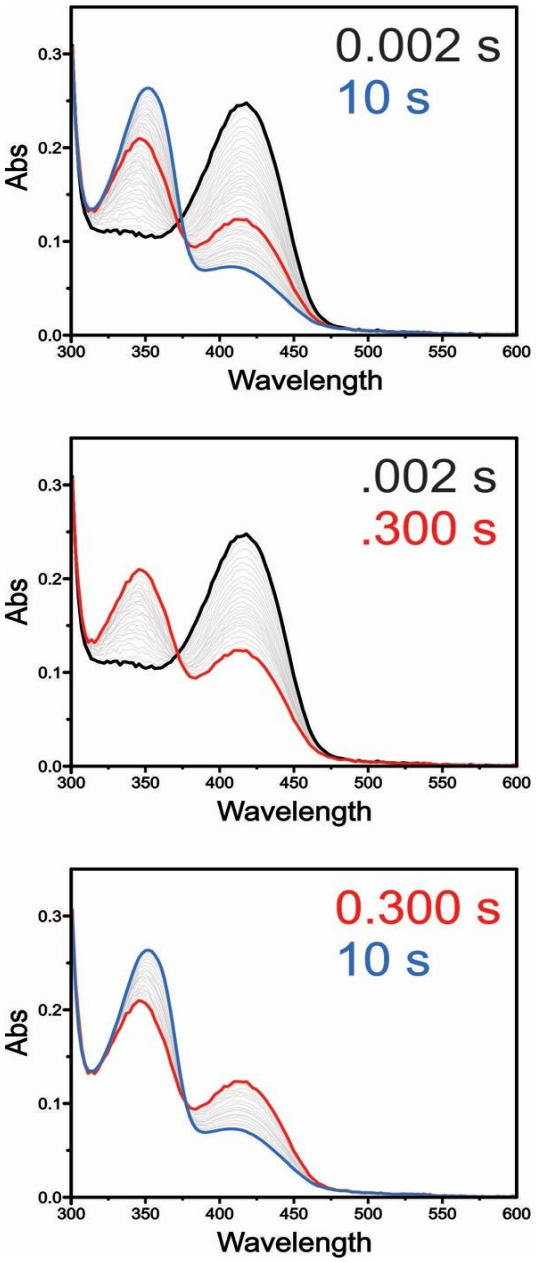

Figure 2.10. SufS H123A spectra after mixing with 400 µM L-cysteine. *Top*, the overall shift from 418 nm (black trace) to intermediate B at 0.3 sec (red trace) followed by intermediate C at 10 sec (blue trace). *Middle*, the point of maximal accumulation of intermediate B at 345 nm at 0.3 sec (red trace). *Bottom*, the conversion of intermediate B at 345nm (red trace, 0.3 sec) to intermediate C at 351nm (blue trace, 10 sec).

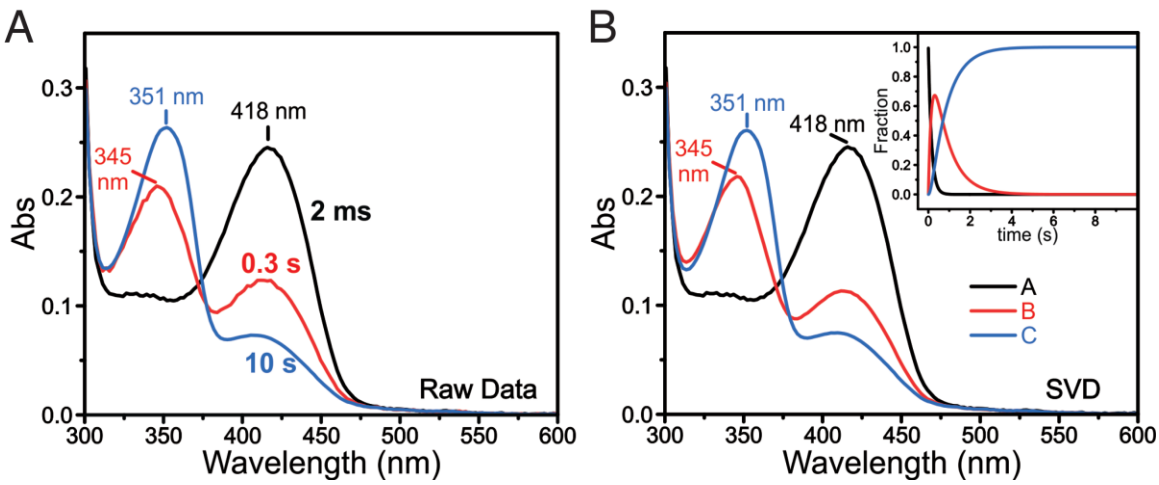

Figure 2.11. UV-visible absorption features of 37.5 μM H123A SufS (post-mix) with 400 μM L-cysteine fit to an A to B to C transition where A, B, and C represent distinct species (see text for details). (A), Spectra obtained from indicated time points after mixing of H123A SufS and cysteine.(B) Pure component spectra of H123A SufS determined using global fitting SVD analysis of PDA data. (B) *Inset*, Fractional concentration of each species in the H123A SufS spectra over time after L-cysteine addition.

incubated with L-cysteine. In agreement with previous experiments,, this did not yield electron density for a trapped intermediate but instead showed electron density for a sub-stoichiometric amount of Cys-364-persulfide, the product of the cysteine desulfurase reaction (Figure 2.12).[24, 25] Next, the structure of SufS C364A was solved following incubation of the crystal with L-cysteine. The crystallization conditions have a pH of 7 with polyethylene glycol as the precipitant and therefore possess a native chemical environment for the enzyme. Diffraction data were collected to 1.85 Å and the structure was solved by molecular replacement using PDB 1jf9 with all heteroatoms removed. The resulting unbiased $F_o - F_c$ difference electron density maps revealed a strong signal for a ligand covalently bound to PLP and a lack of electron density between Lys-226 and PLP indicating the loss of the Lys-aldimine (Figure 2.13A). The electron density indicated the presence of seven non-H atoms in the ligand consistent with a Cys-aldimine intermediate. Inspection of the C_α atom revealed tetrahedral geometry suggesting the substrate C_α was participating in four covalent bonds as expected for the Cys-aldimine intermediate (Figure 2.13A). We also measured anomalous diffraction data on the Cys soaked C364A crystal with 1.74 Å X-rays and observed an anomalous signal confirming the presence of the S atom in the ligand and its identity as Cys-aldimine (Figure 2.13B). Additional anomalous signal is present for the P atom of PLP as expected and also for a solvent ion, most likely Cl^- adjacent to Cys-364 (Figure 2.13B). In sum the data indicate the C364A mutation blocked progression of cysteine desulfurase chemistry at the Cys-aldimine step.

To determine whether additional changes to the structure of SufS C364A occured upon formation of the Cys-aldimine state, a superposition of the homodimer with the WT SufS homodimer was performed (Figure 2.13C). The superposition indicated no gross-

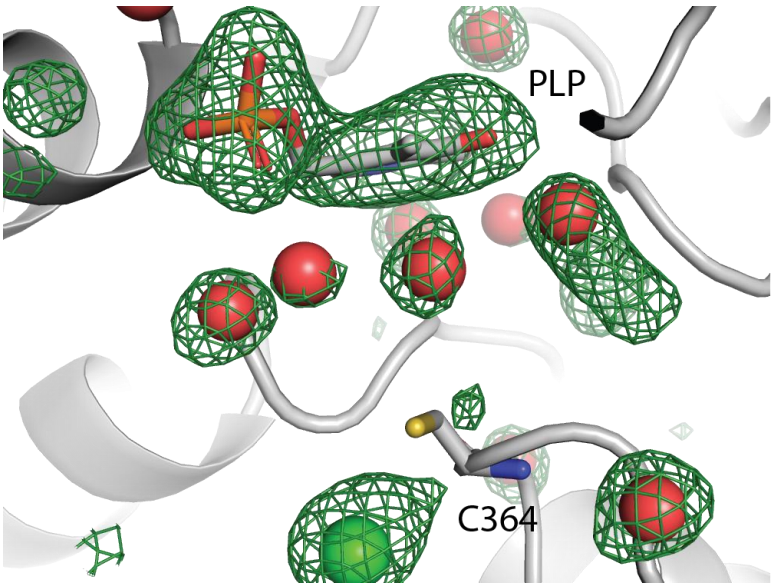

Figure 2.12. Fo – Fc difference electron density for wild-type SufS soaked with L-cysteine. Solvent ions modeled as water are colored red and solvent modeled as Cl^- is colored green. The map is contoured at 3 σ.

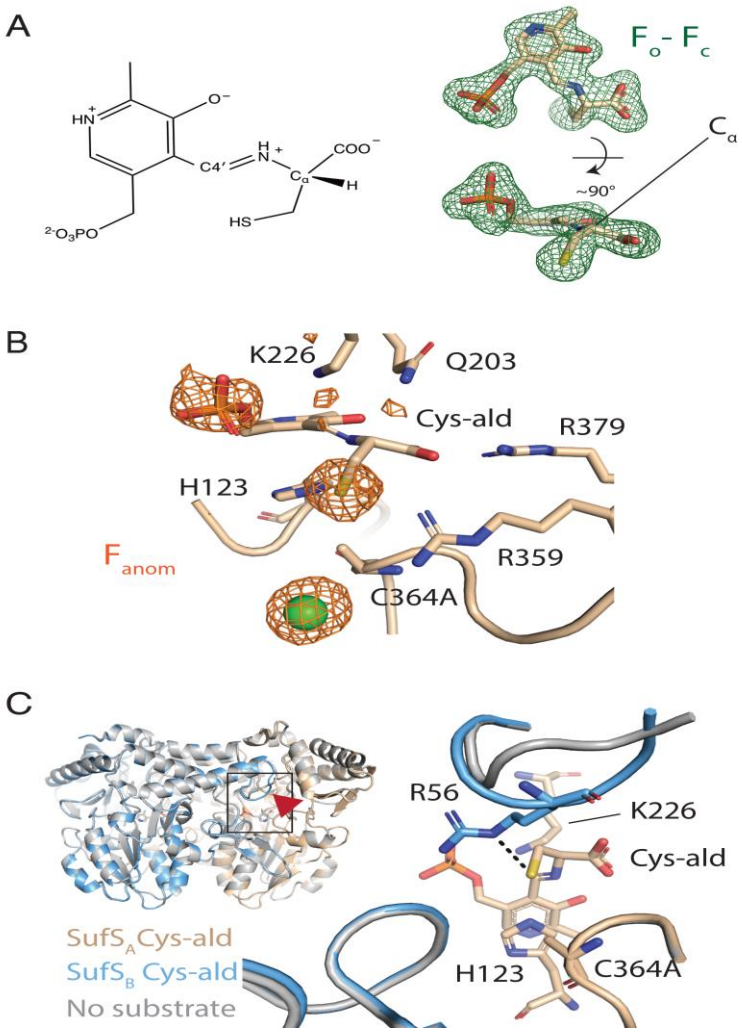

Figure 2.13. (A) Unbiased F_o – F_c difference electron density maps of C364A crystals incubated with L-cysteine possess electron density for a Cys-aldimine enzymatic intermediate covalently bound to PLP. A tetrahedral arrangement of the atoms bonded to C_α indicates sp^3 hybridization consistent with assignment of the intermediate as Cys-aldimine. A line drawing of Cys-aldimine is also shown. (B) Anomalous electron density maps of the active site of SufS C364A with Cys-aldimine, contoured at 3 σ, possess a strong signal indicating the presence of the Cys-aldimine S atom. Anomalous signals are also observed corresponding to the P atom of PLP and a solvent molecule that is most likely Cl^-. (C) A superposition of SufS Cys-364 with Cys-aldimine in the active site versus SufS wild-type with no substrate is shown. A sharp kink in the region of Arg-56 in SufS monomer B unfurls to allow hydrogen bonding between Arg-56 and the sulfhydryl of Cys-aldimine.

structural changes resulted upon formation of the Cys-aldimine state but revealed a restructuring of a loop adjacent to the active site (Figure 2.13C). The loop contains residue Arg-56 that forms a hydrogen bond to the sulfhydryl of the Cys-aldimine intermediate, an interaction that may play a role in substrate C_α deprotonation (Figure 2.13C).

The X-ray crystal structure of a SufS Cys-ketimine

To determine the identity of the reaction intermediate observed by UV-visible absorption spectroscopy, the structure of SufS H123A incubated with L-cysteine was solved. SufS H123A crystals at pH 6.5 with NaCl as the precipitant were incubated with L-cysteine and then frozen in liquid N_2 for X-ray data collection. During incubation with L-cysteine, the crystals gradually lost their yellow color, associated with 420 nm absorbance, and became clear (Figure 2.14A). Molecular replacement was used to solve the structure. Unbiased $F_o - F_c$ difference electron density maps possessed a strong signal for a reaction intermediate, containing seven non-H atoms covalently linked to PLP (Figure 2.14B). Inspection of the geometry at the substrate C_α indicated a trigonal planar arrangement of atoms surrounding C_α consistent with a Cys-ketimine, a reaction intermediate formed just prior to C-S bond cleavage (Scheme 2.1, Figure 2.14B). Anomalous diffraction data were collected and the corresponding maps indicated the presence of an S atom in the position expected for Cys-ketimine (Figure 2.14C).

A superposition was performed between the homodimer of SufS H123A in the Cys-ketimine state and the WT SufS homodimer (Figure 2.14D). The alignment intimated that the two SufS H123A monomers had rotated relative to one another

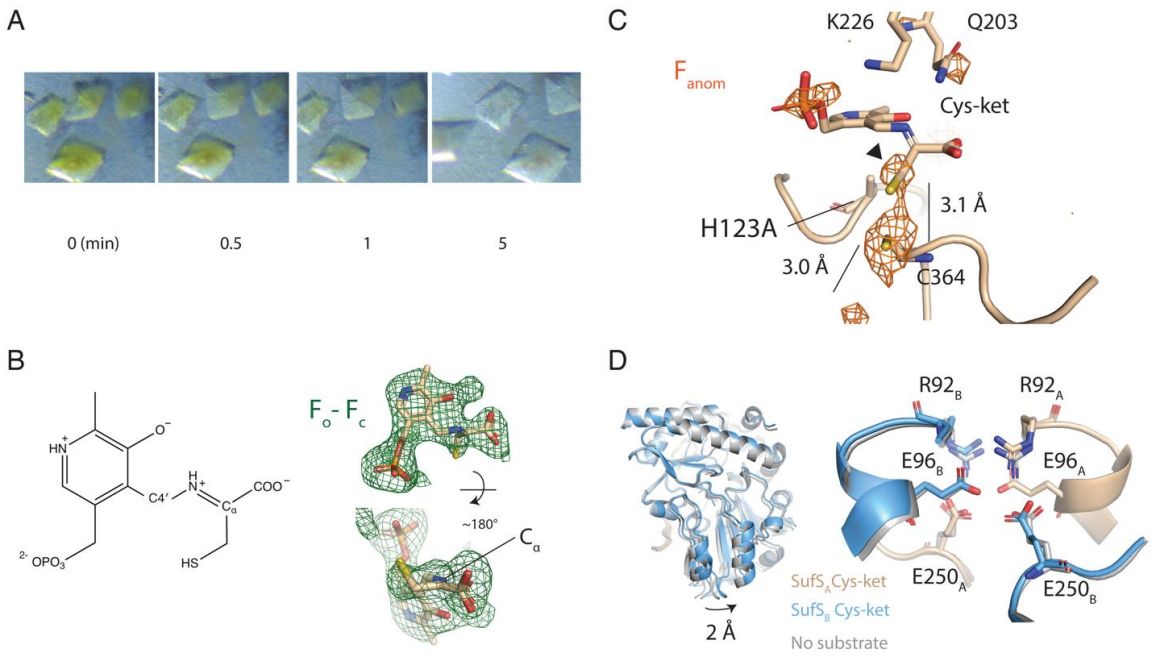

Figure 2.14. (A) Crystals of SufS H123A lose 420 nm absorbance (loss of yellow color) upon incubation with L-cysteine. (B) Unbiased $F_o - F_c$ difference electron density maps of H123A crystals incubated with L-cysteine possess electron density for a Cys-ketimine enzymatic intermediate covalently bound to PLP. A planar arrangement of the atoms bonded to C_α indicates sp^2 hybridization consistent with assignment of the intermediate as Cys-ketimine. A line drawing of Cys-ketimine is also shown. (C) Anomalous diffference electron density maps of the active site of SufS H123A with Cys-ketimine, contoured at 3 σ, possess a strong signal indicating the position of the Cys-ketimine S atom. Anomalous signals are also observed corresponding to the S atom of Cys-364 and a solvent atom adjacent to Cys-364. The solvent atom has been previously observed in WT SufS structures and is most likely Cl^-. A weak anomalous signal is observed for the P atom of PLP. (D) A superposition of SufS H123A without substrate and H123A in the Cys-ketimine state reveals rotation of the SufS monomers occurs in the Cys-ketimine state. Subtle changes to the electrostatic interactions at the SufS dimer interface occur as part of the monomer rotation.

partially altering electrostatic interactions at the dimer interface (Figure 2.14D). Since SufS H123A and WT SufS are superimposable in the absence of a ligand (see Figure 2.5C and 2.5D), these data suggest that formation of the Cys-ketimine state is coincident with a reordering of the SufS subunits relative to one another. Previous HDX-MS studies of SufS dynamics indicated that dimer rearrangement is associated with reaction progression.[27]

Discussion

Early sequence analysis of cysteine desulfurases identified two distinct groups of enzymes: type I typified by IscS or NifS and type II enzymes exemplified by SufS.[12] Recent automated sequence analysis by InterPro confirms these early results clustering ~19,000 sequences together in the IPR010970, SufS family. SufS homologs are present in the genomes of Gram positive and Gram negative bacteria, cyanobacteria and plant plastids. SufS model systems have emerged from each of these phylogenetic groups with SufS deletion mutant phenotypes and SufS interacting partners having been described by several groups.[11, 14, 17, 18, 28, 29] While SufS is not essential in *E. coli* due to functional overlap with IscS, genetic investigations of SufS in *B. subtilis*, *Synechocystis* and *A. thaliana* have found that it is indispensable in each of these organisms. Further, the role of SufS in Fe-S cluster biosynthesis has been confirmed in multiple model organisms.[11, 14, 28] The function of conserved active site residues in the mechanism of SufS, however, is not well resolved. Using new data reported here, alongside existing SufS structural data, we composed a model detailing the progression of SufS from Cys binding to C-S bond

cleavage (Scheme 2.2 and Figure 2.15). Our results highlight new functions of Arg-56, His-123 and Cys-364 in the steps on the pathway to C-S bond cleavage.

Assignment of PLP-intermediates in UV-Vis spectra

The identification and characterization of PLP intermediates in enzymes is often complicated by significant overlap in their spectral properties and that several species can coexist in rapid equilibria. For example, both internal and external aldimine species are expected to absorb in the 400-420 nm region. However, tautomerization from the ketoenamine to the enolimine form of aldimine results in a shift in absorbance to the 330 nm region as well.[30] The 330-350 nm region is also home to absorbance maxima from the *gem*-diamine and ketimine-PLP intermediates .[31, 32] Only the quinonoid-PLP intermediate has a distinct absorption spectra with a peak in the 500 nm region.[33, 34] Given these complications, integration of the kinetic and structural data described above are essential for assignment.

Results from UV-Vis and stopped-flow monitored rapid reaction experiments show that all three enzymes share an initial step upon exposure to L-cysteine, conversion of the stable resting state ~420 nm species (assigned as the internal Lys-226-aldmine) to new species at 340-345 and 424 nm. The linear dependence of the fast phase on cysteine concentration and zero-intercept suggest that this step is dominated by the rate constant of the cysteine binding step. The irreversible nature of this stage, which may be anticipated for formation of a covalent PLP adduct, uncouples the slow phase from cysteine. The rate of this transition is very similar in all three enzymes suggesting the two substitutions have not affected this step in the reaction.

Scheme 2.2.

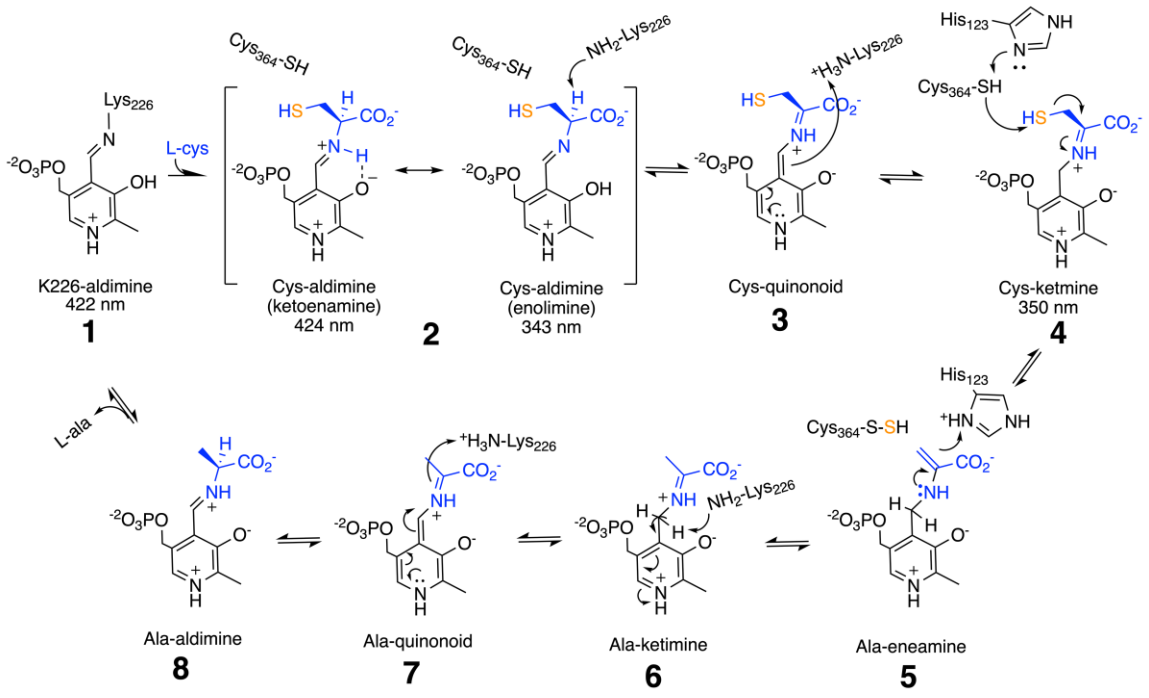

Scheme 2.2. Updated cysteine desulfurase reaction scheme for SufS based on results presented in this work. L-cysteine substrate is shown in blue (C, H, O, N) and orange (S). PLP and SufS active site residues are in black.

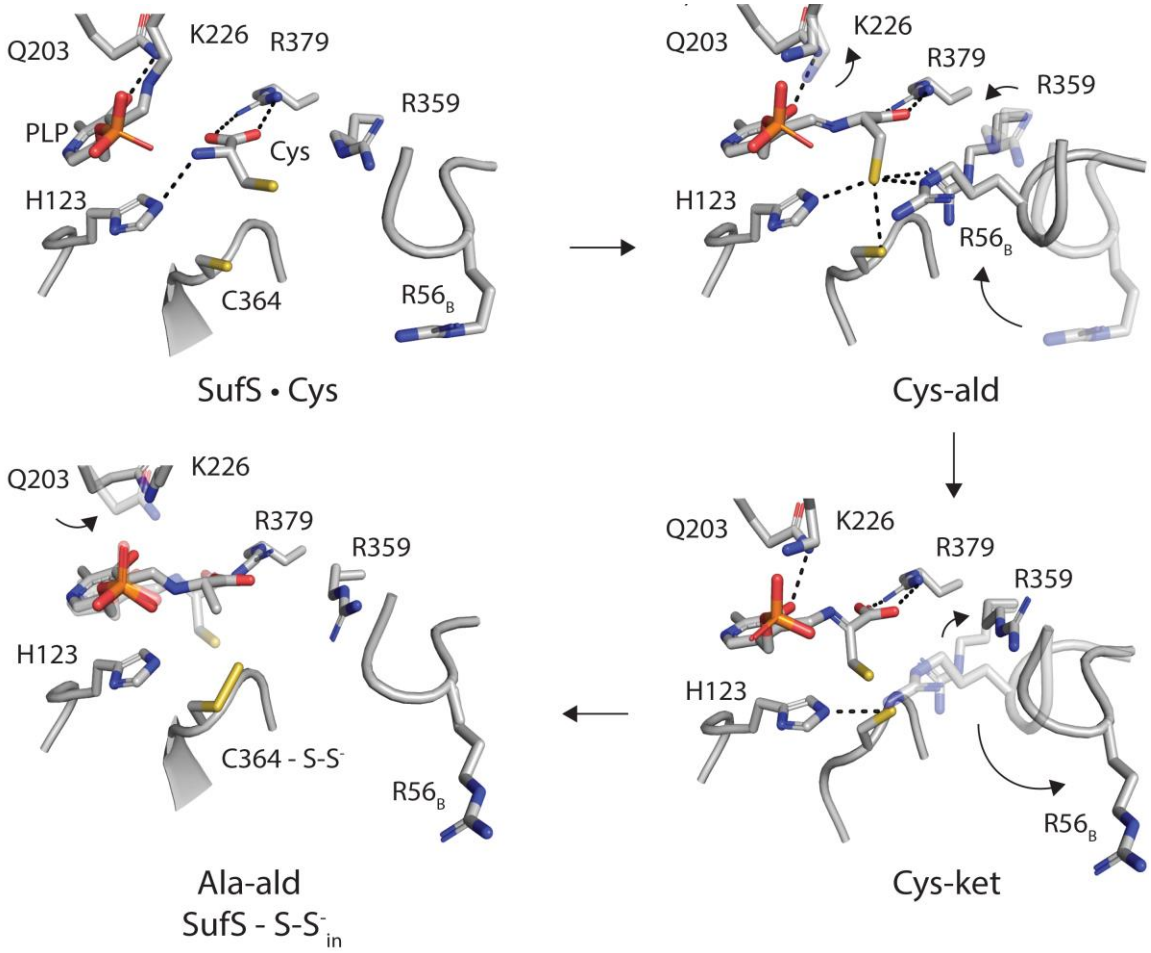

Figure 2.15. The roles of active site residues in the SufS cysteine desulfurase mechanism. Active site residues implicated in type II cysteine desulfurase function are labeled. Arrows show residues which change conformation during reaction progression. Dotted lines represent hydrogen bonds or electrostatic interactions. SufS-S-S$^{-}_{in}$ indicates the persulfide covalently linked to SufS Cys-364 is positioned towards PLP. Coordinate super-positions used to generate the model are described in the Experimental Procedures. SufS bound to L-cysteine is derived from 5db5. The Cys-aldimine and Cys-ketimine structures were created by modeling Cys-364 or His-123 into the corresponding mutant structures (6O11 and 6O13). The Ala-aldimine structure was modeled by combining 1i29 (external aldimine) and 6mr2 (S-S$^{-}_{in}$ and Arg-56).

Absorbances in the 340 nm region are consistent with either a ketimine or *gem*-diamine PLP intermediate. Assignment of the initial 343 nm signal as the ketimine intermediate is not supported by the spectroscopic and structural results with H123A SufS described below. Further, the *gem*-diamine intermediate is short-lived with typical formation rates >45 s^{-1} and would therefore be unlikely to accumulate on the timescale of minutes as observed in WT and C364A SufS upon L-cysteine addition (Figures 2.5 and 2.6).[21, 31, 35]

As mentioned above, the external Cys-aldimine can exist in two tautomers with distinct UV-visble absorption maxima in the 340 and 420 nm region. In some cases, such as for the cyanobacterial C-DES enzyme, these species are stable over a timescale of minutes.[36] The structure of C364A SufS clearly shows the external Cys-aldimine as the trapped intermediate, although x-ray crystallography cannot distinguish the individual tautomers (Figure 2.13). Since the C364A SufS has an absorption spectra upon L-cysteine binding very similar to WT SufS (Figure 2.6), we assign the 343 nm and 424 nm species formed upon L-cysteine binding in WT and C364A SufS as the enolimine and ketoenamine tautomers of the Cys-aldimine respectively (Scheme 2.2, **2**).

The failure to observe further reactions intermediates beyond the Cys-aldimine tautomers in the WT SufS reaction with L-cysteine was unexpected. On sufficiently long timescales of multiple minutes, WT SufS by itself can undergo a single turnover (Table 2.4).[10, 11] However, the rate of persulfide production by SufS alone is approximately 0.12 (nmol product min^{-1})/(nmol SufS) Under the stopped-flow conditions, using approximately 5.6 nmol SufS, it would take 8.3 min to produce one equivalent of persulfide. This relative lack of activity over these short time scales is consistent with the

lack of observable intermediates beyond the Cys-aldimine stage of the cysteine desulfurase reaction for WT SufS.

For true catalytic activity, SufS requires the SufE persulfide acceptor. It is possible that the stalling of the wild-type reaction at the Cys-aldimine stage when SufS is alone reflects coordinated regulation of the combined cysteine desulfurase-transpersulfuration reaction. Since *E. coli* SufS is specfically expressed under conditions that disrupt Fe-S cluster metabolism, including oxidative stress, the enzyme may remain in the Cys-aldimine state until the SufE acceptor interacts with it. This regulation would prevent premature formation of the reactive persulfide species prior to having SufE present to accept the persulfide from SufS Cys-364. It has previously been shown that the SufS-SufE persulfide generation is more resistant to disruption by H_2O_2 than other Type I cysteine desulfurases like IscS.[10] Further experiments are underway to test if SufE regulates the cysteine desulfurase activity of SufS (in addition to participating in the transpersulfuration reaction).

In contrast to the relative stability of the 343/424 nm spectra produced in WT and C364A SufS, H123A SufS forms a transient 345 nm peak in the first 0.3 s after mixing with L-cysteine, which rapidly converts to a stable species with a peak absorbance of 350 nm. The stable 350 nm species is assigned as the Cys-ketimine intermediate on the basis of several lines of evidence. Electron density in the crystal structure of H123A SufS can be fit well with the Cys-ketimine structure (Figure 2.14B). Additionally, both the anomalous diffraction (Figure 2.14C) and kinetic data (Table 2.4) are consistent with an intact C-S bond on the PLP intermediate. The initial 345 nm peak formed upon L-cysteine binding to H123A SufS is assigned as the enolimine tautomer of the Cys-

aldimine that is slightly red-shifted by by loss of the nearby histidine and its π-π stacking interaction. This assignment is also consistent with known PLP chemistry since the enolimine is predicted to be the more reactive of the Cys-aldimine tautomers and would logically proceed to the Cys-ketimine seen at 350 nm.[37, 38]

A role for His-123 as an acid-base catalyst

The findng that loss of His-123 in SufS traps the Cys-ketimine intermediate (Figures 2.6 and 2.15) suggests a key mechanistic role for His-123 in catalysis. Structurally, His-123 is adjacent to the PLP ring where it can influence the PLP cofactor through π-π stacking interactions. While tyrosine and phenylalanine residues are often found in this position in aminotransferase enzymes, decarboxylase enzymes commonly utilitze a histidine.[38] Based on the structural evidence, His-123 is optimally placed to act in an acid/base capacity to deprotonate/protonate the C4' position of the PLP (2.7 Å) in a step involving Cys-ketimine formation or to interact with the C_α (3.1 Å) or C_β (2.7 Å) of the amino acid-PLP adduct. Identification of the Cys-ketimine intermediate in the H123A variant rules out His-123 as the residue responsible for protonation at the C4' position to form the ketimine (conversion of **4** to **5** in Scheme 2.1). A role for C_α protonation/deprotonation is also ruled out as the proton is located on the face of the C_α atom pointing away from His-123. This leaves interactions at the C_β position as the only viable option. His-123 acting to protonate the PLP-Ala-eneamine after C-S bond cleavage (Scheme 2.1, **6**) fits nicely with the structural and spectroscopic data as a stalled Ala-eneamine would likely revert back to the more stable Cys-ketimine. His-123 is also located near the sulfhydryl group of Cys-364 (4.1 Å) and could play a role in

deprotonation of the nucleophilic -SH group prior to C-S bond cleavage as well as protonating the resulting Ala-eneamine intermediate after C-S bond cleavage.

The ability of the H123A SufS mutant to move beyond the Cys-aldimine to the Cys-ketimine stage of the reaction while both WT and C364A remain at that earlier step is at first puzzling. However, loss of π-π stacking interactions with PLP in the H123A mutant seems to favor accumulation of the enolimine tautomer of the Cys-aldimine as seen by the asymmetry in 343/424 nm signal intensity (Figures 2.6, 2.8, 2.11). A similar phenomenon is predicted by metadynamics calculations carried out on the PLP-dependent serine hydroxymethyltransferase (SMHT) enzyme.[37] Those previous studies suggested that the π-π interaction of the PLP pyridine ring with SHMT His122 is weakened in the enolimine tautomer of the external aldimine of SHMT. This shift in the equilibium between Cys-aldimine tautomers may explain the ability of the H123A SufS to move to the Cys-ketimine intermediate before stalling.

A role for Cys-364 in orienting C_α toward catalysis

The identification of the external cys-aldimine as the trapped intermediate in C364A seems counterintuitive at first glance. Loss of C364A should prevent C-S bond cleavage, which one would predict to stall at the Cys-ketimine intermediate. Nonetheless, the lack of persulfide production and detailed structural results are consistent with C364A SufS being stalled at the Cys-aldimine intermediate. Therefore, Cys-364 may play a mechanistic role in conversion of the Cys-aldimine to the Cys-ketimine intermediate. Cys-364 is too far from the C_α to act directly in the deprotonation step. The simplest

interpretation of these results is that Cys-364 engages in a hydrogen bonding interaction with the Sγ atom of Cys-aldimine required to properly position C_α for deprotonation by another active site residue.

Lys-226 is likely responsible for C_α -H bond breakage to form the cys-ketimine intermediate

On the basis of the Cys-aldimine structure, it appears the Lys-226, which forms the Schiff base linkage with the internal PLP aldimine, is responsible for the 1,3 proton shift to generate the Cys-ketimine intermediate from the Cys-aldimine. In the structure, the sidechain of Lys-226 is positioned 3.4 Å from the C4' position of PLP and 4.8 Å from the C_α position. There is a wide pocket of space for the residue to sample, and it is the only potential acid/base residue on the correct face for C_α deprotonation. Under the current experimental conditions, lack of an observable intermediate with absorbance around 500 nm in the H123A SufS reaction suggests that either the quinonoid species decomposes faster than it is formed or that the ketimine species is formed directly from the anionic intermediate.

A detailed mechanism for SufS

Taking all of the data together, a detailed mechanism can be proposed for the desulfurase reation catalyzed by SufS in the absence of SufE (Scheme 2.2). In the first step, L-cysteine reacts with the internal aldimine (**1**) to form a *gem*-diamine species that rapidly converts to a mix of enolimine (343 nm) and ketoenamine (424 nm) tautomers of the Cys-aldimine (**2**). This concerted proces occurs with a second-order rate constant of

~5000 $M^{-1}s^{-1}$. As this equilibrium state is the sole intermediate state, deprotonation of the C_α position is likely rate-determining in the desulfurase reaction with all subsequent steps in the return to Lys-226-aldimine occurring rapidly. Lys-226 can act as a general base to deprotonate the C_α position forming the Cys-quinonoid intermediate (**3**), which is not observable under current reaction conditions. Lys-226 may then transfer the proton to the C4' position on PLP converting it to the Cys-ketimine intermediate (350 nm) (**4**). Following formation of the Cys-ketimine, Cys-364 attacks the sulfhydryl on the Cys-ketimine to break the C-S bond. His-123 may assist in this step by deprotonating Cys-364 to produce the nucleophilic sulfide form. The Ala-eneamine (**5**) produced by C-S bond cleavage is protonated by His-123 to produce the Ala-ketimine intermediate (**6**). Lys-226 then acts as an acid/base catalyst to cycle back to the Ala-aldimine species (**7 & 8**). Finally, Lys-226 stimulates release of L-alanine and formation of the internal aldmine while passing through a transient *gem*-diamine species. It is important to note that these experiments were performed in the absence of the persulfide acceptor SufE which limits SufS to no more than a single turnover under these conditions (and in fact less than a full turnover as noted above). Addition of SufE to the system certainly impacts the transpersulurase activity of SufS by providing the physiological substrate for the second half of the ping-pong reaction. The addition of SufE greatly enhances SufS activity up to 200-fold over SufS alone. Previous studies have suggested that SufE also influences the SufS active site allosterically and could impact specific steps in the cysteine desulfurase reaction as well.[39, 40]

SufS conformational changes during reaction progression

The spectroscopic analysis of WT, H123A, and C364A SufS show that all three proceed with L-cysteine binding through a biphasic process with similar kinetic rate constants. The fast phase of 340 nm formation represents formation of the Cys-aldimine tautomers in all three enzymes. However, it is difficult to assign the slow phases to a specific event in the reaction progression. It may reflect a slow protein conformational change that occurs after formation of the most stable intermediate. Alternatively, it might reflect progression forward to an intermediate with nearly identical absorption maxima but a greater molar extinction coefficient.

A structure of *E. coli* SufS trapped in an external aldimine state through the use of the substrate analog L-propargylamine was interpreted to indicate that no conformational changes occur during the cysteine desulfurase reaction cycle.[23] The lack of conformational change in the SufS-L-propargylamine structure is explained by the fact that the analog possesses a Cγ atom rather than the Sγ of Cys so that the hydrogen bonding interactions to Arg-56 or Arg-359 cannot occur. Additionally, the analog Cγ atom was disordered and not visible in electron density and therefore the structure more appropriately models a product complex than a substrate complex.[23] We identified both local and long-range conformational changes associated with cysteine desulfurase reaction intermediates. Arg-56 and Arg-359 undergo changes to assist in positioning Cys-aldimine for C_α-H bond cleavage. Cys-364 hydrogen bonding to Cys is also required for correct positioning of Cys-aldimine. The structure reported herein is the first observation of a cysteine desulfurase captured with a Cys-aldimine intermediate. The structure is consistent with the principles of PLP facilitated chemistry: only a small rotation is

required to place C_α-H perpendicular to the pyridine ring of PLP, the ideal location for promoting C_α-H bond breaking.[41, 42] The dynamics of the α3-α4 loop of SufS, which contains Arg-56, have also been identified as important during SufS binding to SufE/SufU, indicating there are multiple functional roles for this active site 'flap'.[43, 44] The global rotation of the SufS monomers relative to each other in the Cys-ketimine state can be compared with previous studies showing that formation of an active site persulfide alters SufS dynamics.[27] HDX-MS and structural data of SufS dimer interface mutants identified a pathway for active site crosstalk in the SufS homodimer.[24] The conformational changes observed in Figure 2.14D are reminiscent of the monomer rotations associated with transpersulfuration and indicate that the monomers rearrange relative to each other during both the desulfurase and transpersulfuration reactions. Mounting evidence infers both local and global conformational changes are required for SufS function.

We examined how widely these functional roles may be conserved in SufS family enzymes, by constructing a multiple sequence alignment of members spanning the sequence diversity of IPR010970 and found that Arg-56, His-123 and Cys-364 are conserved in all sequences inspected (Figure 2.1). Additionally, structural superpositions of SufS family members with known structures indicated these active site amino acids occupy similar positions in all known structures (Figure 2.1). For these reasons we believe sulfur mobilization by SufS occurs by a conserved mechanism in all family members.

Two main structural differences in the vicinity of the active site distinguish type I from type II cysteine desulfurases: the presence of the extended flexible loop containing

the active site Cys in type I enzymes and the presence of the β-hairpin (or β-hook) in type II enzymes.[19, 44] These structural differences provide the possibility for diverging dynamics and mechanisms in the two types of cysteine desulfurases. However, structural superpositions of the type I *E. coli* IscS with SufS illustrate that Arg-56 and His-123 are conserved and occupy a similar structural environment (data not shown). Mammalian selenocysteine lyases are also PLP-dependent enzymes with structural similarity to SufS and recent studies indicate that an active site Cys is required for positioning selenocysteine to promote external aldimine formation.[45] Additionally, it was observed that mammalian selenocysteine lyase undergoes an 'open to closed' rotation of the dimer subunits reminiscent of the rotation of SufS in the Cys-ketimine state (Figure 2.14).[45] We believe our identification of the functional role of SufS active site residues and the accompanying structural model for reaction progression will provide a testable model for analysis of diverse cysteine desulfurases and related enzymes.

References

1. Blahut, M., Wise, C. E.; Dong, G.; Bruno, M.; Makris, T.; Frantom, P.; Dunkle, J.; Outten, F.W., Direct observation of intermediates in the SufS cysteine desulfurase reaction reveals functional roles of conserved active-site residues. *J Biol Chem* **2019,** *In press*.

2. Fontecave, M., Iron-sulfur clusters: ever-expanding roles. *Nat Chem Biol* **2006,** *2* (4), 171-4.

3. Volbeda, A.; Charon, M. H.; Piras, C.; Hatchikian, E. C.; Frey, M.; Fontecilla-Camps, J. C., Crystal structure of the nickel-iron hydrogenase from Desulfovibrio gigas. *Nature* **1995,** *373* (6515), 580-7.

4. Roche, B.; Aussel, L.; Ezraty, B.; Mandin, P.; Py, B.; Barras, F., Iron/sulfur proteins biogenesis in prokaryotes: formation, regulation and diversity. *Biochim Biophys Acta* **2013,** *1827* (3), 455-69.

5. Tokumoto, U.; Takahashi, Y., Genetic analysis of the isc operon in Escherichia coli involved in the biogenesis of cellular iron-sulfur proteins. *J Biochem* **2001,** *130* (1), 63-71.

6. Fontecave, M.; Choudens, S. O.; Py, B.; Barras, F., Mechanisms of iron-sulfur cluster assembly: the SUF machinery. *J Biol Inorg Chem* **2005,** *10* (7), 713-21.

7. Nachin, L.; Loiseau, L.; Expert, D.; Barras, F., SufC: an unorthodox cytoplasmic ABC/ATPase required for [Fe-S] biogenesis under oxidative stress. *Embo J* **2003,** *22* (3), 427-37.

8. Outten, F. W.; Djaman, O.; Storz, G., A suf operon requirement for Fe-S cluster assembly during iron starvation in Escherichia coli. *Mol Microbiol* **2004,** *52* (3), 861-72.

9. Mihara, H.; Maeda, M.; Fujii, T.; Kurihara, T.; Hata, Y.; Esaki, N., A nifS-like gene, csdB, encodes an Escherichia coli counterpart of mammalian selenocysteine lyase. Gene cloning, purification, characterization and preliminary x-ray crystallographic studies. *J Biol Chem* **1999,** *274* (21), 14768-72.

10. Dai, Y.; Outten, F. W., The E. coli SufS-SufE sulfur transfer system is more resistant to oxidative stress than IscS-IscU. *FEBS Lett* **2012,** *586* (22), 4016-22.

11. Selbach, B. P.; Pradhan, P. K.; Dos Santos, P. C., Protected sulfur transfer reactions by the Escherichia coli Suf system. *Biochemistry* **2013,** *52* (23), 4089-96.

12. Mihara, H.; Kurihara, T.; Yoshimura, T.; Soda, K.; Esaki, N., Cysteine sulfinate desulfinase, a NIFS-like protein of Escherichia coli with selenocysteine lyase and cysteine desulfurase activities. Gene cloning, purification, and characterization of a novel pyridoxal enzyme. *J Biol Chem* **1997,** *272* (36), 22417-24.

13. Fujii, T.; Maeda, M.; Mihara, H.; Kurihara, T.; Esaki, N.; Hata, Y., Structure of a NifS homologue: X-ray structure analysis of CsdB, an Escherichia coli counterpart of mammalian selenocysteine lyase. *Biochemistry* **2000,** *39* (6), 1263-73.

14. Tirupati, B.; Vey, J. L.; Drennan, C. L.; Bollinger, J. M., Jr., Kinetic and structural characterization of Slr0077/SufS, the essential cysteine desulfurase from Synechocystis sp. PCC 6803. *Biochemistry* **2004,** *43* (38), 12210-9.

15. Trotter, V.; Vinella, D.; Loiseau, L.; Ollagnier de Choudens, S.; Fontecave, M.; Barras, F., The CsdA cysteine desulphurase promotes Fe/S biogenesis by recruiting Suf components and participates to a new sulphur transfer pathway by recruiting CsdL (ex-YgdL), a ubiquitin-modifying-like protein. *Mol Microbiol* **2009,** *74* (6), 1527-42.

16. Loiseau, L.; Ollagnier-de-Choudens, S.; Nachin, L.; Fontecave, M.; Barras, F., Biogenesis of Fe-S cluster by the bacterial Suf system: SufS and SufE form a new type of cysteine desulfurase. *J Biol Chem* **2003,** *278* (40), 38352-9.

17. Outten, F. W.; Wood, M. J.; Munoz, F. M.; Storz, G., The SufE protein and the SufBCD complex enhance SufS cysteine desulfurase activity as part of a sulfur transfer pathway for Fe-S cluster assembly in Escherichia coli. *J Biol Chem* **2003,** *278* (46), 45713-9.

18. Layer, G.; Gaddam, S. A.; Ayala-Castro, C. N.; Ollagnier-de Choudens, S.; Lascoux, D.; Fontecave, M.; Outten, F. W., SufE transfers sulfur from SufS to SufB for iron-sulfur cluster assembly. *J Biol Chem* **2007,** *282* (18), 13342-50.

19. Black, K. A.; Dos Santos, P. C., Shared-intermediates in the biosynthesis of thio-cofactors: Mechanism and functions of cysteine desulfurases and sulfur acceptors. *Biochim Biophys Acta* **2015,** *1853* (6), 1470-80.

20. Zheng, L.; White, R. H.; Cash, V. L.; Dean, D. R., Mechanism for the desulfurization of L-cysteine catalyzed by the nifS gene product. *Biochemistry* **1994,** *33* (15), 4714-20.

21. Behshad, E.; Bollinger, J. M., Jr., Kinetic analysis of cysteine desulfurase CD0387 from Synechocystis sp. PCC 6803: formation of the persulfide intermediate. *Biochemistry* **2009,** *48* (50), 12014-23.

22. Mihara, H.; Kurihara, T.; Yoshimura, T.; Esaki, N., Kinetic and mutational studies of three NifS homologs from Escherichia coli: mechanistic difference between L-cysteine desulfurase and L-selenocysteine lyase reactions. *J Biochem* **2000,** *127* (4), 559-67.

23. Mihara, H.; Fujii, T.; Kato, S.; Kurihara, T.; Hata, Y.; Esaki, N., Structure of external aldimine of Escherichia coli CsdB, an IscS/NifS homolog: implications for its specificity toward selenocysteine. *J Biochem* **2002,** *131* (5), 679-85.

24. Dunkle, J. A.; Bruno, M. R.; Outten, F. W.; Frantom, P. A., Structural Evidence for Dimer-Interface-Driven Regulation of the Type II Cysteine Desulfurase, SufS. *Biochemistry* **2019,** *58* (6), 687-696.

25. Lima, C. D., Analysis of the E. coli NifS CsdB protein at 2.0 A reveals the structural basis for perselenide and persulfide intermediate formation. *J Mol Biol* **2002,** *315* (5), 1199-208.

26. Edgar, R. C., MUSCLE: multiple sequence alignment with high accuracy and high throughput. *Nucleic Acids Res.* **2004,** *32* (5), 1792-7.

27. Kim, D.; Singh, H.; Dai, Y.; Dong, G.; Busenlehner, L. S.; Outten, F. W.; Frantom, P. A., Changes in Protein Dynamics in Escherichia coli SufS Reveal a Possible Conserved Regulatory Mechanism in Type II Cysteine Desulfurase Systems. *Biochemistry* **2018,** *57* (35), 5210-5217.

28. Van Hoewyk, D.; Abdel-Ghany, S. E.; Cohu, C. M.; Herbert, S. K.; Kugrens, P.; Pilon, M.; Pilon-Smits, E. A., Chloroplast iron-sulfur cluster protein maturation requires the essential cysteine desulfurase CpNifS. *Proc Natl Acad Sci U S A* **2007,** *104* (13), 5686-91.

29. Albrecht, A. G.; Peuckert, F.; Landmann, H.; Miethke, M.; Seubert, A.; Marahiel, M. A., Mechanistic characterization of sulfur transfer from cysteine desulfurase SufS to the iron-sulfur scaffold SufU in Bacillus subtilis. *FEBS Lett* **2011,** *585* (3), 465-70.

30. Zhou, X.; Toney, M. D., pH studies on the mechanism of the pyridoxal phosphate-dependent dialkylglycine decarboxylase. *Biochemistry* **1999,** *38* (1), 311-20.

31. Karsten, W. E.; Cook, P. F., Detection of a gem-diamine and a stable quinonoid intermediate in the reaction catalyzed by serine-glyoxylate aminotransferase from Hyphomicrobium methylovorum. *Biochim Biophys Acta* **2009,** *1790* (6), 575-80.

32. Phillips, R. S., Structure, mechanism, and substrate specificity of kynureninase. *Biochim Biophys Acta* **2011,** *1814* (11), 1481-8.

33. Sun, S.; Toney, M. D., Evidence for a two-base mechanism involving tyrosine-265 from arginine-219 mutants of alanine racemase. *Biochemistry* **1999,** *38* (13), 4058-65.

34. Hirayama, A.; Miyanaga, A.; Kudo, F.; Eguchi, T., Mechanism-Based Trapping of the Quinonoid Intermediate by Using the K276R Mutant of PLP-Dependent 3-Aminobenzoate Synthase PctV in the Biosynthesis of Pactamycin. *Chembiochem* **2015,** *16* (17), 2484-90.

35. Kaiser, J. T.; Bruno, S.; Clausen, T.; Huber, R.; Schiaretti, F.; Mozzarelli, A.; Kessler, D., Snapshots of the cystine lyase C-DES during catalysis. Studies in solution and in the crystalline state. *J Biol Chem* **2003,** *278* (1), 357-65.

36. Campanini, B.; Schiaretti, F.; Abbruzzetti, S.; Kessler, D.; Mozzarelli, A., Sulfur mobilization in cyanobacteria: the catalytic mechanism of L-cystine C-S lyase (C-DES) from synechocystis. *J Biol Chem* **2006,** *281* (50), 38769-80.

37. Soniya, K.; Chandra, A., Free energy landscapes of prototropic tautomerism in pyridoxal 5'-phosphate schiff bases at the active site of an enzyme in aqueous medium. *J Comput Chem* **2018,** *39* (21), 1629-1638.

38. Liang, J.; Han, Q.; Tan, Y.; Ding, H.; Li, J., Current Advances on Structure-Function Relationships of Pyridoxal 5'-Phosphate-Dependent Enzymes. *Front Mol Biosci* **2019,** *6*, 4.

39. Singh, H.; Dai, Y.; Outten, F. W.; Busenlehner, L. S., Escherichia coli SufE sulfur transfer protein modulates the SufS cysteine desulfurase through allosteric conformational dynamics. *J Biol Chem* **2013,** *288* (51), 36189-200.

40. Dai, Y.; Kim, D.; Dong, G.; Busenlehner, L. S.; Frantom, P. A.; Outten, F. W., SufE D74R Substitution Alters Active Site Loop Dynamics To Further Enhance SufE Interaction with the SufS Cysteine Desulfurase. *Biochemistry* **2015,** *54* (31), 4824-33.

41. Eliot, A. C.; Kirsch, J. F., Pyridoxal phosphate enzymes: mechanistic, structural, and evolutionary considerations. *Annu Rev Biochem* **2004,** *73*, 383-415.

42. Toney, M. D., Controlling reaction specificity in pyridoxal phosphate enzymes. *Biochim Biophys Acta* **2011,** *1814* (11), 1407-18.

43. Kim, S.; Park, S., Structural changes during cysteine desulfurase CsdA and sulfur acceptor CsdE interactions provide insight into the trans-persulfuration. *J Biol Chem* **2013,** *288* (38), 27172-80.

44. Blauenburg, B.; Mielcarek, A.; Altegoer, F.; Fage, C. D.; Linne, U.; Bange, G.; Marahiel, M. A., Crystal Structure of Bacillus subtilis Cysteine Desulfurase SufS and Its Dynamic Interaction with Frataxin and Scaffold Protein SufU. *PloS one* **2016,** *11* (7), e0158749.

45. Omi, R.; Kurokawa, S.; Mihara, H.; Hayashi, H.; Goto, M.; Miyahara, I.; Kurihara, T.; Hirotsu, K.; Esaki, N., Reaction mechanism and molecular basis for selenium/sulfur discrimination of selenocysteine lyase. *J Biol Chem* **2010,** *285* (16), 12133-9.

CHAPTER 3

ELUCIDATING THE NOVEL EFFECTOR ROLE OF THE SULFUR SHUTTLE SUFE ON THE CYSTEINE DESULFURASE PROTEIN SUFS IN *E. COLI*

Abstract

PLP-dependent cysteine desulfurases perform the vital function of removing sulfur from cysteine to fulfill many significant roles, such as Fe-S cluster biogenesis. *E. coli* SufS serves this desulfurase function as a member of the Suf pathway responsible for Fe-S cluster synthesis under iron limiting and oxidative stress conditions. However, as a type II cysteine desulfurase, SufS requires the sulfur shuttling protein SufE to optimally function. SufE enhances the activity of SufS up to 50-fold by removing the produced persulfide, but little is understood about the mechanism through which this enhancement results. Previous analysis has indicated conformational shifts occur around the active site cysteine of SufE upon interaction with SufS, indicating a potential allosteric effector role. Here, structural and kinetic analysis reveal a novel effector role exhibited by SufE inducing important modifications around the SufS PLP active site resulting in the accumulation of cysteine desulfurase intermediates as well as elucidating the specific intermediates involved in the process.

Introduction

With the potentially harmful nature of unregulated cellular iron levels, careful management of this vital transition metal is required. A major function of cellular iron is in the construction of iron-sulfur (Fe-S) clusters, which operate as cofactors involved in, but not limited to, electron transport, protein structure, and substrate binding.[1] In *E. coli*, the two systems associated with Fe-S cluster biogenesis are the Isc, iron-sulfur cluster, and Suf, sulfur transport, biogenesis pathways. The Isc pathway dominates Fe-S cluster production under normal growth conditions. Suf, however, manages Fe-S development when the cell incurs oxidative stress or iron-limited environments as this system is better equipped to handle these harsher circumstances.[2, 3] Suf has also been shown to completely replace Isc in *E. coli* when the *isc* genes are deleted.[2, 4, 5]

Despite the distinct conditions in *E. coli* during which Isc and Suf operate, they share proteins of similar functionality.[6, 7] Both possess cysteine desulfurases (IscS and SufS) as well as A-type carrier proteins (IscA and SufA). The cysteine desulfurases IscS and SufS are both pyridoxal-5'-phosphate (PLP)-bound proteins accountable for removing the sulfur from free cellular cysteine to produce both alanine and persulfide capable of supplying the necessary component of Fe-S clusters.[8-11] Although these two desulfurases perform the same function and share structural and sequential homology, key characteristics distinguish IscS and SufS into separate categories designated type I and type II cysteine desulfurases, respectively.[12]

Two major distinguishing features between type I and type II cysteine desulfurases involve amino acid insertions following the active site cysteine (type I) or the PLP-bound lysine (type II). Cysteine desulfurases classified as type I possess an

insertion of 12 residues after the active site cysteine that creates a structural loop including the catalytic cysteine responsible for accepting the persulfide. In *E. coli* IscS, this loop is observed to be partially disordered.[13, 14] Homologues to IscS in other organisms are observed as having large distances between this cysteine and the PLP position, indicating the potential for this loop to swing into and out of the active site during the desulfurase reaction. Additionally, the flexible loop grants type I enzymes the chance to interact with various sulfur acceptor proteins as opposed to a single protein, which is the case with the type II enzymes.[13, 15-17]

The active site cysteine for type II cysteine desulfurases, however, are located on a smaller, more defined fixed loop with minimal mobility restricting the options for sulfur acceptors to one.[18, 19] This difference necessitates the existence of a defined sulfur shuttling protein capable of interacting with the desulfurase.[20] In *E. coli*, SufE and CsdE serve this role for the cysteine desulfurases SufS and CsdA, respectively. The impact of this specificity is so pronounced that *E. coli* SufE has no notable effect when expressed as part of a homologous Suf pathways but enhances *E. coli* SufS activity up to 50-fold.[21, 22] This enrichment appears to stem from a two-step ping-pong reaction in which the cysteine desulfurase reaction is the first stage resulting in alanine release followed by involvement of the sulfur shuttle in performing the transpersulfuration reaction.[23, 24] As determined by Selbach et al., the strong reductant tris(2-carboxyethyl)phosphine (TCEP) further enhances the ability of SufS-SufE to perform the desulfurase activity.[25] The exact manner by which the shuttle influences the process is not fully elucidated, with the function believed to be strictly in enhancing turnover of the reaction. From a structural standpoint, the type II CsdA-CsdE complex may offer insight.

CsdA is a third *E. coli* cysteine desulfurase assisted by the sulfur shuttle CsdE. Kim et al. characterized the structure of the CsdA-CsdE complex.[26] The dimeric CsdA complex was observed with two CsdE monomers bound, each to a separate CsdA. While the interaction resulted in no observable alterations to the CsdA protein or active site, CsdE undergoes prominent structural shifts upon binding. The most substantial change involves the active site cysteine loop moving ~11Å from the initial position in a low access hydrophobic cavity, similar to SufE, potentially enhancing the ability of the active cysteine to perform the transpersulfuration reaction.[26-28] The importance of these findings in relation to the currently uncharacterized SufS-SufE complex structure involve the sequence homology shared between SufS and CsdA (~43%) and SufE and CsdE (~35%). The possibility has been indicated that a similar effect exists in the SufS-SufE complex.[29]

With only recent advances in understanding the precise mechanism by which *E. coli* SufS performs a desulfurase reaction on cysteine, we focus on further mechanistic assignment of this protein alone in addition to analyzing the impact of SufE on the mechanism. This was accomplished using UV-visible spectroscopy combined with stopped-flow rapid mix spectroscopy to analyze both the steady-state and pre-stead-state mechanism adopted by SufS in in the presence and absence of SufE. Furthermore, the use of 5-((((2-Iodoacetyl)amino)ethyl)amino)Naphthalene-1-Sulfonic Acid (IAEDANS) labeling in conjunction with NMR and protein crystallography using crosslinking will provide an evaluation of the structural impact that the sulfur shuttle inflicts onto SufS. Due to the significance of Suf in the viability of various pathogenic bacteria, our work will potentially offer new targets for drug design.

Materials and Methods

Strains and plasmid preparation

SufS, SufS mutants, SufE, and SufE mutants were all expressed using the pET21a vector (Novagen) as previously described.[21] Mutations were built following the QuikChange II site-directed mutagenesis protocol (Agilent) prior to confirmation with sequencing analysis. Transformation of each plasmid into BL21(DE3) cells was performed for expression and purification. All primers and strains are defined in Tables 1 and 2 respectively.

Protein expression and purification

SufS, SufE, and their respective mutants were expressed and purified separately as previously described.[21] Expression was initiated using BL21(DE3) cells grown in Lennox Broth (LB). Cells containing the required vectors (pET21a_SufS and pET21a_SufE) had overnight starter cultures grown in LB with 100 µg/mL ampicillin (Amp) at 37 °C. The starter was then diluted 1:100 into fresh LB Amp and cultured at 37 °C with shaking at 200 rpm to an OD_{600} of 0.5-0.6 prior to induction with 500 µM of IPTG.

For SufS expression, the temperature was dropped to 18 °C and the cells incubated for 18 hours. Following induction, the cells were harvested via centrifugation at 7460 xg for 10 minutes at 4 °C and stored at -80 °C until further use. To purify SufS, harvested cells were resuspended in Q-sepharose loading buffer, which consisted of 25mM Tris-HCl, 10 mM β-mercaptoethanol (βME), at pH 8.0 followed by addition of 1 mM phenylmethylsulfonyl fluoride. Cells were lysed via sonication using two 2-min cycles

Table 3.1 Primer sequences for plasmid construction of *pET21a_sufS*, *pET21a_sufE* and for site-directed mutagenesis to construct *pET21a_sufE C51A*, *pET21a_sufS C364A*

Protein	Primer Sequence
SufS	5'-GAGGGGATCCATGATTTTTTCCGTCGACAA-3' 5'-TGCCCTCGAGTTATCCCAGCAAACGGTGAA-3'
SufE	5'-AGGCCATATGGCTTTATTGCCGGATAA-3' 5'-TCCTGGATCCTTAGCTAAGTGCAGCGGCTT-3'
SufS C364A	5'-CGTACCGGACATCACGCCGCAATGCCATTGATG-3' 5'-CATCAATGGCATTGCGGCGTGATGTCCGGTACG-3'
SufE C51A	5'-CAAAATAGCATTCAGGGCGCACAGAGTCAGGTGTGGATTG-3' 5'-CAATCCACACCTGACTCTGTGCGCCCTGAATGCTATTTTG-3'

Table 3.2. Strains used in this study for storage and expression of proteins

Strain Name	Genotype/characteristics	Source or Reference
BL21(DE3)		Laboratory Strain
DH5α		Laboratory Strain
MB153	DH5α pET21a_sufS Amp^R	
MB155	DH5α pET21a_sufS(C364A) Amp^R	[30]
MB156	DH5α pET21a_sufE Amp^R	
MB156	DH5α pET21a_sufE(C51A) Amp^R	This study
MB157	BL21(DE3) pET21a_sufS Amp^R	
MB159	BL21(DE3) pET21a_sufS(C364A) Amp^R	Blahut [30]
MB160	BL21(DE3) pET21a_sufE Amp^R	
MB160	BL21(DE3) pET21a_sufE(C51A) Amp^R	This study

at 50% amplitude of one second on and 2 seconds off performed with a Branson digital sonifier 450. 1% streptomycin sulfate was administered to the cells followed by centrifugation at 31000 xg for 35 minutes at 4 °C. Purification then proceeded via FPLC using anion exchange (Q-sepharose), hydrophobic interaction (phenyl FF), and gel filtration (Superdex 200) (GE Healthcare) chromatography resins sequentially. A linear gradient from 25 mM Tris-HCl, 10 mM βME, pH 8.0 to 25 mM Tris-HCl, 10 mM βME, pH 8.0, 1 M NaCl was used on the Q-sepharose column. Prior to addition to the phenyl column, ammonium sulfate was added to a final concentration of 1 M in the protein sample. The protein was then eluted using the phenyl FF column with a linear gradient of 25 mM Tris-HCl, pH 8.0, 10 mM βME, 100 mM NaCl, and 1 M ammonium sulfate to 25 mM Tris-HCl, pH 8.0, 10 mM βME. The Superdex200 column was run using 25 mM Tris-HCl, pH 8.0, 10 mM βME, and 150 mM NaCl. Protein purity was measured using SDS-PAGE. SufS was then concentrated with a 10 kDa molecular weight Amicon Ultra concentration filter (Millipore) and frozen in liquid nitrogen prior to storage at -80 °C until further use.

Expression and purification of SufE was completed using a similar protocol to SufS with a few alterations. SufE induction was achieved by adding 500 µM IPTG at 37 °C for 3 hours with 200 rpm shaking. The purification of SufE was performed using anion exchange and gel filtration chromatography with the same buffers as those described for SufS.

Cysteine desulfurase activity assay

Cysteine desulfurase activity in the presence and absence of SufE was evaluated following the protocol used by Dai *et al.*[21] Activity was measured by evaluating the formation of methylene blue. SufS was diluted to 1 µM and SufE diluted to 4 µM using 25 mM Tris-HCl, 150 mM NaCl, pH 7.4. These proteins were incubated together in the sample for 5 min prior to the addition of 2 mM L-cysteine and 2 mM dithiothreitol (DTT) with the final reaction volume being 800 µL. The reaction then proceeded for 10 min before quenching with the addition of 100 µL of 20 mM *N*,*N*-dimethyl-*p*-phenylenediamine sulfate (NNDP) in 7.2 M HCl and 100 µL of 30 mM $FeCl_3$ in 1.2 M HCl. The reaction then proceeded for 30 min in the dark prior to centrifugation at 16000 xg. The methylene blue produced in the supernatant was then measured on a UV-visible spectrophotometer at 670 nm and compared to a standard graph made using Na_2S.

PLP quantification

SufS PLP content was analyzed as previously described. Using 10 mM Tris, pH 8.0, SufS was diluted to ~1.5 mg/mL as part of an 800 µL sample. 5 M NaOH was added to SufS followed by incubation at 75 °C for 10 min. Next, 85 µL of 12 M HCl was added to SufS proceeded by 2 min of centrifugation at 16000 xg with the supernatant transported to a cuvette. Absorbance at 390 nm was recorded with the resulting value analyzed against a free PLP quantification standard line to calculate the amount of PLP per SufS monomer.

UV-visible absorption spectroscopy

An Agilent 8453 UV-Visible absorption spectrophotometer was used to kinetically monitor the spectra of 30 µM WT and C364A SufS in the presence and absence of 60 µM SufE. Varying concentrations of L-cysteine were added to the sample in addition to 2 mM TCEP with kinetic traces measured with 5 second intervals for 1000 seconds. Key wavelengths specifically monitored were 330 nm, 340 nm, 420 nm, and 506 nm.

Stopped-flow absorption spectroscopic analysis

Using an Applied Photophysics Ltd. SX20 stopped-flow spectrophotometer, stopped-flow absorption experiments were performed at 4 °C using a PDA. L-cysteine was prepared with 25 mM Tris-HCl, 150 mM NaCl, pH 8.0, and 4 mM TCEP. Samples of SufS and/or SufE were diluted to 60 µM and 120 µM, respectively, using 25 mM Tris-HCl, 150 mM NaCl, and pH 8.0. Concentrations of cysteine ranging from 800 µM to 2 mM (premix), were mixed 1:1 with 60 µM SufS and 120 µM SufE (premix), and full spectral (PDA) was collected for 1000 seconds.

SufS-bound persulfide identification using IAEDANS

50 nmol of SufS or SufS mutants with/without 200 nmol SufE C51A were incubated for 20 seconds with 400 nmol L-cysteine suspended in 25mM Tris-HCl, 150 mM NaCl, pH 8.0. Then, 300nmol of 1,5-I-AEDANS was added to the reaction and allowed to proceed for 30 minutes. In order to remove excess 1,5-I-AEDANS, a 10 kDa Amicon Ultra centrifugal filter was used with the sample washed in the previously mentioned buffer three times before bringing the volume back to 1 mL with the buffer.

The 1 mL sample was then split into two 500 uL aliquots. One aliquot was treated with DTT at a concentration of 5 mM while the other sample treated strictly with an equal volume of buffer to serve as a control. Samples treated with DTT were incubated for 30 minutes and had any formed persulfide (disulfide bond) reduced resulting in a loss of the fluorescent compound. Removal of the unbound IAEDANS was achieved by again using a 10 kDa Amicon Ultra filter and washing the sample three times with buffer before finally bringing the final concentration to 500uL. Protein was quantified via Bradford assay and the relative persulfide percentage determined using a BioTek Synergy H1 Hybrid Reader with λ_{ex} of 336 nm and λ_{em} of 490 nm.[31]

Results

WT and C364A SufS transition through different quinonoid intermediates during the desulfurase reaction.

During the pre-steady state mechanistic phases previously suggested by Blahut et al., the initial internal aldimine phase of the PLP bound to SufS progresses through Cys-aldimine and Cys-ketimine intermediates during persulfide generation.[30] Earlier investigation into PLP cysteine desulfurases has suggested the formation of a quinonoid intermediate between these two stages but no absorbance feature around 500 nm was previously visualized during stopped-flow analysis on *E. coli* SufS.[32, 33] As illustrated in Figure 3.1, both WT and C364A provide an absorption signal around 506 nm when treated with 500 μM L-Cys for extended time periods. The new WT species initially absorbs around 512 nm after 30 minutes before shifting to 500 nm upon decay at 180 minutes (Figure 3.1). Although quinonoid species absorb in this region, the mechanism by which PLP-dependent cysteine desulfurase occurs offers two possible quinonoid

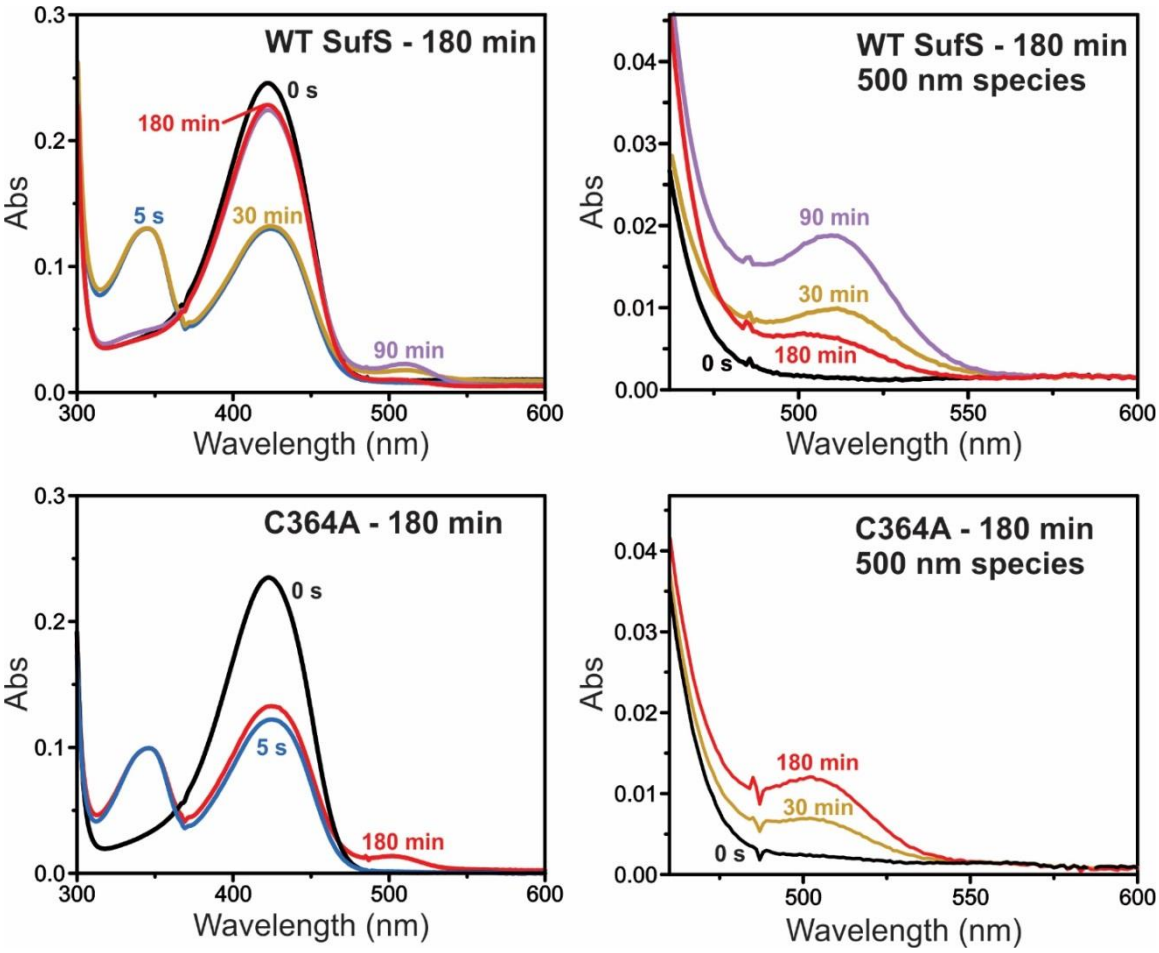

Figure 3.1. UV-visible absorption spectra for WT (Top) and C364A (Bottom) SufS treated in the presence of 2 mM TCEP with 500 μM L-cysteine. Spectra were measured immediately after addition of L-cys and up to 180 minutes after the addition while sitting at room temperature. Spectra on the right illustrate a zoomed in view of the 500 nm species.

intermediates, the Cys- and Ala-quinonoids.[32, 33] With two potential sources of absorption in the 500 nm region, multiple factors must contribute to the assignment. Addition of lower cysteine concentration at sub stoichiometric levels to WT SufS results in a reversible reaction after formation of the ketimine intermediate with no observable signal around 512 nm, while previous work showed that higher cysteine concentrations prevent this reversibility. Also, considering the ability of WT SufS to pass through the entire desulfurase reaction, the 512 nm species more likely corresponds to the second quinonoid intermediate (Ala-quinonoid).

After treatment with excess cysteine, C364A generates an absorbance at 506 nm that does not shift after 180 minutes. Contrary to the cysteine desulfurase activity of WT SufS alone, the C364A mutant fails to generate persulfide due to the lack of the cysteine responsible for accepting sulfur. Previous structural work determined that this mutant stabilizes in the Cys-aldimine conformation, while kinetic analysis supported a biphasic nature indicative of the Cys-ketimine conformation.[30] Decreasing the amount of cysteine in the reaction (Figure 3.2) reveals an increased accumulation of the 506 nm intermediate. The suggestion that C364A is capable of reaching Cys-ketimine but reverts back to the aldimine over time is supported by the increased amount of the potential Cys-quinonoid when considering the reduction in cysteine to drive the reaction forward. When combining this data with the perturbed absorbance in comparison to WT SufS, it is reasonable that C364A generates the Cys-quinonoid absorbing at 506 nm while WT SufS passes through the Ala-quinonoid while producing persulfide.

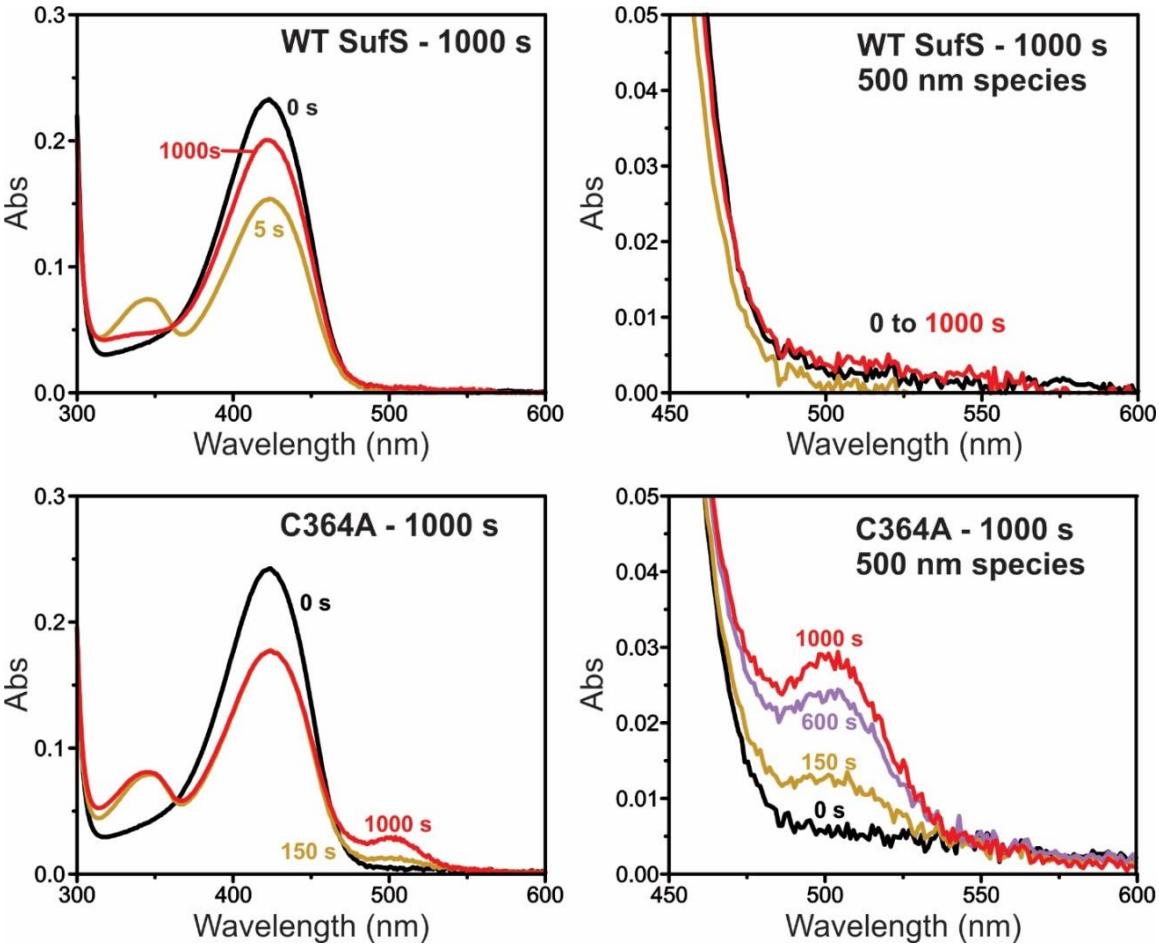

Figure 3.2. UV-visible absorption spectra for WT (Top) and C364A (Bottom) SufS treated with varying concentrations of L-Cys (60 μM for WT and 200 μM for C364A) in the presence of 2 mM TCEP. Scans were recorded every 5 seconds for 1000 seconds total with select spectra shown. Spectra on the right illustrate a zoomed in view of the 500 nm species.

Besides enhancing cysteine desulfurase activity through sulfur shuttling, SufE allosterically activates SufS through a previously undefined effector role.

In addition to SufS alone, the influence of SufE on the cysteine desulfurase mechanism has not been fully elucidated. Initial UV-visible absorption analysis of 30 µM SufS with 60 µM SufE in the presence of 500 µM L-cysteine and 2 mM TCEP (to drive turnover) revealed accumulation of several formerly unseen species that will be covered in the upcoming paragraph. The influence of SufE on formation of the intermediates as opposed to strictly removing the sulfur, which should not influence intermediate formation in the first half of the ping-pong reaction, indicates a potential effector role for the protein.

Previous pre-steady state kinetic analysis was conducted without SufE or a strong reductant in order to prevent SufS from proceeding through the transpersulfuration step. Here we added 4 mM TCEP to the syringe containing cysteine and mixed 1:1 with SufS resulted in the formation of two previously uncharacterized species as demonstrated in Figure 3.3. The first at ~313 nm and the second at ~500 nm. As previously mentioned, the 500 nm species likely corresponds to the Ala-quinonoid intermediate due to the distinct wavelength at which quinonoids absorb, although the 313 nm species is difficult to assign.

Upon addition of SufE to the experiment, several more states are observed with an increased accumulation at 313 nm as well as the quinonoid at 506 nm. Additionally, the 420 nm species demonstrates the previously observed red shift to around 423 nm at the start of the reaction. However, comparing the line in Figure 3.4 at 421 nm to all the peaks at the same wavelength reveals a blue shift to 418 nm after the formation of the 423 nm

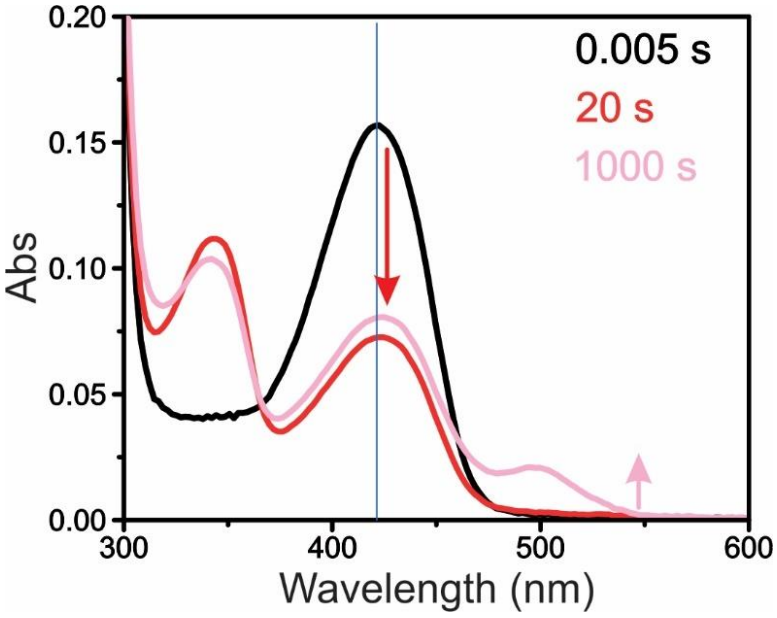

Figure 3.3. Stopped-flow analysis of 30 μM WT SufS (post-mix) mixed with 1000 μM L-Cys in the presence of 2 mM TCEP. Absorbance spectra at various times were collected for 1000 seconds at 4 °C with select time points displayed. The line runs through 421 nm.

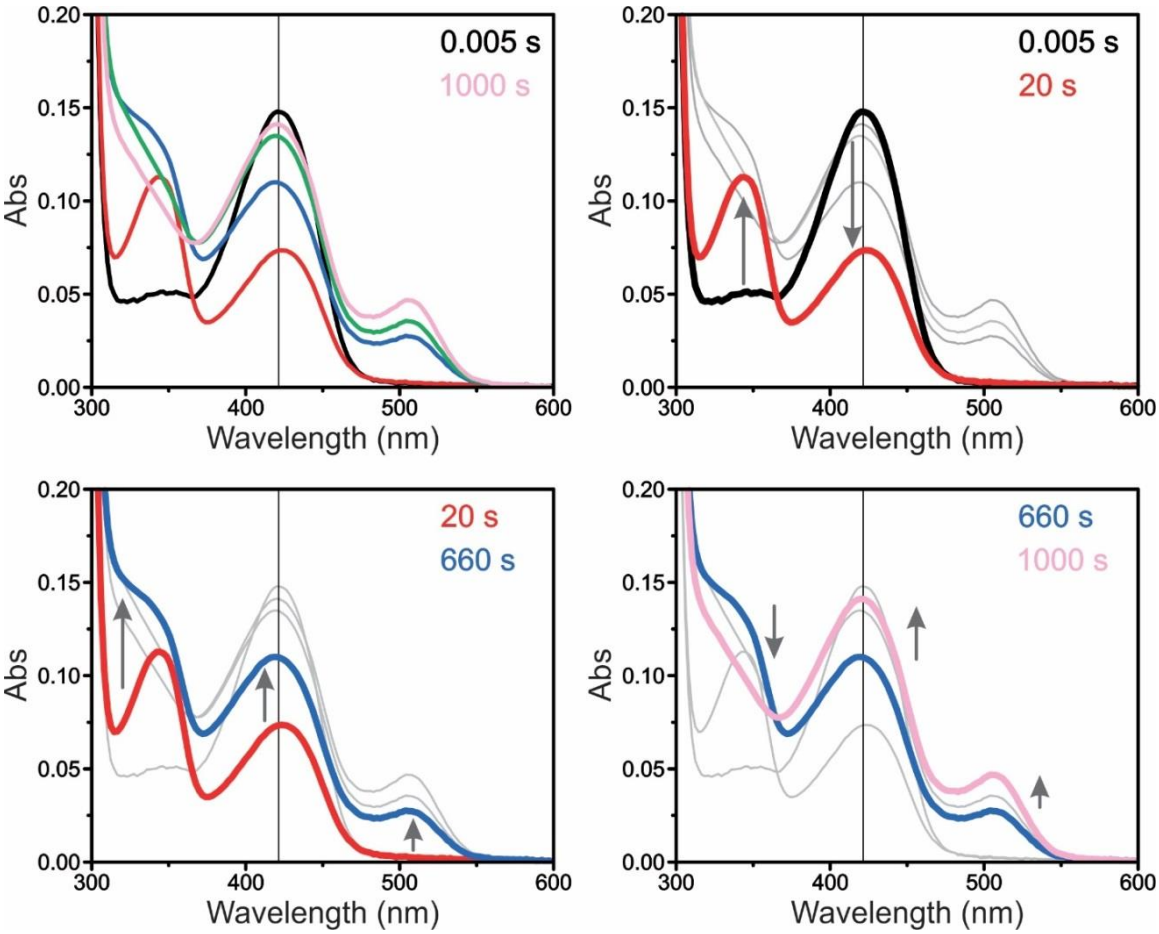

Figure 3.4. Stopped-flow analysis of 30 μM WT SufS (post-mix) with 60 μM WT SufE mixed with varying concentrations of L-Cys in the presence of 2 mM TCEP. Absorbance spectra at various times were collected for 1000 seconds at 4 °C with select time points displayed. The line runs through 421 nm.

species. Analysis of the 313, 340, 420, and 506 nm absorbance over 1000 seconds using stopped-flow as shown in Figure 3.4 and 3.5 reveals the order of formation as the 340 nm, 313 nm, 418 nm, and the 506 nm species last. Assignment of the species generated corresponding to each of these wavelengths is the primary objective with the proposed designations illustrated in Figure 3.6.

At 340 nm, the resulting Cys-ketimine was already observed in studying SufS alone by Blahut et al. However, the next absorbance max around 313 nm has yet to be vetted.[30] This species may result from at least two intermediates absorbing in the same region and, based on the resulting spectra illustrated at various cysteine concentrations over time, accumulates to a greater extent with increasing cysteine concentration, indicating that either this stage is cysteine dependent or the phase before depends on cysteine (Figure 3.5). Due to the region in which it absorbs, the 313 nm species likely corresponds to either the Ala-eneamine or the Ala-ketimine species, or potentially both (Figure 3.6).

The third previously unobserved intermediate to accumulate after cysteine addition shown in Figure 3.4 likely occurs as a combination of two species resulting from the separate PLP sites. The initial absorbance around 420 nm representative of the internal aldimine proceeds through a slight red shift upon addition of L-cysteine to about 423 nm, which was previously characterized.[30] After the formation of the Cys-aldimine and Cys-ketimine species where the 420 nm is at a minimum, however, a slight blue shift to around 418 nm is apparent with a maximum around 660 seconds when treated with 1000 µM L-cysteine. The 423 nm species potentially remains contributing to this

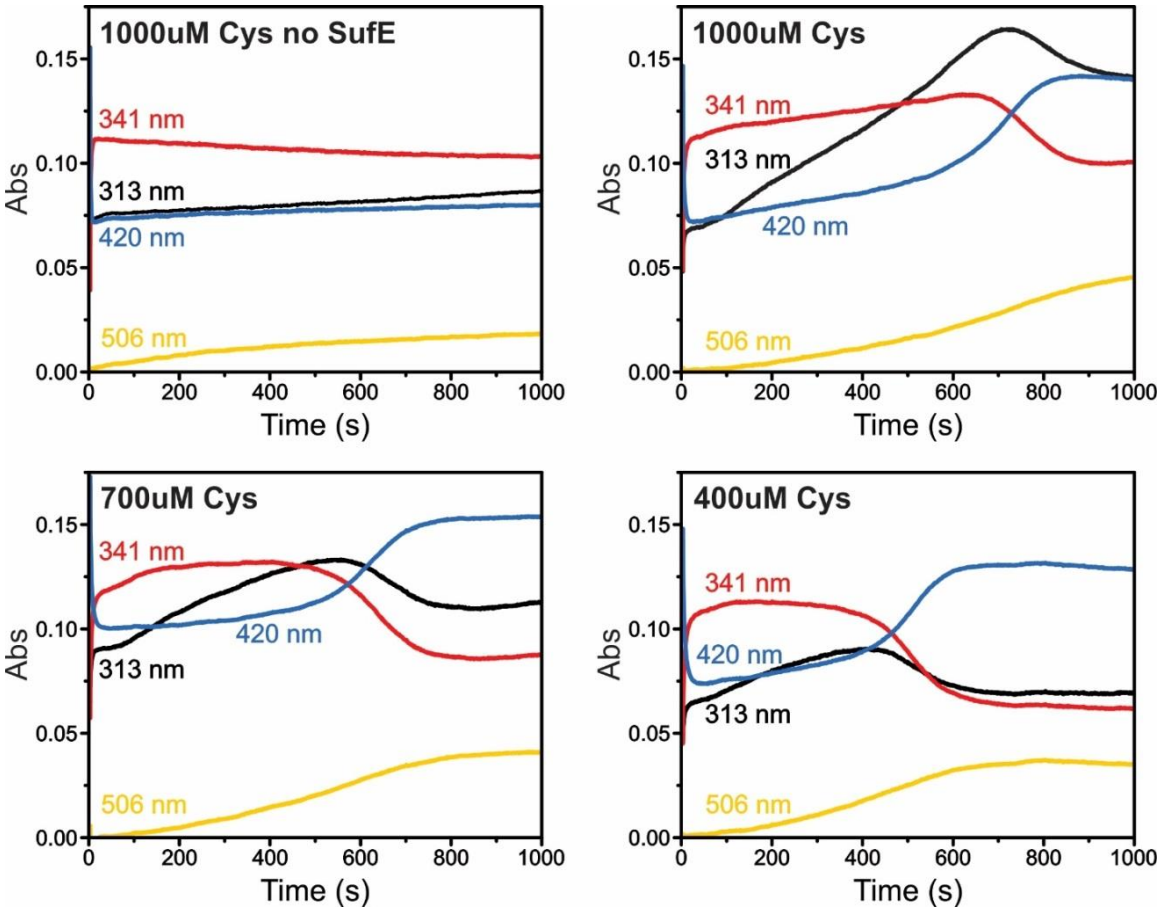

Figure 3.5. Stopped-flow analysis of 30 μM WT SufS (post-mix) without/with 60 μM WT SufE mixed with varying concentrations of L-Cys in the presence of 2 mM TCEP. Absorbance spectra versus time were collected for 1000 seconds at 4 °C with select time points displayed.

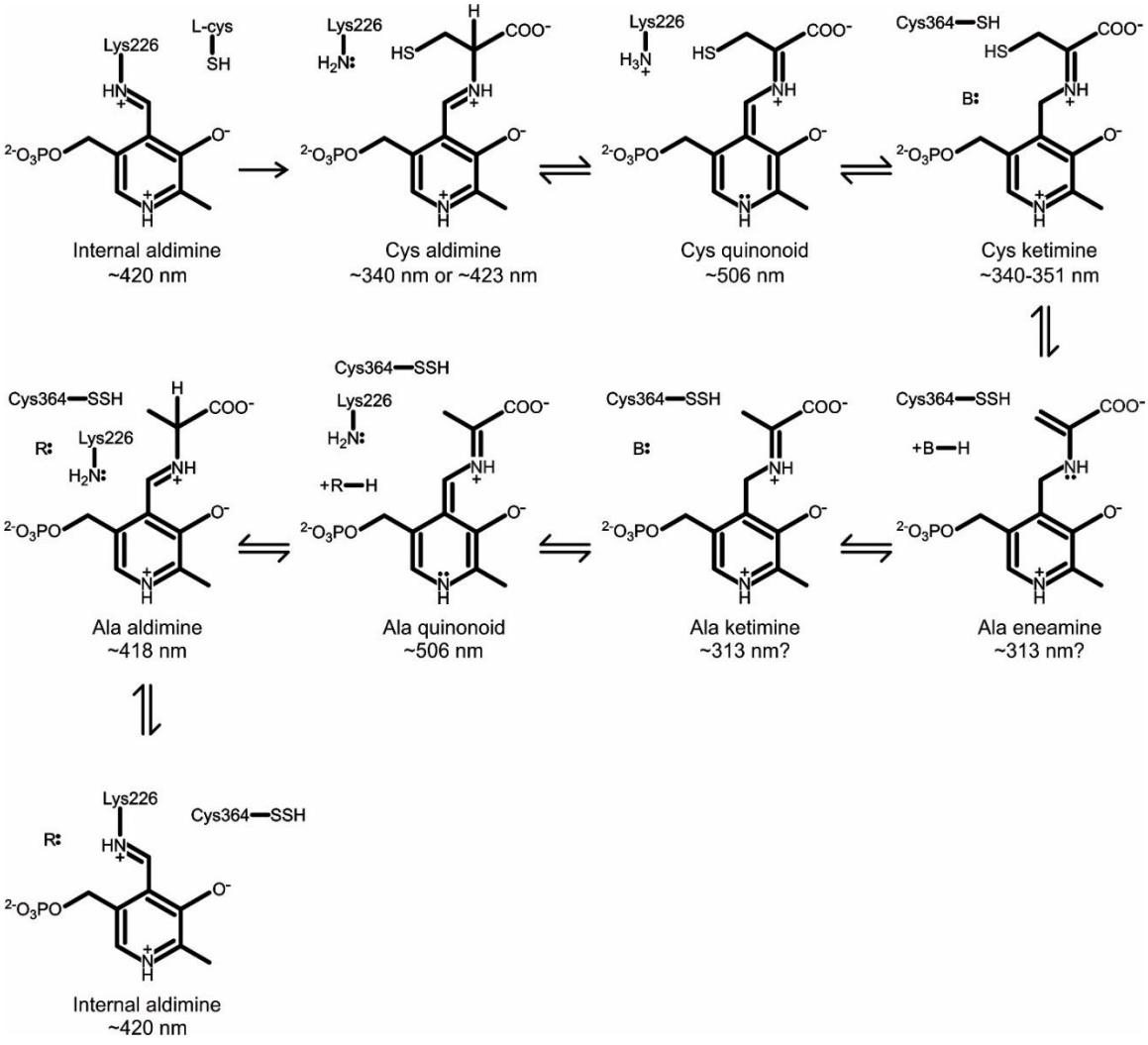

Figure 3.6. Scheme by which SufS performs cysteine desulfurase activity. H123A, which functions in the proton transfer, is represented as B, while a second uncharacterized proton transfer source is labeled as R.

absorbance, but the perturbation is likely a product of the generation of the Ala-aldimine species.

Finally, the quinonoid displays a max absorbance around 506 nm after 1000 seconds, showing a spectral perturbation compared to the previously observed 512 nm and 500 nm (Figure 3.4). To further confirm that this is indeed the Ala-quinonoid as opposed to the Cys-quinonoid, the plot of absorbance versus time reveals that this species accumulates after at least 700 seconds following the other observed intermediates. Due to the Cys-quinonoid forming prior to the 340 nm Cys-ketimine species that develops in the first 5 seconds, the Cys-quinonoid can be ignored as the potential cause for the 506 nm absorbance.

To further characterize this influence, WT SufS was mixed with SufE C51A and SufS C364A mixed with WT SufE to examine specific steps within the overall reaction. The spectra remained similar to those generated by SufS alone with the final visible species around 340 nm, likely the Cys-ketimine, after 1000 seconds. By removing the two primary amino acids through which the persulfide is transferred, SufS C364 and SufE C51, only interactive binding between the two proteins could impact the desulfurase reaction. The resulting spectra being comparable to SufS only indicates that the C51 of SufE is required to alter the mechanism with the impacted stages occurring after the formation of the Cys-ketimine species around 340 nm. Whether SufE C51 is involved in separate uncharacterized reactions with SufS has yet to be determined.

Addition of SufE also enhances persulfide formation on SufS

Two vital amino acids required for SufS cysteine desulfuration to occur and be enhanced by SufE are SufS C364, where the persulfide forms on SufS, and SufE C51, the cysteine responsible for accepting the persulfide. To analyze the formation and enhancement of persulfide on SufS C364, SufE C51A was used as it would bestow the potential enhancing effects on SufS without removing the persulfide. Quantification of the persulfide produced on C364 involved the use of 1,5-I-AEDANS, which is a fluorescent alkylating agent capable of binding exposed thiols or persulfide sulfurs (Figure 3.7). Examination of SufS persulfide formation in the presence and absence of SufE C51A was performed by mixing the two proteins followed by cysteine addition. IAEDANS was then added to the reaction to interact with the sulfur targets followed by persulfide reduction using DTT. As shown in Figure 3.8, formation of a persulfide on C364 results in a DTT cleavable disulfide bond leading to the IAEDANS being cleaved, which means higher fluorescence corresponds to lower persulfide generation. SufS C364A was used as a control for calculating background alkylation with SufE C51A. By comparing the results for SufS in the presence and absence of SufE C51A against the background species, it was determined that SufS alone possessed approximately 62.4% of C364 bound to persulfide. The presence of SufE C51A increased the percent bound to about 91.1% (Figure 3.8).[31] This result illustrates the ability of SufE to allosterically enhance persulfide generation without shuttling sulfur as the presence of the mutant SufE increased the abundance of persulfurated C364 by approximately 50%.

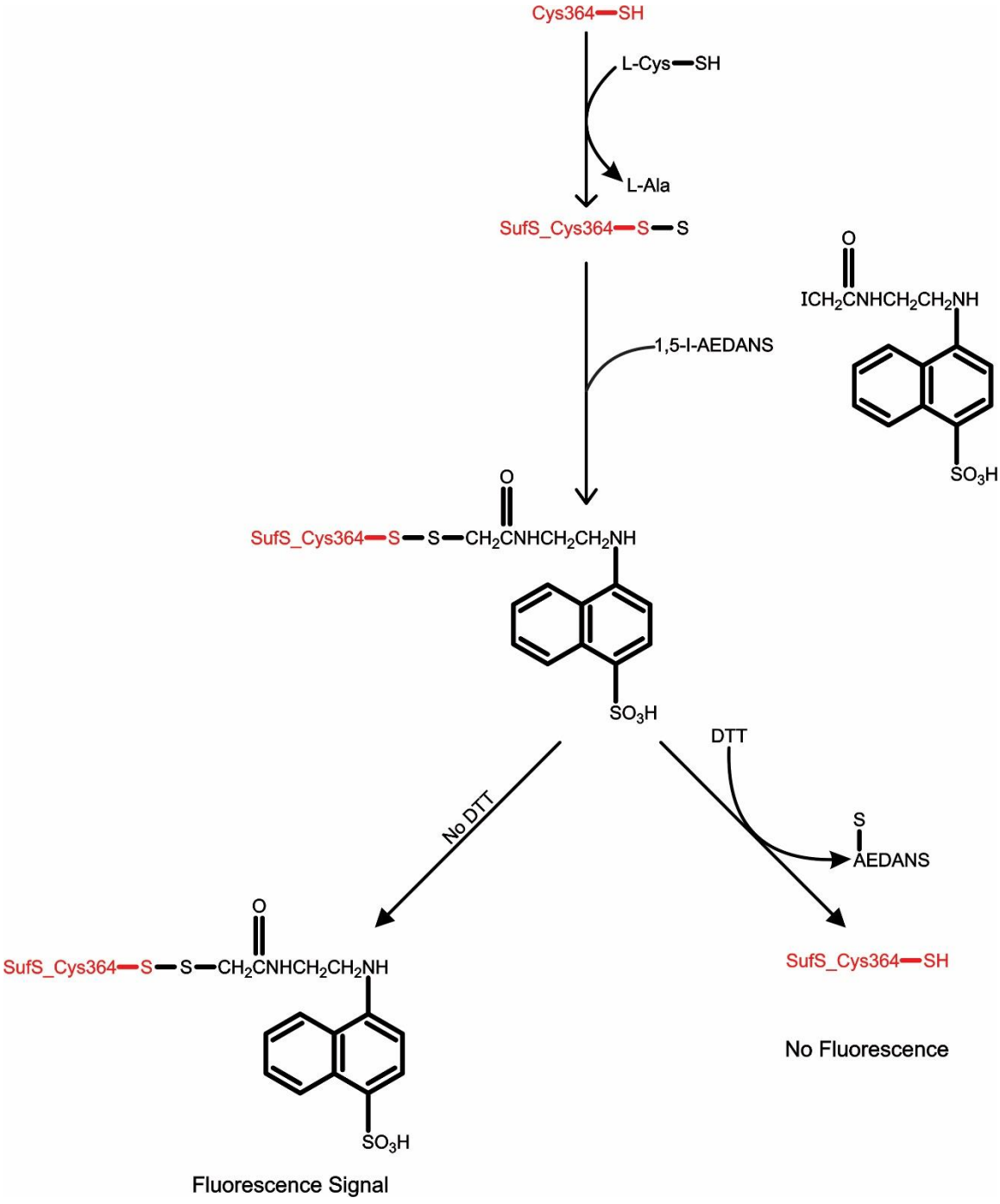

Figure 3.7. Scheme by which IAEDANS interacts to elicit fluorescent response.

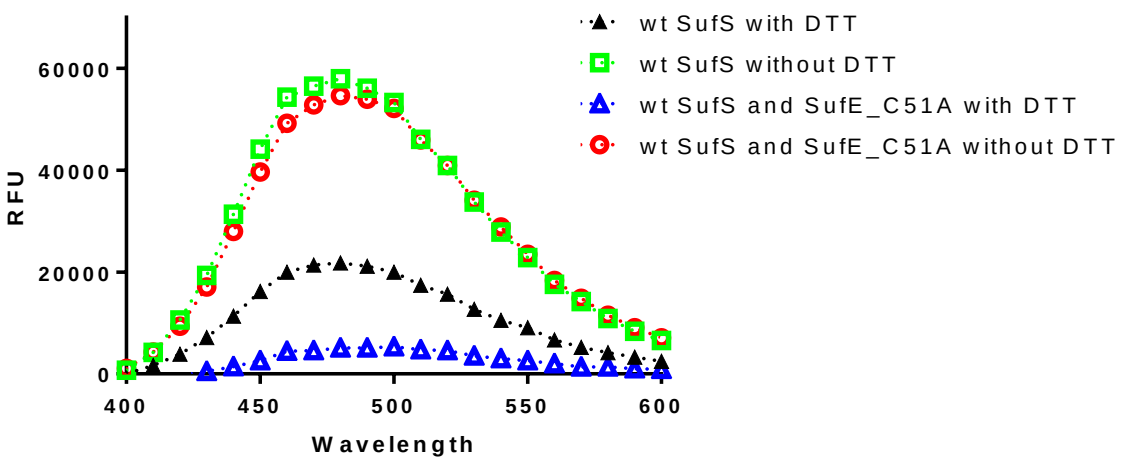

Figure 3.8 Fluorescence spectrum of SufS and L-Cys with/without SufE C51A. 50 nmol WT SufS with or without 50 nmol SufE C51A is incubated with 400 nmol L-cysteine prior to measuring SufS-bound persulfide. Increased fluorescence indicates decreased persulfide formation.[31]

Discussion

The impact of the sulfur shuttle SufE is not restricted to enhancing the cysteine desulfurase activity of SufS but operates as an effector performing a novel function during the mechanism. Previous HDX-MS analysis suggested that SufE interaction with SufS resulted in allosteric changes involved in influencing catalysis by SufS.[29, 34] As Figures 3.4 and 3.5 indicate, drastic increases in accumulation of the 313 nm and the 506 nm species result from addition of SufE and TCEP in addition to a previously uncharacterized blue shift around 420 nm. Without SufE, the 313 nm intermediate appears, although at much lower levels as is also the case with the species around 506 nm. However, without SufE, this conformation absorbs around 500 nm instead of 506 nm. This red shift with the addition of SufE and TCEP supports a perturbation of this structure that likely corresponds to the Ala-quinonoid intermediate due to the wavelength at which it absorbs combined with the late formation in comparison to the other intermediates. The fluctuating absorbance around 420 nm creates some difficulty as a mix of species likely contributes with one being the regenerated internal aldimine resulting late in the cycle. The blue shifted 418 nm mixed species may also result from the formation of the Ala-aldimine intermediate as PLP aldimines tend to absorb around 420 nm. Finally, despite likely resulting from another mix of species, the 313 nm intermediate potentially corresponds to either the Ala-ketimine or the Ala-eneamine as ketimines absorb around 340 nm but ruling out the potential for the eneamine is not yet possible.

The identification of an allosteric activator role for SufE as opposed to only serving the function of enhancing SufS turnover opens a novel branch of type II cysteine

desulfurase research. Other observable modifications to SufS may include structural changes to the active site or other uncharacterized intermediates. While the scope of this work focuses on the *E. coli* pathway, the potential exists for similar effector roles to occur in the Suf pathway of other organisms such as *M. tuberculosis* in which Suf is the only Fe-S biogenesis pathway. Further elucidation of the effector function can potentially contribute to the recognition of other intermediates as potential inhibitory targets for drug design.

In addition to the effector role of SufE, the SufS mutant C364A indicates the potential importance of C364 to stabilizing the Cys-ketimine conformation. The lack of cysteine at this location resulted in the apparent reversion of Cys-ketimine to Cys-aldimine, which was the observed form using X-ray crystallography. The most insightful aspect of the spectra involved the generation of the species at 506 nm most likely representative of the proposed Cys-quinonoid species that exists between the aldimine and ketimine structures. Due to the importance of C364 to the desulfurase mechanism, we can suggest that this quinonoid is the first of two formed during the process. Additionally, the accumulation at 506 nm illustrates the path by which the Cys-aldimine becomes the Cys-ketimine.

Further support for the effector role of SufE is established by the IAEDANS experiment conveying an increase in persulfide generation in the presence of SufE C51A, which lacks the ability to shuttle sulfur. If the sole function of SufE with regards to SufS was to abstract the available sulfur, then this mutant would not alter persulfide formation. However, the diminished fluorescence represents enhanced persulfide production indicative of a secondary effect from SufE.

Future Directions

Due to limited time with this project, not all desired experiments have been performed to vet the impact of SufE on both the structure and activity of SufS during the desulfurase reaction. Structural evaluation of the CsdA-CsdE complex by Kim et al. propositions an impact on the SufE homologue CsdE leading to a potential effect during the interaction between SufS and SufE. Unfortunately, the complex formed by SufS and SufE does not provide the long-term stability required for X-ray crystallographic analysis like CsdA-CsdE, despite the relatively tight K_d of 3.5μM. To overcome this obstacle, we will hopefully use crosslinking with two-step coupling via 1-ethyl-3-(3-dimethylaminopropyl)carbodiimide hydrochloride (EHS) combined with N-hydroxysuccinimide (NHS). The crosslinked complex can hopefully then be evaluated using X-ray crystallography to identify the potential alterations experienced by both proteins both with and without soaking in L-cysteine.

In addition to crystallography, phosphorous-31 nuclear magnetic resonance (NMR) will closely monitor the SufS-PLP active site in both the presence and absence of SufE. This experiment will permit close examination of structural alterations proximal to the PLP phosphorous. In combination with crystallography, this NMR will help resolve if SufE effects the active site around PLP further exhibiting an effector role in the formation of the SufS-SufE complex.

Finally, further kinetic analysis must be performed using stopped-flow to evaluate any potential impact on the pre-steady state kinetics with the addition of both SufE and TCEP. Additionally, a control in which TCEP is mixed with WT SufS and WT SufE must also be performed to make sure that the observed spectroscopic changes are not

altered or induced by TCEP with its only function being reducing the persulfide to turn over the reaction.

The lack of true mechanistic understanding of type II cysteine desulfurases offers a pressing need to identify the intermediates of the reaction as well as the impact of the sulfur shuttling protein on the mechanism. With the experiments performed until now, we have confirmed the quinonoid in addition to three other intermediates with enhanced accumulation resulting from the addition of SufE. Hopefully, the future structural analysis will enable verification on whether the sulfur shuttling protein simply obtains the sulfur, impacts the general structure of SufS, or affects the active site PLP to enhance cysteine desulfurase activity.

References

1. Fontecave, M., Iron-sulfur clusters: ever-expanding roles. *Nat Chem Biol* **2006,** *2* (4), 171-4.

2. Outten, F. W.; Djaman, O.; Storz, G., A suf operon requirement for Fe-S cluster assembly during iron starvation in Escherichia coli. *Mol Microbiol* **2004,** *52* (3), 861-72.

3. Nachin, L.; Loiseau, L.; Expert, D.; Barras, F., SufC: an unorthodox cytoplasmic ABC/ATPase required for [Fe-S] biogenesis under oxidative stress. *EMBO J* **2003,** *22* (3), 427-37.

4. Takahashi, Y.; Tokumoto, U., A third bacterial system for the assembly of iron-sulfur clusters with homologs in archaea and plastids. *J Biol Chem* **2002,** *277* (32), 28380-3.

5. Tokumoto, U.; Kitamura, S.; Fukuyama, K.; Takahashi, Y., Interchangeability and distinct properties of bacterial Fe-S cluster assembly systems: functional replacement of the isc and suf operons in Escherichia coli with the nifSU-like operon from Helicobacter pylori. *J Biochem* **2004,** *136* (2), 199-209.

6. Py, B.; Barras, F., Building Fe-S proteins: bacterial strategies. *Nat Rev Microbiol* **2010,** *8* (6), 436-46.

7. Py, B.; Moreau, P. L.; Barras, F., Fe-S clusters, fragile sentinels of the cell. *Curr Opin Microbiol* **2011,** *14* (2), 218-23.

8. Ayala-Castro, C.; Saini, A.; Outten, F. W., Fe-S cluster assembly pathways in bacteria. *Microbiol Mol Biol Rev* **2008,** *72* (1), 110-25, table of contents.

9. Roche, B.; Aussel, L.; Ezraty, B.; Mandin, P.; Py, B.; Barras, F., Iron/sulfur proteins biogenesis in prokaryotes: formation, regulation and diversity. *Biochim Biophys Acta* **2013,** *1827* (3), 455-69.

10. Johnson, D. C.; Dean, D. R.; Smith, A. D.; Johnson, M. K., Structure, function, and formation of biological iron-sulfur clusters. *Annu Rev Biochem* **2005,** *74*, 247-81.

11. Fontecave, M.; Ollagnier-de-Choudens, S., Iron-sulfur cluster biosynthesis in bacteria: Mechanisms of cluster assembly and transfer. *Arch Biochem Biophys* **2008,** *474* (2), 226-37.

12. Mihara, H.; Kurihara, T.; Yoshimura, T.; Soda, K.; Esaki, N., Cysteine sulfinate desulfinase, a NIFS-like protein of Escherichia coli with selenocysteine lyase and cysteine desulfurase activities. Gene cloning, purification, and characterization of a novel pyridoxal enzyme. *J Biol Chem* **1997,** *272* (36), 22417-24.

13. Shi, R.; Proteau, A.; Villarroya, M.; Moukadiri, I.; Zhang, L.; Trempe, J. F.; Matte, A.; Armengod, M. E.; Cygler, M., Structural basis for Fe-S cluster assembly and tRNA thiolation mediated by IscS protein-protein interactions. *PLoS Biol* **2010,** *8* (4), e1000354.

14. Cupp-Vickery, J. R.; Urbina, H.; Vickery, L. E., Crystal structure of IscS, a cysteine desulfurase from Escherichia coli. *J Mol Biol* **2003,** *330* (5), 1049-59.

15. Smith, A. D.; Agar, J. N.; Johnson, K. A.; Frazzon, J.; Amster, I. J.; Dean, D. R.; Johnson, M. K., Sulfur transfer from IscS to IscU: the first step in iron-sulfur cluster biosynthesis. *J Am Chem Soc* **2001,** *123* (44), 11103-4.

16. Ikeuchi, Y.; Shigi, N.; Kato, J.; Nishimura, A.; Suzuki, T., Mechanistic insights into sulfur relay by multiple sulfur mediators involved in thiouridine biosynthesis at tRNA wobble positions. *Mol Cell* **2006,** *21* (1), 97-108.

17. Kambampati, R.; Lauhon, C. T., Evidence for the transfer of sulfane sulfur from IscS to ThiI during the in vitro biosynthesis of 4-thiouridine in Escherichia coli tRNA. *J Biol Chem* **2000,** *275* (15), 10727-30.

18. Fujii, T.; Maeda, M.; Mihara, H.; Kurihara, T.; Esaki, N.; Hata, Y., Structure of a NifS homologue: X-ray structure analysis of CsdB, an Escherichia coli counterpart of mammalian selenocysteine lyase. *Biochemistry* **2000,** *39* (6), 1263-73.

19. Lima, C. D., Analysis of the E. coli NifS CsdB protein at 2.0 A reveals the structural basis for perselenide and persulfide intermediate formation. *J Mol Biol* **2002,** *315* (5), 1199-208.

20. Outten, F. W.; Wood, M. J.; Munoz, F. M.; Storz, G., The SufE protein and the SufBCD complex enhance SufS cysteine desulfurase activity as part of a sulfur transfer pathway for Fe-S cluster assembly in Escherichia coli. *J Biol Chem* **2003,** *278* (46), 45713-9.

21. Dai, Y.; Outten, F. W., The E. coli SufS-SufE sulfur transfer system is more resistant to oxidative stress than IscS-IscU. *FEBS Lett* **2012,** *586* (22), 4016-22.

22. Loiseau, L.; Ollagnier-de-Choudens, S.; Nachin, L.; Fontecave, M.; Barras, F., Biogenesis of Fe-S cluster by the bacterial Suf system: SufS and SufE form a new type of cysteine desulfurase. *J Biol Chem* **2003,** *278* (40), 38352-9.

23. Selbach, B.; Earles, E.; Dos Santos, P. C., Kinetic analysis of the bisubstrate cysteine desulfurase SufS from Bacillus subtilis. *Biochemistry* **2010,** *49* (40), 8794-802.

24. Kim, D.; Singh, H.; Dai, Y.; Dong, G.; Busenlehner, L. S.; Outten, F. W.; Frantom, P. A., Changes in Protein Dynamics in Escherichia coli SufS Reveal a Possible Conserved Regulatory Mechanism in Type II Cysteine Desulfurase Systems. *Biochemistry* **2018,** *57* (35), 5210-5217.

25. Selbach, B. P.; Pradhan, P. K.; Dos Santos, P. C., Protected sulfur transfer reactions by the Escherichia coli Suf system. *Biochemistry* **2013,** *52* (23), 4089-96.

26. Kim, S.; Park, S., Structural changes during cysteine desulfurase CsdA and sulfur acceptor CsdE interactions provide insight into the trans-persulfuration. *J Biol Chem* **2013,** *288* (38), 27172-80.

27. Liu, G.; Li, Z.; Chiang, Y.; Acton, T.; Montelione, G. T.; Murray, D.; Szyperski, T., High-quality homology models derived from NMR and X-ray structures of E. coli proteins YgdK and Suf E suggest that all members of the YgdK/Suf E protein family are enhancers of cysteine desulfurases. *Protein Sci* **2005,** *14* (6), 1597-608.

28. Goldsmith-Fischman, S.; Kuzin, A.; Edstrom, W. C.; Benach, J.; Shastry, R.; Xiao, R.; Acton, T. B.; Honig, B.; Montelione, G. T.; Hunt, J. F., The SufE sulfur-acceptor protein contains a conserved core structure that mediates interdomain interactions in a variety of redox protein complexes. *J Mol Biol* **2004,** *344* (2), 549-65.

29. Dai, Y.; Kim, D.; Dong, G.; Busenlehner, L. S.; Frantom, P. A.; Outten, F. W., SufE D74R Substitution Alters Active Site Loop Dynamics To Further Enhance SufE Interaction with the SufS Cysteine Desulfurase. *Biochemistry* **2015,** *54* (31), 4824-33.

30. Blahut, M.; Wise, C.E.; Dong, G.; Bruno, M.; Makris, T.; Frantom, P.; Dunkle, J.; Outten, F.W., Direct observation of intermediates in the SufS cysteine desulfurase reaction reveals functional roles of conserved active-site residues. *J Biol Chem* **2019,** *In press*.

31. Dong, G. Characterization of SufS and SufE of Suf Pathway for Fe-S Cluster Assembly in Escherichia Coli. University of South Carolina, 2017.

32. Zheng, L.; White, R. H.; Cash, V. L.; Dean, D. R., Mechanism for the desulfurization of L-cysteine catalyzed by the nifS gene product. *Biochemistry* **1994,** *33* (15), 4714-20.

33. Behshad, E.; Bollinger, J. M., Jr., Kinetic analysis of cysteine desulfurase CD0387 from Synechocystis sp. PCC 6803: formation of the persulfide intermediate. *Biochemistry* **2009,** *48* (50), 12014-23.

34. Singh, H.; Dai, Y.; Outten, F. W.; Busenlehner, L. S., Escherichia coli SufE sulfur transfer protein modulates the SufS cysteine desulfurase through allosteric conformational dynamics. *J Biol Chem* **2013,** *288* (51), 36189-200.

CHAPTER 4

CONSERVED CYSTEINE RESIDUES ARE NECESSARY FOR NICKEL-INDUCED ALLOSTERIC REGULATION OF THE METALLOREGULATORY PROTEIN YQJI (NFER) IN *E. COLI*[1]

[1] Blahut, M., Dzul, S., Wang, S., Kandegedara, A., Grossoehme, N.E., Stemmler, T., Outten, F.W. Conserved cysteine residues are necessary for nickel-induced allosteric regulation of the metalloregulatory protein YqjI (NfeR) in *E. coli*. *Journal of Inorganic Biochemistry* **2018**, 184, 123-133.

Abstract

Transition metal homeostasis is necessary to sustain life. First row transition metals act as cofactors within the cell, performing vital functions ranging from DNA repair to respiration. However, intracellular metal concentrations exceeding physiological requirements may be toxic. In *E. coli*, the YqjH flavoprotein is thought to play a role in iron homeostasis. YqjH is transcriptionally regulated by the ferric uptake regulator and a newly discovered regulator encoded by *yqjI*. The apo-form of YqjI is a transcriptional repressor of both the *yqjH* and *yqjI* genes. YqjI repressor function is disrupted upon binding of nickel. The YqjI N-terminus is homologous to nickel-binding proteins, implicating this region as a nickel-binding domain. Based on function, *yqjI* and *yqjH* should be renamed Ni-responsive Fe-uptake regulator (*nfeR*) and Ni-responsive Fe-uptake flavoprotein (*nfeF*), respectively. X-ray Absorption Spectroscopy was employed to characterize the nickel binding site(s) within YqjI. Putative nickel binding ligands were targeted by site-directed mutagenesis and resulting variants were analyzed in vivo for repressor function. Isothermal titration calorimetry and competitive binding assaywere used to further quantify nickel interactions with wild-type YqjI and its mutant derivatives. Results indicate plasticity in the nickel binding domain of YqjI. Residues C42 and C43 were found to be required for in vivo response of YqjI to nickel stress, though these residues are not required for in vitro nickel binding. We propose that YqjI may contain a vicinal disulfide bond between C42 and C43 that is important for nickel-responsive allosteric interactions between YqjI domains.

Introduction

Effective homeostatic management of iron, a biologically-abundant transition metal, is essential for most organisms. Iron is a cofactor for proteins with roles in metabolism (ie. cellular respiration and photosynthesis), dioxygen storage and transport, and redox sensing and signaling mechanisms. Iron primarily exists in ferrous (Fe(II)) and ferric (Fe(III)) oxidation states. Fe(III), the predominant oxidation state in aerobic environments, has limited solubility at neutral pH making iron acquisition difficult for many organisms. Under conditions of limited iron availability, microbial organisms can produce iron chelators known as siderophores to facilitate metal solubility and transport into the cell.[2] However, excess Fe(II) in the cell can lead to redox cycling with hydrogen peroxide to generate radical species that can oxidize lipids, DNA, and amino acids.[3]

Due to the delicate balance required to maintain necessary iron levels without accruing a damaging excess, the genes governing iron uptake, use, and export are meticulously regulated at the transcriptional and post-transcriptional levels. The ferric uptake regulator (Fur) controls expression of more than 100 genes that are involved in iron usage or homeostasis in the Gram-negative bacterium *Escherichia coli*.[4] Under iron-rich conditions the Fe^{2+}-Fur dimer represses target genes, but this repression is relieved under iron-deficient conditions, allowing for increased expression of genes involved in iron homeostasis.[5, 6] The gene *yqjH* is one member of the Fur regulon. The YqjH enzyme catalyzes the flavin adenine dinucleotide (FAD)-dependent reduction of ferric iron to the ferrous state. Previous studies have established that YqjH catalyzes iron-release from a variety of chelators, such as ferric dicitrate and ferric triscatecholate, using an NADPH dependent reduction mechanism.[7] This work suggested an in vivo role

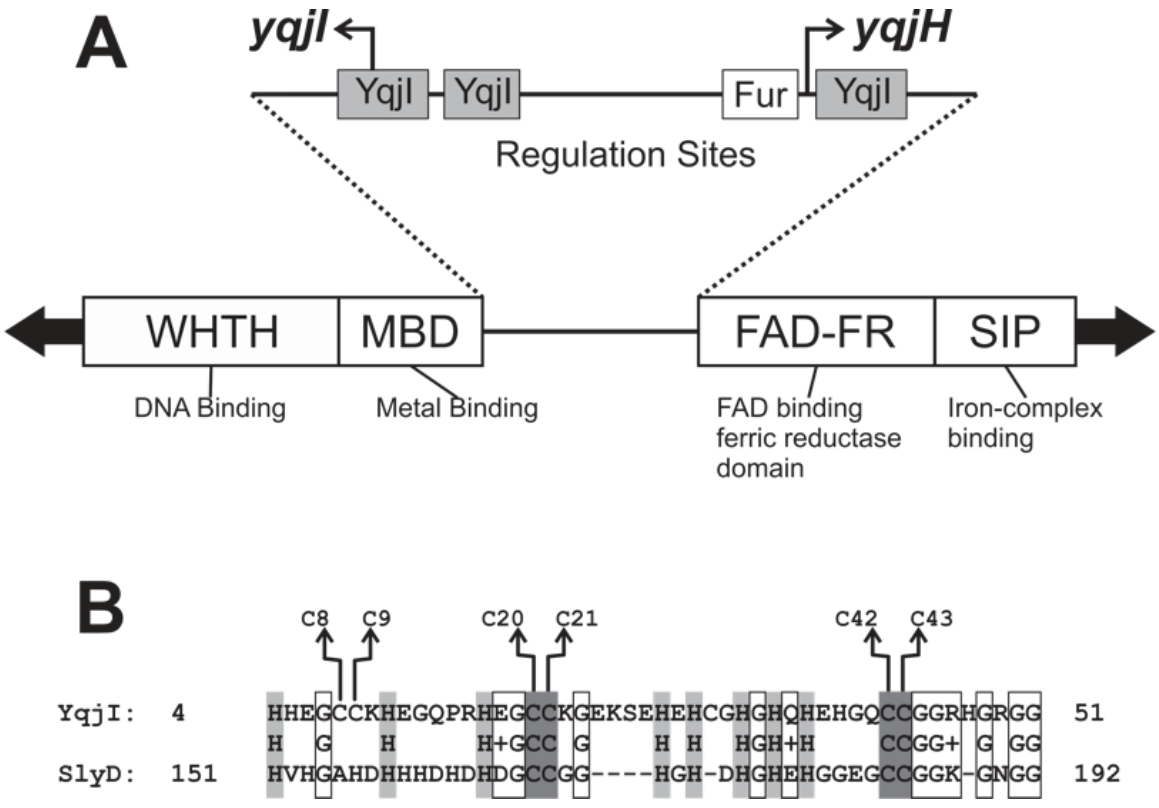

Figure 4.1. Intergenic region between *yqjH* and *yqjI* genes as well their genetic coding regions. Binding sites for YqjI and Fur in the promoters of both genes are indicated in the top image. **B**. Metal binding N-terminus of YqjI showing homology to the nickel-binding region of SlyD. Light grey boxes indicate conserved His residues, dark grey boxes indicate conserved Cys residues, and open boxes indicate other conserved residues.

for YqjH in the reduction of ferric iron from multiple siderophores.[7] Based on these studies we propose that the hypothetical gene name *yqjH* be replaced in the literature with Nickel-responsive Fe-uptake Flavoprotein, abbreviated as *nfeF*.

Intriguingly, transcription of *yqjH* is also strongly repressed independently of Fur by the YqjI protein. The *yqjI* gene is encoded adjacent to the 5'-end of the *yqjH* gene, but is transcribed in the opposite direction, as shown in Figure 4.1A. YqjI residues 57 to 207 are homologous to the PadR family of transcriptional regulators, suggesting a possible function for YqjI as a transcriptional repressor.[8-10] Earlier work established that YqjI binding to sites within the promoter regions of both *yqjI* and *yqjH* results in transcriptional repression of both genes (Figure 4.1A).[11] Wang *et al.* determined that three similar, palindromic binding sites for YqjI are present within the promoter regions. Two of these sites are near the *yqjI* transcriptional start site while the third is proximal to the start site for *yqjH*.[12] By suppressing *yqjH* gene expression, YqjI indirectly prevents iron reduction, and thus iron release from siderophores.[7]

The N-terminus of the YqjI protein includes a ~52 residue-long region consisting of 7 cysteine, 12 histidine, and 7 glutamate residues. This region lacks any predicted secondary structure and may be disordered (Figure 4.1B).[11] Sequence analysis reveals that this region is similar to a nickel-binding region within the peptidyl-prolyl cis-trans isomerase SlyD also present in *E. coli*. The binding of nickel ions to SlyD regulates its isomerase activity.[13] In addition, the YqjI N-terminus also resembles the nickel-binding region within the metal exporter RcnA.[14] Previously, it was shown that addition of Ni(II) or Fe(II) could disrupt YqjI DNA-binding in vitro.[11] Further investigation revealed that in vivo repression of *yqjH* and *yqjI* transcription by YqjI is abolished upon addition of

high levels of nickel but addition of iron had no effect.[11] Together these results suggest that nickel binding to the YqjI N-terminus may negatively regulate YqjI DNA-binding activity such that transcription of the *yqjH* ferric reductase is increased under high nickel conditions. Based on these studies we propose that the hypothetical gene name *yqjI* be replaced in the literature with Nickel-responsive Fe-uptake Regulator, abbreviated as *nfeR*.

In the current study, we present the first detailed characterization of nickel-binding to YqjI (NfeR). Simulations of the Extended X-ray Absorption Fine Structure (EXAFS) region of the nickel K-edge XAS spectra were used to identify the types of ligands responsible for YqjI nickel-binding, and their relevant metal-ligand bond lengths. Site-directed mutagenesis coupled with in vivo gene regulation studies were used to determine the functional relevance of the candidate ligands within the YqjI N-terminus. Then competitive nickel-binding assays and chemical analyses were performed to probe the YqjI-nickel interactions. The results indicate that nickel-dependent regulation of YqjI requires several conserved Cys residues in the N-terminus. Furthermore, the conformational flexibility and ligand-rich nature of the YqjI N-terminus may allow for multiple nickel-binding modes.

Materials and Methods:

Strains and Plasmid Preparation

YqjI and its mutant derivatives were expressed from the pET21a vector (Novagen) as previously described.[11] Mutations to YqjI cysteines were constructed following the QuikChange II site-directed mutagenesis protocol (Agilent). All mutations were confirmed by sequencing and mutated plasmids were transformed into BL21(DE3)

cells for expression and purification of YqjI. All strains and primers can be found in Tables 4.1 and 4.2.

ApoYqjI and NiYqjI Expression and Purification

YqjI was expressed from a pET21a vector in *E. coli* BL21(DE3) cells as previously described but with some modifications.[11] Briefly, cells grown overnight in LB with 100mg/L Ampicillin (Amp) were diluted 1:100 in fresh LB Amp (100mg/L) and grown at 37°C with 200rpm shaking to an OD_{600} of 0.7 to 0.8. For expression of apoYqjI, the cells were induced with 10µM isopropyl β-D-1-thiogalactopyranoside for 24 hours at 25°C after which they were harvested via centrifugation at 7460 x g for 10 minutes and stored at -80°C until use. Cells were resuspended in heparin binding buffer consisting of 20mM HEPES, 200mM NaCl, 5% glycerol, 10mM β-mercaptoethanol (βME), pH =7.5 with 1mM phenylmethylsulfonyl fluoride added. After resuspension, the cells were lysed via sonication for two 2-minute intervals of one second on and one second off at 50% amplitude on a Branson digital sonifier 450. Lysed cells were treated with 1% streptomycin sulfate and centrifuged for 40 minutes at 31000 x g. Purification was performed following the previously established protocol using the cation exchange (Hitrap), nickel (Histrap), and gel filtration chromatography (Superdex200) columns in sequence.[12] The monomeric form of YqjI was isolated by gel filtration (Figure 4.2A). Purity of final YqjI fractions was determined using SDS-PAGE and the protein was concentrated via a 10kDa molecular weight Amicon Ultra concentration filter (Millipore). Concentrated aliquots of YqjI were flash frozen in liquid nitrogen and stored at -80°C.

Table 4.1: Strain list

Strain Name	Genotype/characteristics	Source/Reference
MG1655	Wild type *E. coli* K12	Laboratory strain
NM400	MG1655 mini-λ, Cm^R, Ts	Laboratory strain
BL21(DE3)		Laboratory strain
SW057	MG1655 Δ*yqjI* Φ(*yqjH-lacZ*) Kan^R	[11]
SW058	MG1655 Δ*yqjI* Φ(*yqjI-lacZ*) Kan^R	[11]
SW245	MG1655 Δ*yqjI* pET21a_yqjI Φ(*yqjH-lacZ*) $Kan^R Amp^R$	[11]
MB140	MG1655 Δ*yqjI* pET21a_yqjI(C8AC9A) Φ(*yqjH-lacZ*) $Kan^R Amp^R$	This study
SW247	MG1655 Δ*yqjI* pET21a_yqjI(C20AC21A) Φ(*yqjH-lacZ*) $Kan^R Amp^R$	This study
SW248	MG1655 Δ*yqjI* pET21a_yqjI(C42AC43A) Φ(*yqjH-lacZ*) $Kan^R Amp^R$	This study
MB141	MG1655 Δ*yqjI* pET21a_yqjI(C42A) Φ(*yqjH-lacZ*) $Kan^R Amp^R$	This study
MB142	MG1655 Δ*yqjI* pET21a_yqjI(C43A) Φ(*yqjH-lacZ*) $Kan^R Amp^R$	This study
MB143	MG1655 Δ*yqjI* pET21a_yqjI(C31A) Φ(*yqjH-lacZ*) $Kan^R Amp^R$	This study
MB144	MG1655 Δ*yqjI* pET21a_yqjI(C153A) Φ(*yqjH-lacZ*) $Kan^R Amp^R$	This study
MB145	MG1655 Δ*yqjI* pET21a_yqjI Φ(*yqjI-lacZ*) $Kan^R Amp^R$	This study
MB146	MG1655 Δ*yqjI* pET21a_yqjI(C42AC43A) Φ(*yqjI-lacZ*) $Kan^R Amp^R$	This study
MB147	BL21(DE3) pET21a_yqjI Amp^R	This study
MB148	BL21(DE3) pET21a_yqjI(C8AC9A) Amp^R	This study
MB149	BL21(DE3) pET21a_yqjI(C20AC21A) Amp^R	This study
MB150	BL21(DE3) pET21a_yqjI(C42AC43A) Amp^R	This study
MB151	MG1655 Δ*yqjI* pET21a_yqjI(C8AC9A) Φ(*yqjI-lacZ*) $Kan^R Amp^R$	This study
MB152	MG1655 Δ*yqjI* pET21a_yqjI(C20AC21A) Φ(*yqjI-lacZ*) $Kan^R Amp^R$	This study

Table 4.2: Primer List

Primer Name	Sequence (5'-3')	Purpose
YqjIC8AC9A_F	ATGAGCCATCATCACGAAGGGGCTG CTAAACATGAAGGCCAGCCACGC	C8/C9 to Ala mutagenesis
YqjIC8AC9A_R	GCGTGGCTGGCCTTCATGTTTAGCAG CCCCTTCGTGATGATGGCATCAT	C8/C9 to Ala mutagenesis
YqjIC20AC21A_F	GGCCAGCCACGCCATGAGGGCGCCG CCAAAGGTGAGAAGTCAGAACAC	C20/C21 to Ala mutagenesis
YqjIC20AC21A_R	GTGTTCTGACTTCTCACCTTTGGCGG CGCCCTCATGGCGTGGCTGGCC	C20/C21 to Ala mutagenesis
YqjIC42AC43A_F	CACCAGCATGAACACGGTCAAGCCG CCGGTGGTCGCCACGGTCGCGGC	C42/43 to Ala mutagenesis
YqjIC42AC43A_R	GCCGCGACCGTGGCGACCACCGGCG GCTTGACCGTGTTCATGCTGGTG	C42/43 to Ala mutagenesis
YqjIC42A_F	CACCAGCATGAACACGGTCAAGCCT GTGGTGGTCGCCACGGTCGCGGC	C42 to Ala mutagenesis
YqjIC42A_R	GCCGCGACCGTGGCGACCACCACAG GCTTGACCGTGTTCATGCTGGTG	C42 to Ala mutagenesis
YqjIC43A_F	CACCAGCATGAACACGGTCAATGTG CCGGTGGTCGCCACGGTCGCGGC	C43 to Ala mutagenesis
YqjIC43A_R	GCCGCGACCGTGGCGACCACCGGCA CATTGACCGTGTTCATGCTGGTG	C43 to Ala mutagenesis
YqjIC31A_F	GGTGAGAAGTCAGAACACGAGCACG CCGGACACGGTCACCAGCATG	C31 to Ala mutagenesis
YqjIC31A_R	CATGCTGGTGACCGTGTCCGGCGTGC TCGTGTTCTGACTTCTCACC	C31 to Ala mutagenesis
YqjIC153A_F	GAAGAACGCATCAAAGCGCGTGCCG TTGGCGCGGCGCTGCGCCAGAAC	C153 to Ala mutagenesis
YqjIC153A_R	GTTCTGGCGCAGCGCCGCGCCAACG GCACGCGCTTTGATGCGTTCTTC	C153 to Ala mutagenesis

For preparation of Ni^{2+}-YqjI, 500µM $NiCl_2$ was added to the LB media at the time of induction. Additionally, the Histrap column was omitted and the Superdex200 buffer contained 500mM NaBr instead of NaCl and β-mercaptoethanol was omitted to avoid formation of adventitious nickel-βME compounds in the X-ray Absorption Spectroscopy (XAS) experiments. The nickel concentration of purified YqjI was measured using the 4-(2-pyridylazo)-resorcinol (PAR) assay [15] as well as inductively-coupled plasma mass spectrometry (ICP-MS).

In addition to the Ni^{2+}-YqjI samples eluting as a monomer using gel filtration, the size and homogeneity of all YqjI samples treated with Ni^{2+} were verified using a Superdex200 10/300 GL analytical gel filtration column (Figure 4.2B). The buffer used for this elution was 20mM HEPES, 5% glycerol, 500mM NaCl, pH = 7.5. High molecular weight and low molecular weight standards (GE) were used to obtain a calibration curve and compared to the gel filtration elution profile for YqjI (Figure 4.2C). In all instances, Ni^{2+}-YqjI eluted as a homogeneous peak consisting of monomer at the same elution volume as apo-YqjI with a weight of 30kDa, slightly above the predicted weight of 23.4kDa.

Inductively-coupled plasma mass spectrometry (ICP-MS)

Samples for ICP-MS were initially prepared by diluting concentrated YqjI protein to 100µM in 20mM HEPES, 500mM NaCl, 5% glycerol, 10mM βME, pH=7.5. All 1.5mL microcentrifuge tubes in which YqjI was stored and prepared were washed using concentrated, ultrapure 70% HNO_3. YqjI was then diluted to 20µM in 70% HNO_3 before being heated at 90°C for 2 hours. After heating the samples, they were diluted 1:20 using

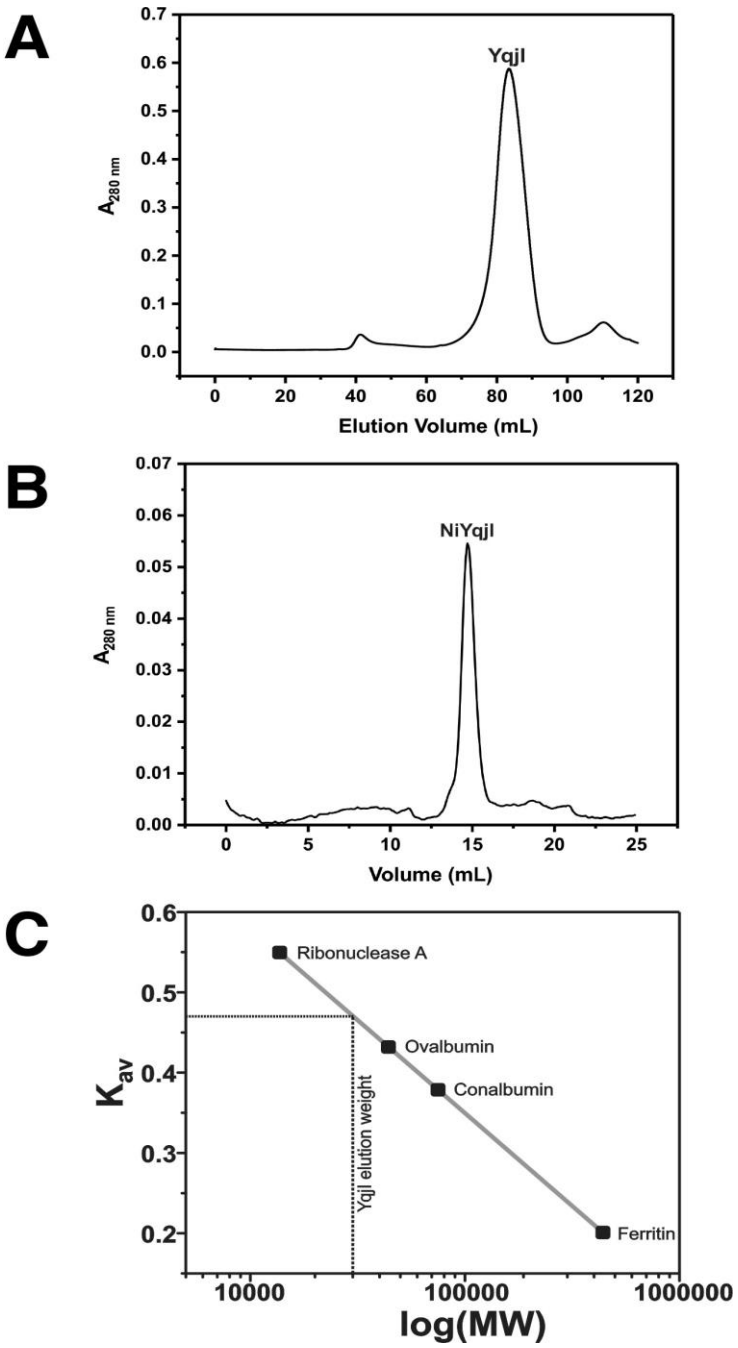

Figure 4.2. (A) Prep grade Superdex200 elution profile for wild-type YqjI (NfeR) during protein purification. (B) Analytical Superdex200 elution profile for wild-type YqjI (NfeR) reconstituted with Ni^{2+}. (C) Gel filtration graph for GE protein standards indicating the molecular weight at which YqjI elutes. In the presence or absence of Ni^{2+}, the point at which YqjI elutes remains unchanged.

50µL of sample in 950µL MQ water to create a matrix of 3.5% HNO_3. Metal standards were prepared the same way. Samples were analyzed on a Thermo Element 2 High Resolution ICP-MS instrument at the CEMS at the University of South Carolina.

X-ray Absorption Spectroscopy (XAS)

XAS was used to characterize the Ni and Zn atomic structure and electronic properties of metal bound to wild-type and the C42A-C43A YqjI double mutant. Wild-type and mutant XAS samples were prepared at protein concentrations of 0.3 to 0.6 mM, respectively, in 20 mM HEPES buffer (pH 7.5), 500 mM NaBr and 30% glycerol. Samples were loaded in leucite sample cells wrapped with kapton tape, then flash frozen and stored in liquid nitrogen until data collections. XAS data were collected at the National Synchrotron Light Source (NSLS) on beamline X3-b. This beamline utilized a Si[111] single crystal monochromator equipped with a harmonic rejection mirror for simultaneous beam focusing and removal of higher order harmonics. During data collection, samples were maintained at 24 K using a He Displex Cryostat. Protein fluorescence excitation spectra were collected using a 30-element Canberra Ge solid-state detector. Background fluorescence noise was removed by placing a 0.3 µm Co or a 0.6 µm Cu fluorescence filter between the cryostat and detector during either Ni or Zn XAS data collection, respectively. Energy calibration spectra were collected simultaneously with protein spectra by placing either a Ni or Zn foil between terminal ionization detectors inline with the X-ray path through the cryostat. Data collection details for Ni or Zn XAS are reported elsewhere.[16, 17] Independent duplicate spectra were collected for

each sample and each element to ensure sample reproducibility. Data represent the average of between 7 to 12 individual scans for each independent sample.

XAS data were processed using the Macintosh OS X version of the EXAFSPAK program suite integrated with the Feff v8 software for theoretical model generation.[18, 19] Data reduction utilized a Gaussian function in the pre-edge region and a three-region cubic spline throughout the EXAFS region. Data were converted to k-space using a Ni E_0 value of 8,333 eV or a Zn E_0 value of 9,668 eV. In both elements, k^3 -weighted EXAFS was truncated at 1.0 and 13.0 $Å^{-1}$ for filtering purposes. This k range corresponds to a spectral resolution of ca. 0.12 Å for all metal-ligand interactions; therefore only independent scattering environments above 0.12 Å were considered resolvable during the EXAFS simulation analysis.[20] EXAFS fitting analysis was performed on raw/unfiltered data. EXAFS data were fit using both single and multiple scattering amplitude and phase functions calculated with the program Feff v8. Single scattering theoretical models were calculated for metal-carbon, nitrogen, oxygen, and sulfur coordination to best simulate nearest-neighbor ligand scattering environments. Scale factors (Sc) and E_0 values used during the simulations were calibrated by fitting crystallographically characterized Ni and Zn models; specific values include a Scale Factor of 0.9 (Ni) and 1.0 (Zn), and E_0 values for metal-O/N/C and metal-S of -10.55 and -12.22 eV (for Ni), and a combined value of -15.25 eV (for Zn). Criteria for judging the best-fit simulation utilized both the lowest mean square deviation between data and fit (F'), corrected for the number of degrees of freedom, and a reasonable Debye-Waller factor upper limit of $< 6.0 \times 10^{-3}$ A^2.[21, 22]

β-galactosidase Assay

The pET21a vector with genes coding for *yqjI* and its cysteine mutants were transformed into MG1655 Δ*yqjI* Φ(*yqjH-lacZ*) or MG1655 Δ*yqjI* Φ(*yqjI-lacZ*) cells. Overnight cultures were diluted 1:100 in LB Amp (100mg/L) and cultured at 37°C to an OD_{600} of approximately 0.1. At this point, 5mL aliquots of cultures were split into separate 50mL conical tubes with desired concentrations of nickel added. The cultures were grown for 30 additional minutes at 37°C after which the OD_{600} was measured. Cells at all nickel concentrations were collected via centrifugation for 10 minutes at 1800 x g and 4°C and resuspended in Z-buffer (100mM sodium phosphate, 10mM KCl, 1mM $MgSO_4$, 50mM βME, pH=7) to a final OD_{600} of approximately 0.5. Both 100µL chloroform and 50µL 0.1% SDS were added to a 1mL mix of cells and Z-buffer and the cells were then vortexed for 30 seconds. The mixture incubated at room temperature for 5 minutes before the addition of 200µL o-nitrophenyl-β-D-galactopyranoside (ONPG) (4mg/mL). Cells were vortexed and allowed to sit until the reactions were deemed complete based on the shade of yellow. Further reaction was stopped using 500µL of 1M sodium bicarbonate. The OD_{420} and OD_{550} values were measured and Miller unit calculations were performed using the following formula.[23]

Miller Units = $1000 * (OD_{420} - 1.75 * OD_{550}) / [(\text{volume of cells in mL})(\text{time of reaction in min})(OD_{600})]$

Isothermal Titration Calorimetry (ITC)

Apo forms of wild-type and the C42A-C43A mutant YqjI proteins were prepared for ITC using a 5mL Hitrap desalting column and freshly prepared elution buffer (20mM

HEPES, 500mM NaCl, 5% glycerol, pH = 7.5) in order to remove βME. βME can bind free Ni^{2+} ions leading to an independent metal-buffer side reaction. Fractions containing YqjI were collected and their concentrations determined using a Bradford assay. YqjI, diluted to approximately 50μM for calorimetry, was degassed to remove bubbles, placed in the sample well, and titrated with an initial 2μL injection of 1.5mM $NiCl_2$ (prepared in 20mM HEPES, 500mM NaCl, 5% glycerol, pH = 7.5) followed by 54 injections (5μL) from the injector. ITC was performed using a Malvern Microcal VP-ITC at 298K with a 200 second interval between injections. Analysis of ITC results was done using Origin ITC analysis software provided by MicroCal in combination with VPViewer [24] using a sequential binding model that allowed for determination of binding constants for three nickel sites. ITC experiments were performed in triplicate. Attempts to run ITC at 3.5μM YqjI were made, but no measurable signal above noise was observed (Figure 4.3).

Competition Binding Assays with Mag-Fura-2

YqjI samples were initially eluted through 5mL Hitrap desalting column using a buffer consisting of 20mM HEPES, 150mM NaCl, 5% glycerol, pH=7.5 in order to remove βME. Mag-fura-2 (MF2) was diluted to 10μM in 20mM HEPES, 150mM NaCl, 5% glycerol, pH=7.5 buffer. The concentration of MF2 was confirmed using the extinction coefficient of 22000 M^{-1} at 369 nm.[25] 2.5μM of YqjI or C42A-C43A was added to the MF2. Increasing concentrations of Ni^{2+} from 0μM to 35μM were titrated into the cuvette containing YqjI and MF2. After each titration, the sample was allowed to equilibrate for 5 minutes followed by measurement of the UV-visible absorption spectra on an Agilent 8453 spectrophotometer. Metal binding of MF2 results in a blue

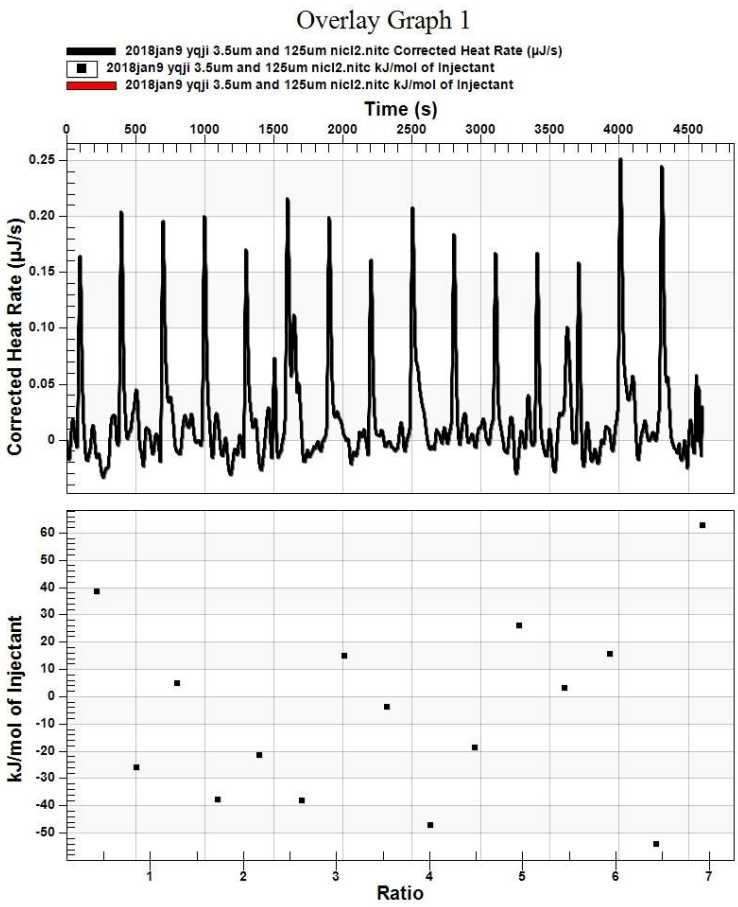

Figure 4.3. ITC data from nickel titration of 3.5 µM YqjI

shift of a feature from 366 nm to 325 nm and a consequent decrease in the 366 nm feature. Following the titration, the change in absorbance at 366 nm was used in combination with the measured K_D of MF2 for Ni^{2+} (150nM) in these buffer conditions to create a custom formula on the software Dynafit using sequential binding for two nickels (Figure 4.4).[26] The raw data from the MF2 competition assay fit best with a sequential binding model for two nickel sites. A script using a two independent sites model (rather than a sequential binding model) resulted in very large error. The goodness of fit for the two-nickel sequential binding model to the experimental data in Dynafit was evaluated by analyzing the residuals and R^2 values. Control experiments monitoring the fluorescence emission and UV-visible absorption spectra of MF2 in the presence of YqjI but in the absence of nickel did not indicate any direct interaction between MF2 and YqjI (data not shown).

Atomic Absorption (AA) Spectroscopy

Samples for AA were prepared as described for ICP-MS except that the 20μM YqjI samples were diluted 1:100 instead of 1:20. Nickel content was measured using a nickel lamp at a wavelength of 233nm. Overall nickel content was determined by comparing sample values to measured nickel standards. All measurements were performed using a Perkin Elmer PinAAcle 900T spectrometer. This technique was used for samples obtained from ITC and MF2 titrations.

[task]

data = equilibria
task = fit

[mechanism]

P + M <==> PM	: K1 dissoc.	; P = YqjI
PM + M <==> PMM	: K2 dissoc.	; M = Nickel
L + M <==> ML	: K3 dissoc.	; L = Mag-Fura-2

[concentrations]
L = 10.2
P = 2.5

[constants]
K1 = 0.001?
K2 = 0.001?
K3 = 0.15

[responses]

L = .02253?
ML = .01?

[data]

variable	M
set	WT

[set:WT]

M, uM	M
0	0.22652
0.5	0.22538
1	0.22306
1.5	0.22143
2	0.21845
2.5	0.2152
3	0.21184

3.5	0.20441
4	0.20348
4.5	0.19748
5	0.19117
5.5	0.1833
6	0.18038
7	0.15378
8	0.14781
9	0.13056
10	0.11725
11	0.09455
12.2	0.08373
13	0.06491
14	0.06034
15	0.04248
16	0.04462
17.5	0.03526
20	0.02333
22.5	0.02118
25	0.01734
27.5	0.01589
30	0.01329
35	0.01264

[output]
  directory ./output/WT_1Abs366.txt

[end]

Figure 4.4. Dynafit script for nickel binding to YqjI

DTNB Assay

All DTNB [5,5'-dithiobis(2-nitro-benzoic acid)] assays were performed in an anaerobic chamber (Coy) following the Thermo Scientific protocol. YqjI aliquots stored in 20mM HEPES, 500mM NaCl, 10mM βME, and 5% glycerol at a pH of 7.5 were treated for 30 min with 8M urea (unfolded), 30 mM tris(2-carboxyethyl)phosphine (TCEP) (native, reduced), or sequentially with 8M urea followed by 30 mM TCEP (unfolded, reduced). All samples containing βME and/or TCEP were desalted anaerobically prior to assaying free thiol content with DTNB. For samples unfolded with 8M urea, urea was maintained in the DTNB assay buffer to prevent refolding. The exact process by which each sample was prepared is shown in Figure 4.5.

Each treated sample and an untreated (but desalted) native YqjI control were concentrated and the protein concentration was measured using the Bradford assay. Next, 5μL of 4mg/mL DTNB was mixed with 250μL of reaction buffer (0.1M sodium phosphate, 1mM ethylenediaminetetraacetic acid, pH=8.0) and 25μL of each sample to give a final DTNB concentration of 71μg/mL. The reactions were allowed to incubate for 15 minutes and the absorbance at 412nm was measured. Total thiol (Cys) content was calculated and converted into a molar ratio per YqjI monomer using the measured YqjI protein concentration. The molar absorptivity (ε) at 412 nm of the 2-nitro-5-thiobenzoate (formed from the reaction with Cys) is 14,150$M^{-1}cm^{-1}$ and becomes 14,290$M^{-1}cm^{-1}$ in the presence of 8M urea.[27]

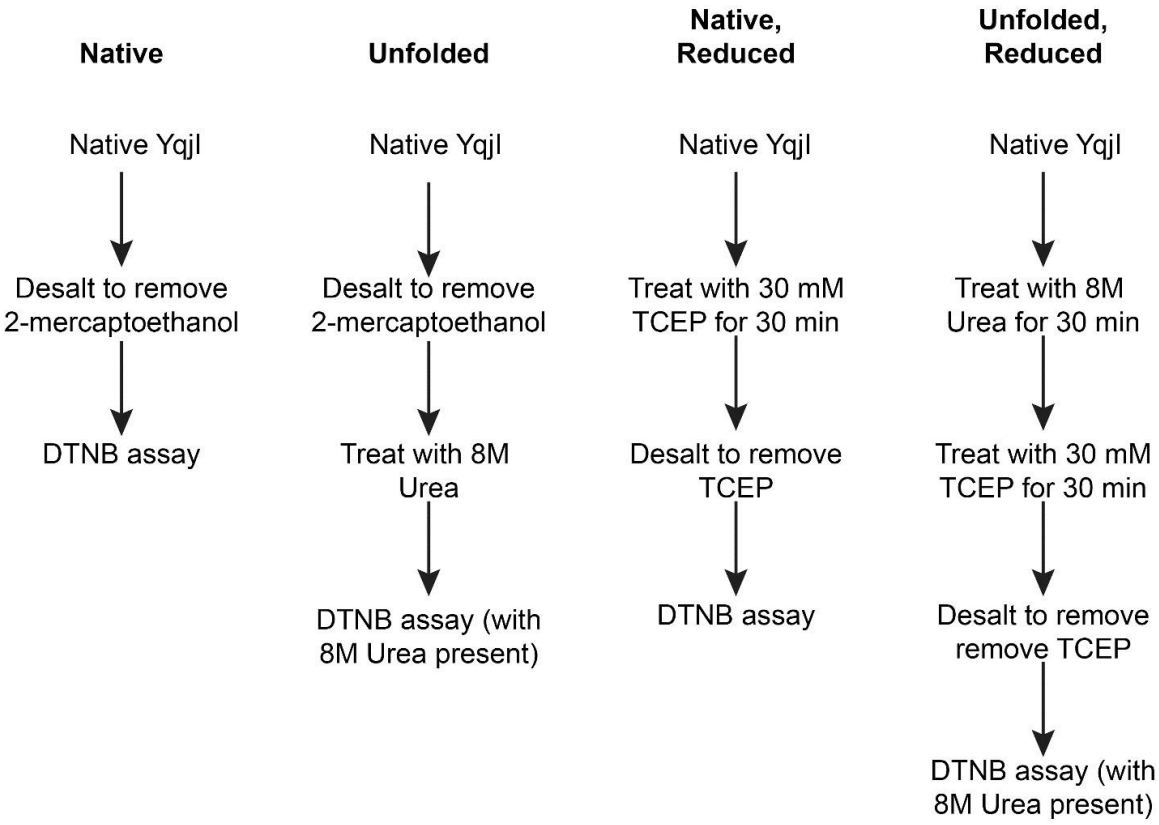

Figure 4.5. Scheme showing flow chart of various treatments used to analyze YqjI free thiol content with the DTNB assay.

Results:

Analysis of the Ni K-edge EXAFS indicates cysteines are key for nickel binding to wild-type YqjI.

As previously reported by Wang *et al.* [11], Ni^{2+} binds to the YqjI protein and inhibits its ability to interact with target DNA sequences within the promoters for both *yqjH* and *yqjI*. In vivo addition of nickel or the deletion of *yqjI* increased transcription from both *yqjH* and *yqjI* promoters showing that YqjI is a nickel-dependent transcriptional repressor of its target promoters. To identify YqjI nickel-binding ligands, Ni^{2+}-YqjI protein was isolated from *E. coli* grown with excess nickel added at the time of induction and protein samples were characterized using XAS. ICP-MS analysis of the nickel content of XAS samples revealed a nickel:YqjI ratio of 1.2:1 following purification. X-ray Absorption Near Edge Structure (XANES) spectra for wild-type protein (Figure 4.6) suggest Ni^{2+} is bound in either a distorted 4 coordinate environment, in a 5 coordinate trigional bipyramidal like ligand geometry, or possibly a heterogeneous mixture of both. The first inflection point of the Ni K-edge XANES occurs at 8342 eV, confirming a Ni^{2+} oxidation state. A small pre-edge feature at 8332 eV (1s →3d transition) was observed at respective dimensionless areas of 0.009, consistent with signals seen in 4 coordinate Ni(II) complexes.[26, 27] However, the lack of an intense edge feature centered at 8338 eV (1s →4p transitions) suggest 5 coordinate trigional bipyramidal Ni-ligand geometry; the low transition area observed for the subtle feature present at 8337 eV is 0.85.[28] Simulations of the nickel Extended X-ray Absorption Fine Structure (EXAFS) data (Figure 4.7) indicate Ni^{2+} is coordinated in a distorted ligand environment constructed by both S and O/N ligands at a coordination number within the

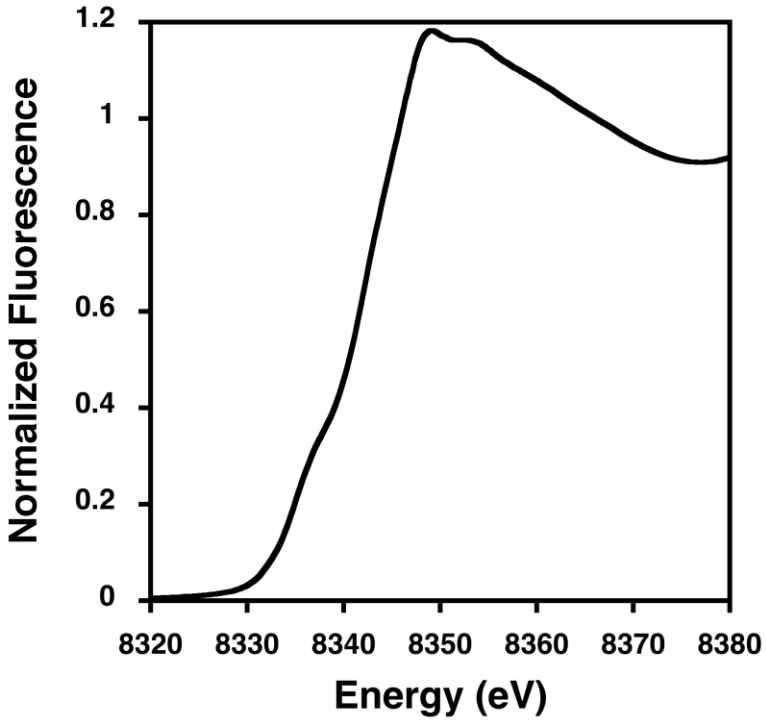

Figure 4.6. Ni K-edge XANES Spectra for wild-type YqjI.

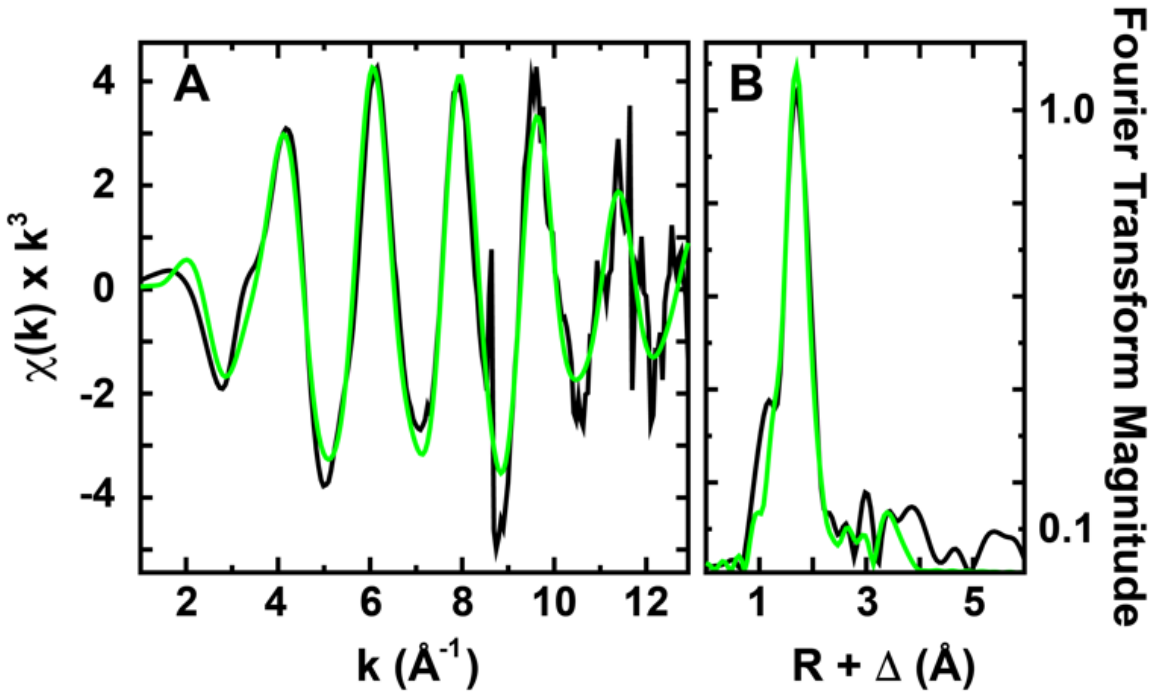

Figure 4.7. EXAFS and Fourier transforms of Ni^{2+} bound to wild-type YqjI. Raw EXAFS data (**A**) and the corresponding Fourier transforms of the EXAFS (**B**) are shown in black. Best fit simulations for both the EXAFS and the Fourier transforms of the EXAFS are shown in green.

range of 4 to 5 ligands. Selection criteria for optimal fits was strict; simulation parameter guidelines [21, 22] are as follows: (a) resolution defined for data was 0.12 Å, so only environments separated by R ≥0.12 Å were acceptable, (b) an upper limit in acceptable Debye-Waller factor was s2 ≤ 0.006 $Å^2$, (c) we vary only the bond length and Debye-Waller factor for each shell in the simulation to reduce the number of degrees of freedom within our simulations and to provide systematic variances in the measurement of the fitting potential energy landscape, and (d) our goodness of fit (F') parameter has a penalty induced for increased numbers of degrees of freedom used in the fit. Bond lengths obtained from protein data were compared to distances/coordination geometries posted in the Cambridge Structural Database.[28] Bond lengths and fitting metrics for the optimal simulations for the protein Ni environments are posted in Table 4.3. Simulation parameters for the Ni-nearest neighbor ligand environments in both samples were consistent with both N/O and S ligand environments at apparent equal distribution. Bond lengths for the Ni-N/O ligand environment (the technique cannot directly distinguish between these 2 atom types) were at 2.01 and 1.93 Å for the wild-type and mutant proteins respectively, while the Ni-S respective bond lengths were at 2.20 and 2.22 Å. The high Debye-Waller factors (σ^2) in the best simulations forced selection of fits with coordination numbers that were lower than reasonable based on the interpretation of coordination geometry from the XANES (distorted 4 to 5 coordinate Ni), indicating a high degree of ligand disorder in the Ni sites. Long range Ni•••C scattering, at bond distances of 2.78 Å, 3.11 Å and 4.04 Å are consistent with patterns observed for C/N signals in the EXAFS, likely from rigid imidazole ring multiple scattering from histidine

Table 4.3. Summary of the best fit EXAFS simulation analysis for Ni site for wild-type and C42A-C43A mutant YqjI. Values reported are the average of two independent data sets.

	Ni-Nearest Neighbor Ligands [a]				Ni-Long Range Ligands [a]				
Sample	**Atom [b]**	**R(Å) [c]**	**C.N. [d]**	**σ^2 [e]**	**Atom [b]**	**R(Å) [c]**	**C.N. [d]**	**σ^2 [e]**	**F' [f]**
Wild-type YqjI	O/N	2.01	1.5	5.71	C	2.78	1.0	4.45	0.48
	S	2.20	2.0	4.21	C	3.11	1.0	5.93	
					C	4.04	2.5	3.57	
C42A-C43A YqjI	O/N	1.93	1.0	4.99	C	2.83	3.0	1.81	0.85
	S	2.22	2.0	4.93	C	3.04	3.0	2.32	
					C	4.01	4.0	3.45	

[a] Independent metal-ligand scattering environment
[b] Scattering atoms: O (Oxygen), N (Nitrogen), C (Carbon) and S (Sulfur)
[c] Metal-ligand bond length
[d] Metal-ligand coordination number
[e] Debye-Waller factor given in $Å^2 \times 10^3$
[f] Number of degrees of freedom weighted mean square deviation between data and simulation

ligands bound directly to the metal.[29] Any attempts to include bromine scattering in the nearest neighbor ligand environment simulations were unsuccessful.

Residues C42-C43 are critical for the normal function of YqjI in vivo.

The presence of sulfur scattering in the XAS of the wild-type protein suggests Cys residues play a direct role in coordinating the metal to YqjI. A surprising number of the Cys residues in the YqjI N-terminus are found adjacent to each other (Figure 4.1B). For each pair of adjacent Cys residues in the N-terminal region of YqjI, both Cys residues were mutated to Ala simultaneously in the same mutant protein. To evaluate the effect of Cys to Ala mutations on in vivo YqjI regulation of its target genes, the wild-type and mutant plasmid constructs were transformed into the Δ*yqjI* strain that lacks a chromosomal copy of the gene. In these backgrounds only the YqjI protein provided in trans on the plasmids can regulate the *yqjH* and *yqjI* promoters. The Δ*yqjI* strains also contained the promoter regions of *yqjH* and *yqjI* fused to the *lacZ* open reading frame, which encodes the β-galactosidase enzyme. The *lacZ* fusion gene reporter constructs were inserted in a separate location in the chromosome from the *yqjH – yqjI* locus. The Δ*yqjI* gene reporter strains were then exposed to nickel and the nickel-responsive transcription from the *yqjH* and *yqjI* promoters was monitored via measurement of β-galactosidase activity.

Levels of *yqjH* transcription in the absence of nickel were approximately the same if wild-type YqjI, C8A-C9A, or C20A-C21A mutant YqjI proteins were provided in trans (Figure 4.8A). In contrast, if the C42A-C43A YqjI protein was provided in trans, basal *yqjH* transcription was more than 3-fold lower compared to the transcription observed in

strains carrying the other YqjI variants (Figure 4.8A). Upon nickel exposure, the transcription of *yqjH* increased due to the nickel-dependent loss of YqjI transcriptional repression as has been previously observed (Figures 4.8A and 4.8B).[11] The nickel-dependent increase in transcription was approximately the same regardless of whether wild-type YqjI, C8A-C9A, or C20A-C21A YqjI proteins were present in trans. However, the C42A-C43A YqjI protein was not as responsive to nickel treatment in vivo and that strain showed only a moderate increase in *yqjH* transcription and only at the higher levels of nickel exposure (Figure 4.8A and 4.8B show same data for WT and C42A-C43A). These results indicate that the transcriptional repression of the *yqjH* promoter by the C42A-C43A YqjI mutant protein is greater than the wild-type YqjI protein, leading to lower basal expression from the *yqjH* promoter. Furthermore, the C42A-C43A mutant protein is not as responsive to nickel addition as the wild-type YqjI in vivo.

Subsequently, the Cys42 and Cys43 cysteines were individually mutated to Ala independently to test if one or both cysteine residues are required for nickel-responsive transcriptional repression by YqjI (Figure 4.8B). Regulation by the individual C42A and C43A mutant YqjI proteins largely mirrored that of the C42A-C43A double mutant YqjI. Both C42A and C43A YqjI proteins repressed basal *yqjH* transcription more markedly than wild-type YqjI and both Cys mutants were less responsive to nickel than the wild-type YqjI protein in vivo. There was some deviation from this trend at the highest nickel concentration tested where the single C42A and C43A mutants showed a level of repression intermediate between wild-type YqjI and the C42A-C43A double mutant YqjI (Figure 4.8B).

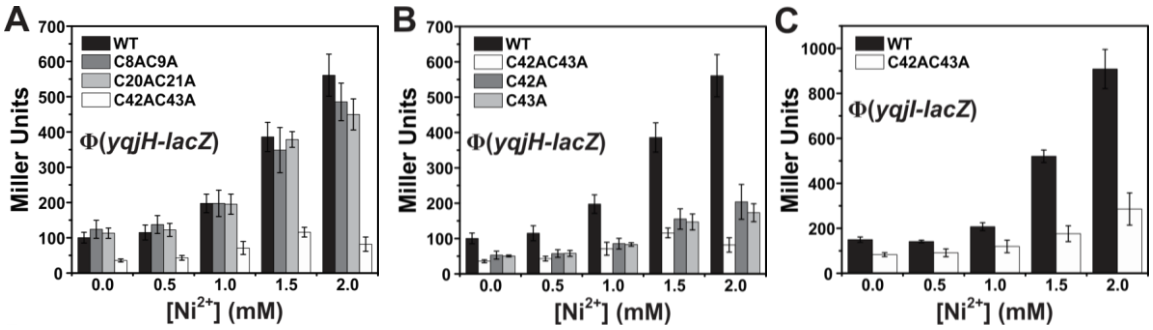

Figure 4.8. MG1655 cells without genomic *yqjI* were treated with nickel for 30 min. All results were performed at least in triplicate. **A**. β-galactosidase assay for *yqjH-lacZ* in the presence of YqjI or its cysteine mutant derivatives. **B**. β-galactosidase assay for *yqjH-lacZ* in the presence of wild-type YqjI or C42A and C43A mutant derivatives. WT and C42A-C43A data is the same as in Figure 4A. **C**. β-galactosidase results for *yqjI-lacZ* in the presence of wild-type YqjI or the C42A-C43A mutant.

We also measured the ability of the C42A-C43A YqjI mutant protein to regulate the *yqjI* promoter in vivo (Figure 4.8C). Similar to the effect observed with the *yqjH* promoter, the C42A-C43A YqjI protein showed increased repression of basal transcription from the *yqjI* promoter and also a decreased response to nickel exposure (Figure 4.8C). Thus, YqjI regulation of both *yqjH* and *yqjI* target promoters is similarly altered by the C42A-C43A mutations

Though the C8A-C9A and C20A-C21A mutations did not alter YqjI regulation of *yqjH*, we also tested their ability to regulate *yqjI* (Figure 4.9). For both double mutants, a 2-fold increase in *yqjI* basal gene expression was observed, indicating a mild defect in the repressor function of these two mutant proteins at the *yqjI* promoter. For comparison, transcription from the *yqjI* promoter in the presence of C8A-C9A or C20A-C21A YqjI was still more than 10-fold lower than the fully de-repressed promoter in the Δ*yqjI* strain that completely lacks a copy of YqjI. Importantly, in the strains carrying the C8A-C9A or C20A-C21A proteins, YqjI-dependent repression of *yqjI* was still lost in response to nickel addition, as was similarly observed for strains carrying wild-type YqjI and during studies on the *yqjH* promoter (Figures 4.8A and 4.5). These results indicate that the C8A-C9A and C20A-C21A mutations do not impair the in vivo nickel-responsiveness of YqjI. Mutation of either of these two pairs of Cys residues may subtly alter the DNA-binding or repressor functions of YqjI, at least at the *yqjI* promoter. It is possible that a similar defect was not observed with *yqjH* due to the ability of Fur to compensate for a mild loss of *yqjH* gene repression.

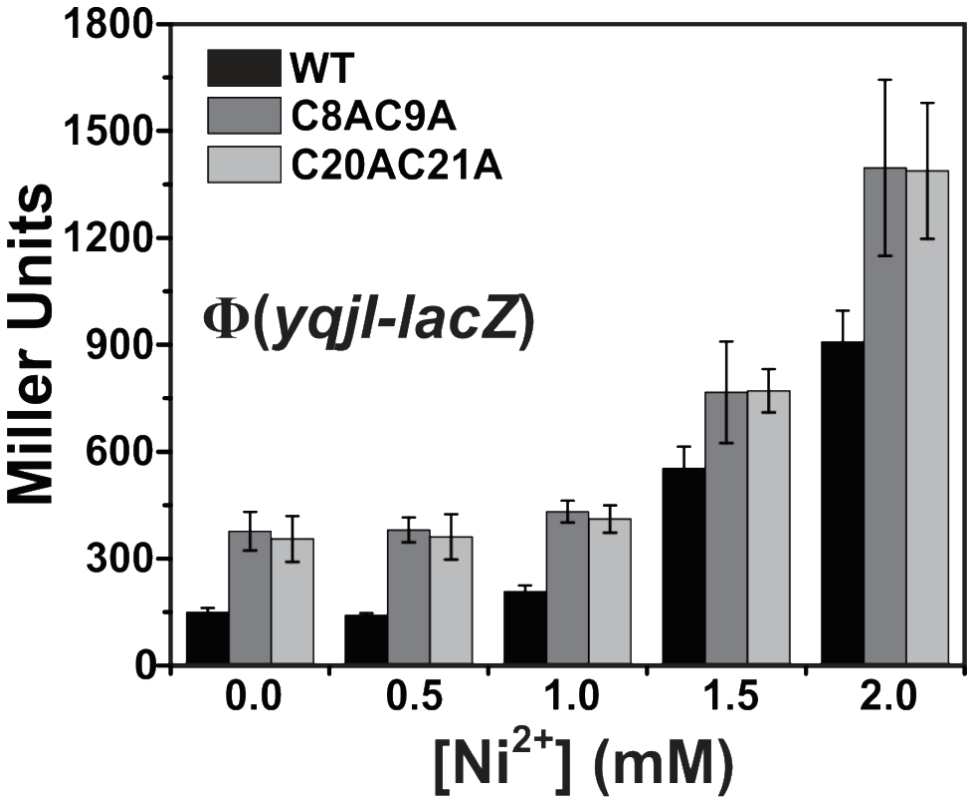

Figure 4.9. MG1655 cells without genomic *yqjI* were treated with nickel for 30 min. All results were performed at least in triplicate. β-galactosidase assay for *yqjI-lacZ* in the presence of YqjI or its cysteine mutant derivatives C8A-C9A and C20A-C21A. Data for WT YqjI is the same shown in Figure 4C.

YqjI also contains Cys31 and Cys153, which are not conserved in the N-terminal region that is homologous to SlyD and RcnA. These two Cys residues were each mutated to Ala in YqjI and the mutant proteins were analyzed for in vivo repression of *yqjH*. The C31A and C153A mutations did not have any noticeable impact on in vivo transcriptional regulation of the YqjI target promoters (data not shown). Overall, the in vivo data indicate that the C8A-C9A and C20A-C21A mutations do not significantly alter in vivo nickel-responsive regulation by YqjI. In contrast, both Cys42 and Cys43 are required for proper nickel-responsive transcriptional regulation by YqjI in vivo.

XAS analysis for Ni^{2+} bound to C42A-C43A mutant.

Following the in vivo characterization of C42A-C43A YqjI, Ni XAS analysis was used to characterize the coordination and electronic states for metal bound to the mutant. Ni XANES spectra for mutant YqjI (Figure 4.10) have an edge inflection energy at 8342 eV, identical to the spectrum seen for wild-type protein, indicating the Ni^{2+} oxidation state. In addition, the presence of a small pre-edge feature at 8330 eV, from a 1s →3d transition, and a larger feature centered at 8336 eV, from the 1s →4p electronic transitions (with respective dimensionless areas of 0.011 and 1.35), is consistent with a coordination number within the range of 4 to 5 ligands, similar to what was observed in the wild-type protein and in other nickel complexes.[28, 30] Subtle changes in the overall edge features were observed between 8340 and 8350 eV when comparing wild-type to C42A-C43A YqjI samples, suggesting that while the geometry is maintained between samples, there is a perturbation in Ni coordination environments for the mutant.

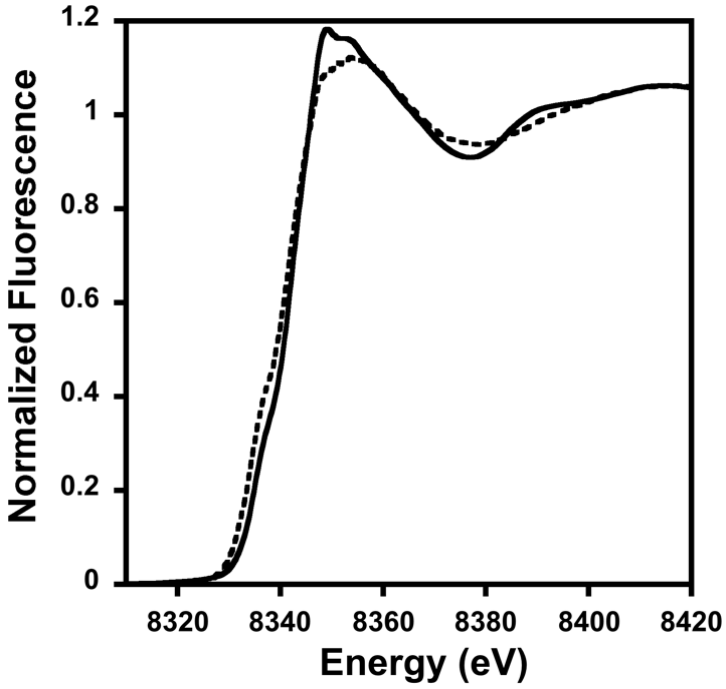

Figure 4.10. Ni XANES Spectra for WT (solid line) and C42A-C43A (dashed line) YqjI double mutant samples.

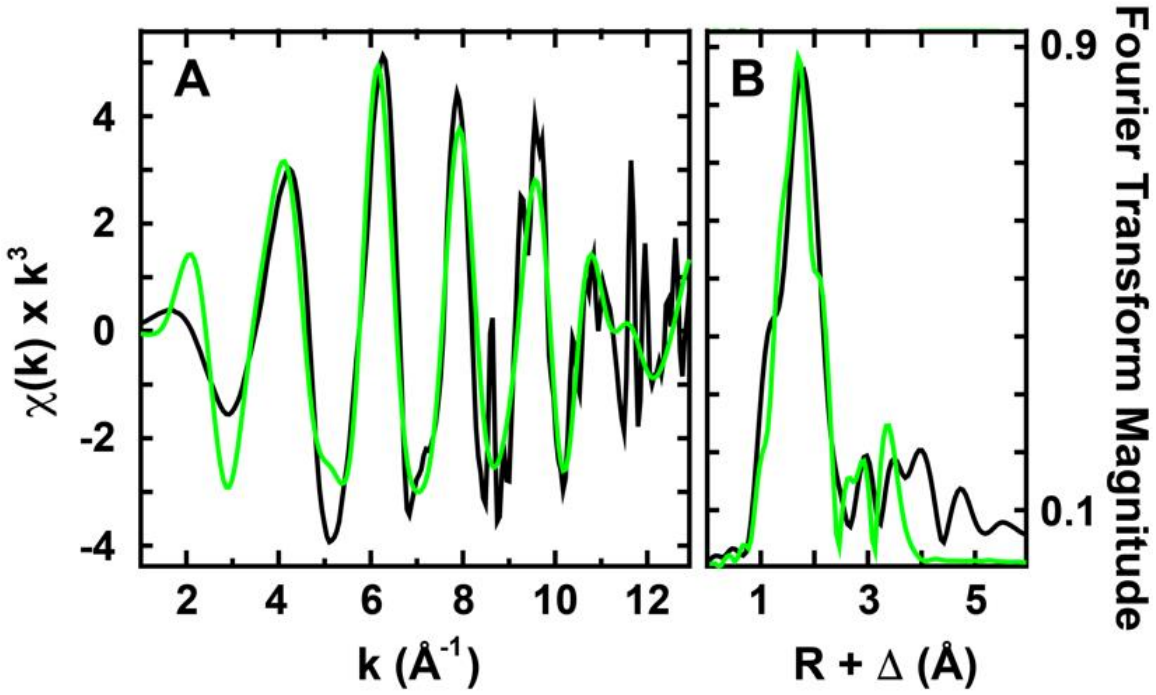

Figure 4.11. EXAFS and Fourier transforms of the Ni site in C42A-C43A YqjI. Raw EXAFS data (**A**) shown in black while Fourier transorms of the raw EXAFS Ni data (**B**) provided adjacent to the EXAFS data. Best fit simulations are shown in green.

Analysis of the Ni EXAFS was used to provide high resolution metrical coordinates for Ni^{2+} bound to C42A-C43A YqjI. Simulations of the raw EXAFS and Fourier transforms of the EXAFS mutant protein, provided in Figure 4.11, are reminiscent of features seen for the wild-type protein. A summary of the EXAFS fitting results for nickel coordination in the wild-type and mutant proteins is provided in Table 4.3. The nickel nearest neighbor ligand environment is again constructed of two unique environments of oxygen/nitrogen and sulfur atoms. An average Ni-O/N bond distance of 1.93 Å is 0.08 Å shorter than the average distance seen for the wild-type protein. The average Ni-S bond distance for the C42A-C43A mutant at 2.22 Å is slightly larger than the value obtained for the wild-type protein at 2.20 Å. These simulated Ni-O/N and Ni-S bond lengths are consistent with the spread of values obtained for Ni-$(O/N)_2S_2$ square planar small molecule compounds although we cannot definitely assign the nickel sites to that geometry.[31] In addition, the long-range Ni•••C scattering observed are at distances consistent with projected carbon scattering from histidine ligand side chains.

XAS analysis for Zn^{2+} bound to wild-type and C42A-C43A mutant YqjI.

Previously it was shown that YqjI also binds a Zn ion that may be important for overall structural stability of the protein. Approximately 0.5 Zn^{2+} bound per monomer of YqjI.[11] However, YqjI DNA-binding activity is not responsive to changing Zn levels in vivo or in vitro, so the separate Zn site does not appear to be regulatory. To ensure that the Cys mutations do not indirectly disrupt YqjI function by altering Zn binding to YqjI, Zn XAS analyses were performed on the wild-type and C42A-C43A mutant YqjI samples. Zn XANES spectra for both wild-type and mutant YqjI (Figure 4.12) are

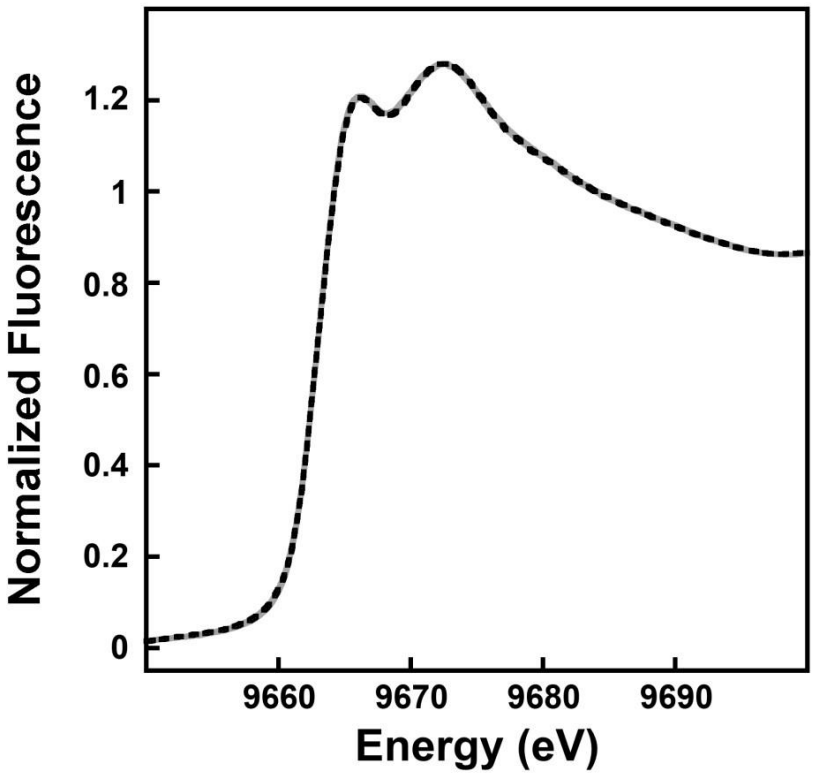

Figure 4.12. Zn XANES spectra for wild-type (solid line) and C42A-C43A (dashed line) YqjI double mutant samples.

consistent with Zn(II) centers with mixed oxygen/nitrogen and sulfur ligand environments.[32] The spectra are identical between the wild-type and C42A-C43A mutant samples, indicating mutation of the C42 and C43 residues does not perturb the Zn binding site within YqjI.

Comparison of the Zn-ligand coordination environments for wild-type and C42A-C43A mutant YqjI suggest identical coordination environments. Raw Zn EXAFS spectra (Figure 4.13) from both samples show a camel back beat pattern at a k value of ~ 4 $Å^{-1}$ and ligand radial distribution profiles at R > 3 Å in the Fourier transforms consistent with Zn–Imidazole scattering from histidine amino acids.[29] Simulations of the Zn-nearest neighbor ligand EXAFS scattering fit best with both samples (Table 4.4) using Zn-O/N and Zn-S bond lengths consistent with Zn-N_2S_2 model compounds in the Cambridge Structural Database.[31] Long range carbon scattering is consistent with C/N multiple scattering patterns for histidine imidazole scattering.[29]

Isothermal titration calorimetry (ITC) analysis for the wild-type and the C42A-C43A mutant of YqjI reveals no major differences in the thermodynamics of nickel binding.

The EXAFS and XANES analyses show that nickel still binds to the C42A-C43A mutant YqjI, although in a slightly altered ligand environment compared to the wild-type YqjI. To evaluate the significance of the altered ligand environment, nickel-binding by wild-type YqjI and the C42A-C43A mutant was analyzed by ITC (Figure 4.14 and Table 4.5).

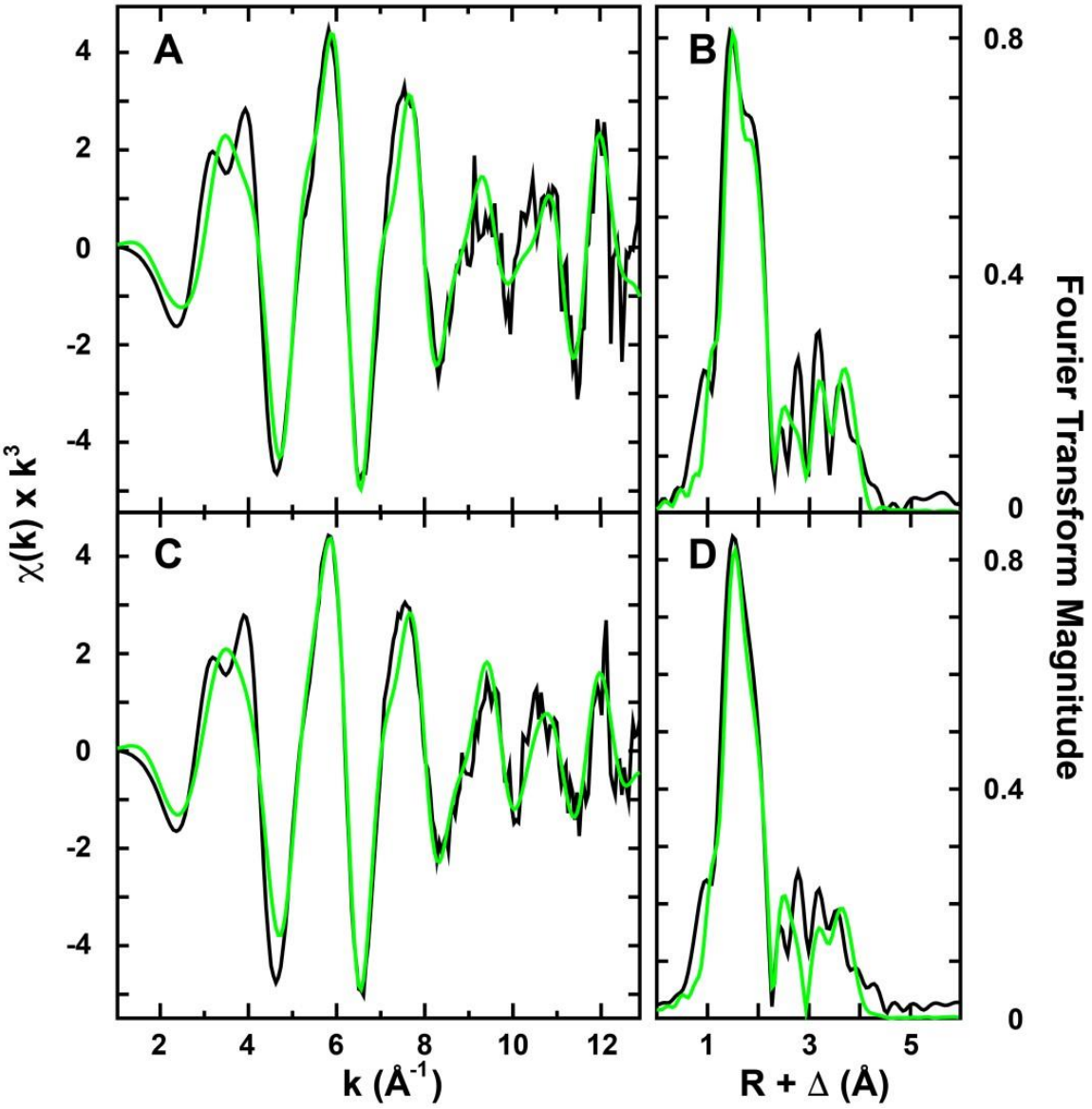

Figure 4.13. EXAFS and Fourier transforms of the Zn site in wild-type and C42A-C43A double mutant YqjI. Raw EXAFS data for wild-type (A) and mutant (C) data shown in black while Fourier transorms of the raw EXAFS data for wild-type (B) and mutant (D) Zn data provided adjacent to the EXAFS data. Best fit simulations are shown in green.

Table 4.4. Summary of the best fit EXAFS simulation analysis for Zn site for wild-type and C42AC43A double mutant YqjI. Values reported are the average of two independent data sets.

	Zn-Nearest Neighbor Ligands [a]				Zn-Long Range Ligands [a]				
Sample	**Atom [b]**	**R(Å) [c]**	**C.N. [d]**	**σ^2 [e]**	**Atom [b]**	**R(Å) [c]**	**C.N. [d]**	**σ^2 [e]**	**F' [f]**
Wild-Type	O/N	1.99	2.0	3.95	C	3.03	1.0	4.34	0.58
	S	2.28	1.0	1.74	C	3.31	2.5	3.09	
					C	4.02	3.0	2.74	
C42A-C43A	O/N	2.00	2.0	3.92	C	3.05	1.5	2.89	0.31
	S	2.28	1.0	2.63	C	3.37	2.0	4.93	
					C	4.02	1.5	2.57	

[a] Independent metal-ligand scattering environment

[b] Scattering atoms: O (Oxygen), N (Nitrogen), C (Carbon) and S (Sulfur)

[c] Metal-ligand bond length

[d] Metal-ligand coordination number

[e] Debye-Waller factor given in $Å^2 \times 10^3$

[f] Number of degrees of freedom weighted mean square deviation between data and simulation

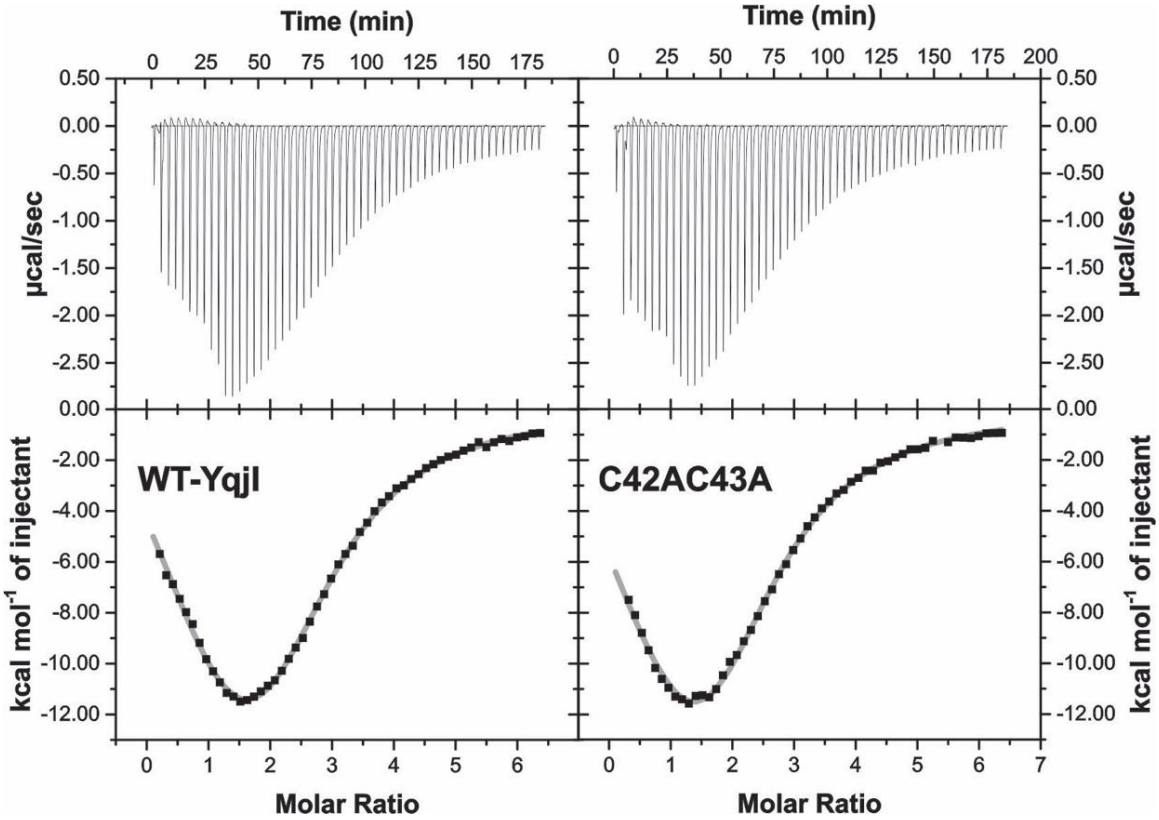

Figure 4.14. ITC scans for monomeric YqjI and the C42A-C43A mutant performed by adding Ni^{2+} to the protein. 1.5mM Ni^{2+} was added in 55 x 5µL injections to 50µM YqjI with 200 second intervals between each injection. Both Ni^{2+} and YqjI were degassed prior to use. Data was processed using ITC analysis software on Origin.

Table 4.5. ITC results for YqjI and the C42A-C43A mutant upon binding to Ni^{2+}.

	K_{D1} (μM)	K_{D2} (μM)	ΔH_1(kcal mol^{-1})	ΔH_2(kcal mol^{-1})	$T\Delta S_1$ (kcal mol^{-1})	$T\Delta S_2$ (kcal mol^{-1})	ΔG_1(kcal mol^{-1})	ΔG_2(kcal mol^{-1})
Wild-type YqjI	**2.2 ± 1.1**	**6.8 ± 2.6**	**-4.0 ± 1.4**	**-18.8 ± 2.0**	**3.9 ± 1.1**	**-11.4 ± 2.2**	**-7.9 ± 0.4**	**-7.4 ± 0.2**
C42A-C43A YqjI	**3.1 ± 0.3**	**10.2 ± 1.3**	**-5.7 ± 0.9**	**-20.7 ± 0.5**	**1.9 ± 0.8**	**-13.7 ± 0.6**	**-7.6 ± 0.1**	**-7.0 ± 0.1**

ITC analysis shows that wild-type YqjI binds a maximum of three nickels in vitro (Figure 4.14). However, subsequent ICP-MS analysis on the same sample revealed that only 2 nickels remained bound to YqjI if the ITC sample was desalted after the last nickel addition. The loss of one nickel during desalting indicates that one nickel is only loosely bound to YqjI. The K_D values measured by ITC for the first two sites were similar at 2.2μM and 6.8μM, while the third site was 10-fold weaker with a K_D of 64.0μM. It should be stressed that these K_D values are only apparent dissociation constants because other coupled equilibria that can alter total heat flow (including ligand protonation/deprotonation or buffer effects) have not been separately evaluated. Interestingly, the thermodynamic data for the two nickel binding sites reveals a major difference in the driving force between the first and second nickel binding reactions. For the first nickel binding site, changes in enthalpy and entropy are both energetically favorable (Table 4.5). However, for the second nickel binding event, there is a significant entropic penalty upon nickel binding ($T\Delta S$ = -11.4 kcal mol^{-1}) that is compensated for by a highly favorable enthalpy change (ΔH = -18.8 kcal mol^{-1}). These thermodynamic differences in the two sites may be responsible for the difference in apparent K_D values between them.

Next, nickel binding to the C42A-C43A mutant of YqjI was analyzed. Despite the Cys pair mutations showing in vivo effects, three nickels still bound C42A-C43A with the third nickel again being lost following desalting. Consistent with the results of the EXAFS, the apparent K_D values for C42A-C43A YqjI were similar to those measured for the wild-type YqjI. The thermodynamic parameters measured by ITC were also quite similar between mutant and wild-type YqjI proteins (Table 4.5). Favorable enthalpy and

entropy changes still drove the first nickel binding while a highly favorable enthalpy change was needed to overcome the entropic penalty of the second nickel binding (Table 4.5 and Figure 4.14).

The C42A-C43A mutant still binds nickel in vitro.

To supplement the ITC analysis, we also utilized an alternative technique to measure the YqjI K_D for nickel binding. The small molecule chelator Mag-fura-2 (MF2) (K_D for nickel = 150nM) was used as a competitor to measure the YqjI K_D values.[15, 33-35] Nickel binding by MF2 can be monitored by changes in absorbance or fluorescence, allowing us to easily monitor the effect of YqjI on MF2 nickel occupancy. All calculations were performed in DynaFit with the observation that two nickels are sequentially bound to wild-type YqjI. Sequential binding was selected over independent binding due to the improved fit observed for the competitive binding assay data (see Materials and Methods).

As shown in Figure 4.15, wild-type YqjI bound Ni^{2+} with a K_{D1} of 4.0 ± 0.5nM and K_{D2} of 76 ± 16.3nM, which illustrates that the first site binds almost 20-fold tighter than the second site. The difference in affinity for the two sites was somewhat greater than the 3-fold difference in apparent K_D values observed by ITC (Table 4.5). The C42A-C43A YqjI mutant protein demonstrated slightly weaker binding of Ni^{2+} at both sites with a K_{D1} of 16.1 ± 6.6nM and a K_{D2} of 142.0 ± 32.7nM. This decrease in affinity, primarily at site 1, could be due to the subtle alteration in the nickel coordination sites observed in XAS and EXAFS data for the C42A-C43A mutant (Figures 4.10 and 4.11, Table 4.3). The slight decrease in nickel binding affinity does not seem to explain inability of the

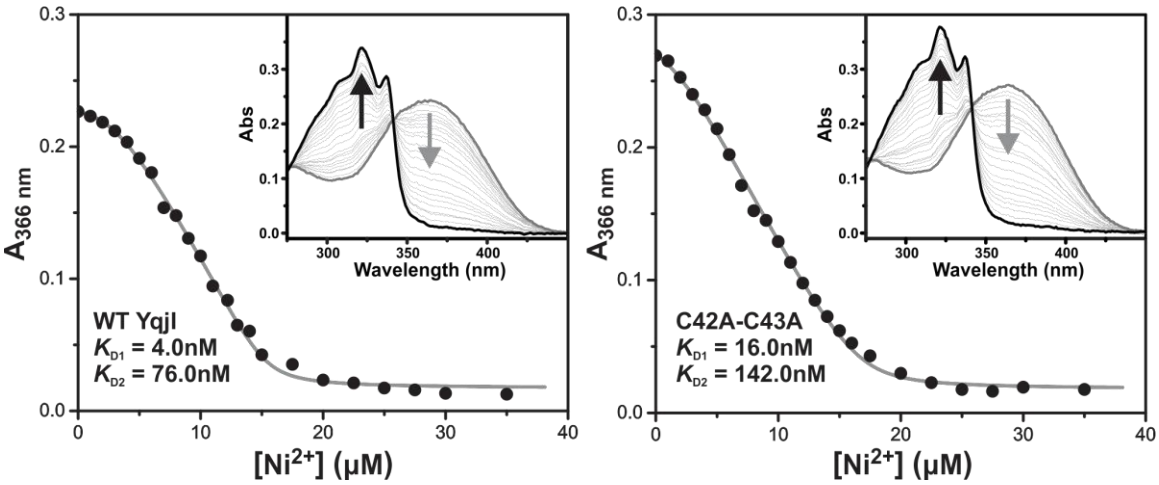

Figure 4.15. Mag-fura-2 titrations of wild-type YqjI and the C42A-C43A mutant YqjI to determine the K_D values for Ni^{2+}. 10μM of Mag-fura-2 and 2.5μM YqjI were titrated with Ni^{2+}. The Abs_{366} was plotted and the values applied to a customized formula in Dynafit under the assumption of sequential two-site nickel-binding to determine the two K_D values.

C42A-C43A mutant to efficiently respond to nickel in vivo (Figure 4.8). This data suggests that C42A and C43A are not obligate ligands for nickel-sensing by YqjI but that mutating them may alter local structure in the N-terminus that indirectly perturbs the YqjI nickel responsiveness (see Results and Discussion below). A third additional site possessing a much lower affinity for nickel was observed using ITC, but the nickel separates after desalting the protein and this site was not required to fit the data gathered during the MF2 competition assay. Overall, nickel binding to both the C42A-C43A mutant and the wild-type protein proceeds via two sequential nickel-binding events with the first being more than a factor of ten tighter than the second. Additionally, the C42A-C43A mutant displays a moderate alteration of binding affinity without losing the ability to bind two nickels.

Assessment of the free thiol status in the YqjI N-terminus.

Based on the extensive EXAFS, ITC, and MF2 competition assays, C42 and C43 do not appear to be obligate ligands for nickel coordination in YqjI. It is possible that C42 and C43 mediate nickel-responsive structural changes within YqjI by stabilizing a specific conformation of the YqjI N-terminus. Although the N-terminus is not predicted to have a defined secondary structure, one or more disulfide bonds in the N-terminus may provide a local level of structural order in that region. In order to determine the redox state of Cys residues in the YqjI N-terminus, the concentration of free thiols in purified YqjI was measured with DTNB under a mix of native, denaturing, and strongly reducing conditions. Table 4.6 shows the results of DTNB assays using wild-type and C42A-C43A YqjI. All proteins were in their apo (nickel-free) forms for these experiments.

Table 4.6. DTNB assay for wild-type YqjI and C42A-C43A YqjI

YqjI protein analyzed	Thiols Detected with DTNB after various treatments (anaerobic)			
	Native	Unfolded †	Native, Reduced ⊥	Unfolded and Reduced †⊥
Wild-Type*	**2.8 ± 0.2**	**2.9 ± 0.1**	**5.8 ± 0.5**	**7.5 ± 0.7**
C42A-C43A	**2.8 ± 0.0**	**2.6 ± 0.0**	**3.9 ± 0.1**	**6.1 ± 0.3**

*Wild-type YqjI contains a total of 8 Cys residues.
† 8M Urea
⊥30 mM TCEP
§ See Figure S4 for scheme describing treatments of each YqjI sample and Materials and Methods for experimental details.

Urea and TCEP were selected as denaturant and reductant, respectively, in order to unfold the protein and to reduce any existing disulfide bonds. All analyses were carried out anaerobically to prevent adventitious Cys oxidation after removal of reductant but prior to the DTNB measurement.

Under native conditions, only 3 of the total 8 cysteines can be detected by reaction with DTNB in the wild-type YqjI protein (Table 4.6). Unfolding YqjI with 8M urea in the absence of reductant did not further expose any additional Cys residues. However, addition of the strong reductant TCEP to native YqjI resulted in the exposure of 3 additional Cys residues. This result could indicate the presence of a disulfide bond that also structurally prohibits the access of DTNB to a third free thiol deeper in the protein interior. When wild-type YqjI was denatured by 8M urea in the presence of TCEP, all 8 of the total Cys residues could be detected by DTNB. Together these results suggest the existence of at least one TCEP-accessible disulfide bond in YqjI that helps maintain a local structure where other Cys residues are less solvent exposed. When the disulfide(s) is present, this local structure is maintained even when other secondary and tertiary structures are unfolded by urea. Since 7 of the 8 Cys residues in YqjI are located in the N-terminal region, the disulfide and the "protected" Cys residues are likely in that region as well.

When the C42A-C43A YqjI mutant was analyzed, it showed the same three DTNB accessible Cys residues as the wild-type YqjI under native conditions and after urea treatment (Table 4.6). However, treatment with TCEP resulted in only a single Cys residue being detected by DTNB (Table 4.6). Treatment of C42A-C43A YqjI with both urea and TCEP resulted in DTNB detection of all 6 Cys residues in that mutant. Based

on these results, it seems logical to infer that C42 and C43 form a vicinal disulfide bond that is TCEP-accessible. The C42-C43 disulfide helps to maintain local structure within the disordered YqjI N-terminus, thereby helping to block DTNB access to other Cys residues.

Discussion

Site-directed mutagenesis, in vivo functional analysis, and spectroscopic characterization revealed that YqjI requires the adjacent C42-C43 residues for proper in vivo function but that these two residues are likely not obligate ligands for nickel binding by YqjI (NfeR). Two different methods were used to assess the nickel-binding affinity of the sites in both mutant and wild-type YqjI. For wild-type YqjI (NfeR), ITC showed K_{D1} = 2μM and K_{D2} = 7μM while a metal chelator competition assay showed K_{D1} = 4nM and K_{D2} = 76nM. At present, we cannot explain the discrepancy between the two methods, although we note that metal-binding analyses of the metalloregulator MntR have shown that ITC provided larger K_D values than competition assays in some cases.[25] Because ITC monitors total changes in heat, the results may not reflect multiple steps occurring during metal binding, such as nickel transiting through binding intermediates, if those preliminary steps do not involve changes in heat. Given that we observe three binding sites and given the plasticity of the N-terminus of YqjI in respect to metal ligands, it is possible that ITC provides a K_D^{App} that reflects a number of steps or processes that occur prior to formation of the final nickel site but which do not necessarily release or consume heat.

In contrast, the competition assay is monitoring the binding process differently. Regardless of the complexity of nickel interactions with YqjI, the competition assay is only assaying the ability of YqjI to compete with MF2 for nickel. The simplicity of the assay could provide a more accurate estimate of K_D although it would not provide important information about the stepwise process or thermodynamics of nickel binding to YqjI. It also is worth pointing out that a chelator competition assay may provide erroneous binding data if the protein physically interacts with the chelator in the absence of metal ligand and alters its metal affinity or other properties. We did not observe any change in MF2 fluorescence or UV-visible absorption features when the chelator was mixed with YqjI without nickel addition, suggesting there is not an artefactual interaction between protein and chelator that would skew the assay used in this study (Figure 4.16 and data not shown). However, this experiment does not completely rule out the possibility of ternary complex formation (YqjI-MF2-Ni^{2+}) during the competition assay that might explain the large discrepancy between the binding constants measured with the two methods.

It is worth noting that the nanomolar K_D values obtained using the competition assay are consistent with the previously measured nickel affinities of *E. coli* NikR and RcnR, which together define the physiological range of cytoplasmic nickel concentration to be 10 – 500 nM in this organism.[36] However, it is possible that transcriptional control of target genes by YqjI (NfeR) responds to a higher concentration of nickel in vivo, providing additional gene regulation in response to excessive nickel stress where cytoplasmic nickel concentrations rise into the μM range. In that case the K_D values from ITC may be the more physiologically relevant. Regardless of this uncertainty, it is clear

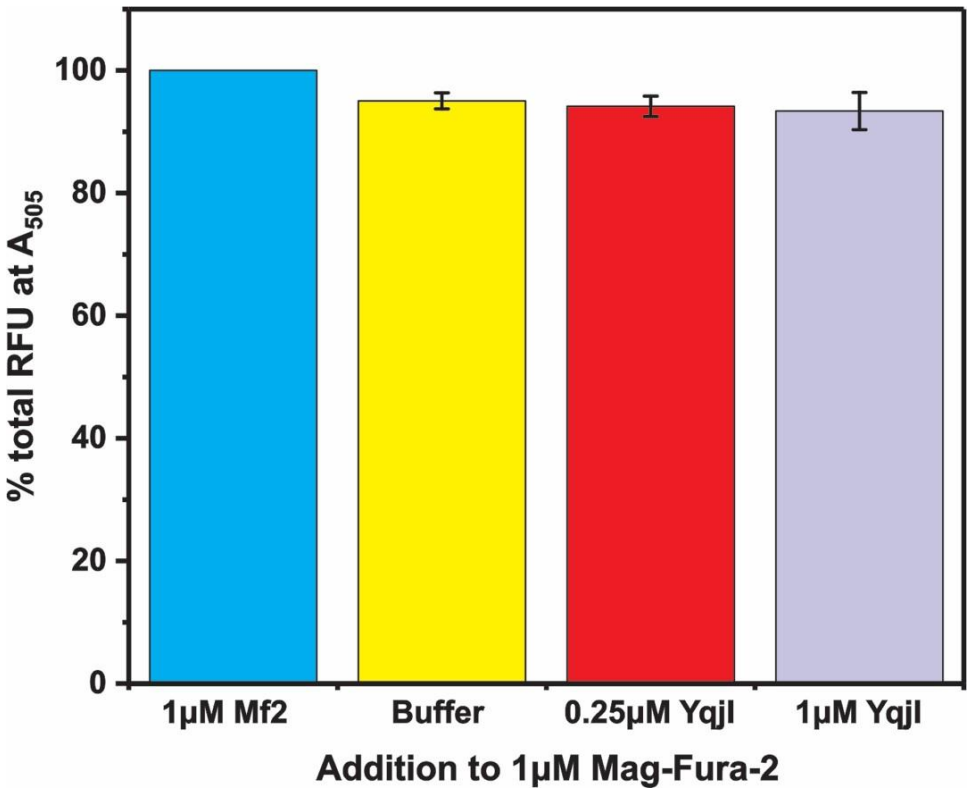

Figure 4.16. Monitoring RFU from intrinsic Mag-Fura-2 fluorescence upon addition of buffer or YqjI (NfeR) to MF2. Assays were conducted in microtiter plate with 1μM MF2. Both 1:4 and 1:1 molar ratios of YqjI:MF2 are tested here (corresponding to 0.25 and 1 μM YqjI with 1 μM MF2). For comparison, a molar ratio of 1:4 YqjI:MF2 is used for the chelator competition assay used to measure the K_D of nickel-binding to YqjI (see main text, Materials and Methods).

that mutation of the C42-C43 residues does not significantly impact nickel binding by YqjI (NfeR).

Analysis of free thiol status in YqjI suggests that C42-C43 form a vicinal disulfide bond that may be required for nickel-responsive gene regulation by YqjI. Although rare, vicinal disulfides have been identified in protein structures and shown to have important roles in protein function.[37] Vicinal disulfides form an eight-membered ring structure consisting of the Cys side chain atoms as well as the backbone α-carbons and the α-amino and α-carboxyl groups that form the peptide bond between the two Cys residues. The constraints of the ring structure lead to high dihedral strain energy for the disulfide bridge and results in a non-planar amide bond between the Cys residues.[37] The conformational restriction of vicinal disulfides can be important for stabilizing a specific local structure within the protein. The presence of a structurally constrained vicinal disulfide may be significant for coordinating nickel binding by the relatively unstructured N-terminus of YqjI with changes in the well-structured DNA-binding domain.

The existence of the vicinal disulfide is supported by analysis of the free thiol status of purified YqjI and by the in vivo functional changes in the YqjI protein where C42 and C43 have been mutated. The regulatory behavior of the two single C42A and C43A YqjI proteins closely resembled that of the C42A-C43A YqjI double mutant in the in vivo gene expression studies. This result would be expected if C42 and C43 form a disulfide since mutation of either Cys residue would disrupt the disulfide structure in YqjI. Additionally, XAS analysis revealed that while the C42A-C43A mutations slightly alter the nickel binding environment in YqjI, they clearly do not block nickel binding. The 2-3 fold reduction in the K_D values for the two nickel sites is unlikely to significantly

alter YqjI nickel-binding in vivo during high nickel stress. The mutant YqjI still bound nickel with 16 nM and 142 nM affinity, which is in the same range as other nickel stress response regulators in *E. coli*, including RcnR (25 nM).[15]

The putative vicinal disulfide between C42 and C43 appears to be critical for the nickel-responsiveness of YqjI. We propose that this disulfide provides a structurally rigid "hinge" by which the actual nickel-binding sites within YqjI can allosterically communicate with the PadR-like DNA binding domain of YqjI. This model is supported by several in vivo results. First, single or double mutations in C42 and C43 result in a YqjI protein that more tightly represses the *yqjH* and *yqjI* target promoters in vivo. This functional change could occur because the DNA binding domain of YqjI has been uncoupled from the regulatory domain in the N-terminus leading to elevated repression of its target promoters. Second, mutation of the C42 and C43 residues diminishes the nickel response of YqjI in vivo. Based on the in vitro nickel-binding studies of YqjI, it is likely that nickel is still binding those mutant proteins but the signal is not being effectively communicated to the YqjI DNA binding domain. Since the effect of nickel is to switch off YqjI repressor function, loss of this allosteric switching in the mutant YqjI leads to less induction of the YqjI target promoters under high nickel conditions in vivo.

This model does not address the surprising failure to isolate Cys mutants in YqjI that directly block nickel binding. Based on the EXAFS and XANES results, the wild-type YqjI nickel binding sites should contain multiple thiols, yet mutation of C8-C9 and C20-C21 did not disrupt YqjI nickel responsiveness in vivo and the C42-C43 mutations only subtly altered nickel binding. However, the answer may lie with the unusual amino acid composition of the first 50 amino acids of the N-terminal region of YqjI. In addition

to 7 Cys residues that may be able to substitute for each other, the N-terminal region also contains 12 His and 7 Glu residues that may replace any thiol ligand(s) missing from the wild-type site. If this is the case, much more extensive mutagenesis of these other putative metal-binding residues will need to be carried out to completely block all nickel-binding activity in YqjI. Unfortunately, this type of mutagenesis may fail to pinpoint the wild-type nickel-binding sites in YqjI as it would only define the entire set of ligands that might bind nickel (depending on the absence or presence of other mutations). Crystallization of wild-type Ni-YqjI may be the only way to convincingly define the wild-type nickel sites in YqjI.

The thermodynamics of nickel binding to YqjI revealed that the two stable nickel sites in YqjI are not equivalent. The favorable changes in entropy and enthalpy associated with the first nickel binding event may explain the higher affinity for that site. A positive (favorable) entropy change could suggest desolvation of Cys and His residues involved in metal ligation or the release of water molecules that are unfavorably ordered around a nonpolar surface in the protein. In contrast, there is a high entropic cost to the second nickel-binding event that is overcome by a much more favorable change in enthalpy. The second nickel binding may lead to bond formation that stabilizes a specific conformation of the YqjI N-terminus. This increased bonding could lead to conformational restriction or a loss of translational/rotational degrees of freedom upon nickel binding to YqjI, thereby leading to the unfavorable change in entropy. Such changes would be consistent with nickel acting as an allosteric regulator of YqjI DNA-binding activity, which likely requires structural or conformational changes. The thermodynamics and enthalpic drive of the second binding site is similar to nickel

binding behavior observed for SlyD [38] and follow the typical process of coordination during which amino acid side chains assume a rigid conformation around a metal ion .[39, 40]

We may then add to our model the nickel-binding plasticity of the N-terminus that allows nickel to still bind and communicate (via the C42-C43 "hinge") to the DNA-binding domain of YqjI, even when the exact nickel binding site is different from the wild-type YqjI. However, such metal-binding plasticity would be rendered moot by the mutation of C42 and/or C43 that would uncouple the sensor region from the DNA-binding domain. Based on this model, the most important sequence determinants in the N-terminus are C42 and C43 that transmit the nickel-binding events from a somewhat indiscriminate nickel-binding "sponge" to the DNA-binding domain of YqjI.

References

1. Blahut, M.; Dzul, S.; Wang, S.; Kandegedara, A.; Grossoehme, N. E.; Stemmler, T.; Outten, F. W., Conserved cysteine residues are necessary for nickel-induced allosteric regulation of the metalloregulatory protein YqjI (NfeR) in E. coli. *J Inorg Biochem* **2018,** *184*, 123-133.

2. Ahmed, E.; Holmstrom, S. J., Siderophores in environmental research: roles and applications. *Microb Biotechnol* **2014,** *7* (3), 196-208.

3. Imlay, J. A., How oxygen damages microbes: Oxygen tolerance and obligate anaerobiosis. *Adv Microb Physiol* **2002,** *46*, 111-153.

4. Hantke, K., Cloning of the repressor protein gene of iron-regulated systems in Escherichia coli K12. *Mol Gen Genet* **1984,** *197* (2), 337-41.

5. Hantke, K., Iron and metal regulation in bacteria. *Curr Opin Microbiol* **2001,** *4* (2), 172-7.

6. McHugh, J. P.; Rodriguez-Quinones, F.; Abdul-Tehrani, H.; Svistunenko, D. A.; Poole, R. K.; Cooper, C. E.; Andrews, S. C., Global iron-dependent gene regulation in Escherichia coli. A new mechanism for iron homeostasis. *J Biol Chem* **2003,** *278* (32), 29478-86.

7. Miethke, M.; Hou, J.; Marahiel, M. A., The siderophore-interacting protein YqjH acts as a ferric reductase in different iron assimilation pathways of Escherichia coli. *Biochemistry* **2011,** *50* (50), 10951-64.

8. Gury, J.; Barthelmebs, L.; Tran, N. P.; Divies, C.; Cavin, J. F., Cloning, deletion, and characterization of PadR, the transcriptional repressor of the phenolic acid decarboxylase-encoding padA gene of Lactobacillus plantarum. *Appl Environ Microbiol* **2004,** *70* (4), 2146-53.

9. Marchler-Bauer, A.; Anderson, J. B.; Chitsaz, F.; Derbyshire, M. K.; DeWeese-Scott, C.; Fong, J. H.; Geer, L. Y.; Geer, R. C.; Gonzales, N. R.; Gwadz, M.; He, S.; Hurwitz, D. I.; Jackson, J. D.; Ke, Z.; Lanczycki, C. J.; Liebert, C. A.; Liu, C.; Lu, F.; Lu, S.; Marchler, G. H.; Mullokandov, M.; Song, J. S.; Tasneem, A.; Thanki, N.; Yamashita, R. A.; Zhang, D.; Zhang, N.; Bryant, S. H., CDD: specific functional annotation with the Conserved Domain Database. *Nucleic Acids Res* **2009,** *37* (Database issue), D205-10.

10. Fibriansah, G.; Kovacs, A. T.; Pool, T. J.; Boonstra, M.; Kuipers, O. P.; Thunnissen, A. M., Crystal structures of two transcriptional regulators from Bacillus cereus define the conserved structural features of a PadR subfamily. *PloS One* **2012,** *7* (11), e48015.

11. Wang, S.; Wu, Y.; Outten, F. W., Fur and the novel regulator YqjI control transcription of the ferric reductase gene yqjH in Escherichia coli. *J Bacteriol* **2011,** *193* (2), 563-74.

12. Wang, S.; Blahut, M.; Wu, Y.; Philipkosky, K. E.; Outten, F. W., Communication between binding sites is required for YqjI regulation of target promoters within the yqjH-yqjI intergenic region. *J Bacteriol* **2014,** *196* (17), 3199-207.

13. Zhang, J. W.; Butland, G.; Greenblatt, J. F.; Emili, A.; Zamble, D. B., A role for SlyD in the Escherichia coli hydrogenase biosynthetic pathway. *J Biol Chem* **2005,** *280* (6), 4360-6.

14. Rodrigue, A.; Effantin, G.; Mandrand-Berthelot, M. A., Identification of rcnA (yohM), a nickel and cobalt resistance gene in Escherichia coli. *J Bacteriol* **2005,** *187* (8), 2912-6.

15. Iwig, J. S.; Leitch, S.; Herbst, R. W.; Maroney, M. J.; Chivers, P. T., Ni(II) and Co(II) sensing by Escherichia coli RcnR. *J Am Chem Soc* **2008,** *130* (24), 7592-606.

16. Steiner, R. A.; Dzul, S. P.; Stemmler, T. L.; Harrop, T. C., Synthesis and Speciation-Dependent Properties of a Multimetallic Model Complex of NiSOD That Exhibits Unique Hydrogen-Bonding. *Inorg Chem* **2017,** *56* (5), 2849-2862.

17. Shimberg, G. D.; Michalek, J. L.; Oluyadi, A. A.; Rodrigues, A. V.; Zucconi, B. E.; Neu, H. M.; Ghosh, S.; Sureschandra, K.; Wilson, G. M.; Stemmler, T. L.; Michel, S. L. J., Cleavage and polyadenylation specificity factor 30: An RNA-binding zinc-finger protein with an unexpected 2Fe-2S cluster. *Proc Natl Acad Sci U S A* **2016,** *113* (17), 4700-4705.

18. Rehr, J. J.; Ankudinov, A. L., Progress and challenges in the theory and interpretation of X-ray spectra. *J Synchrotron Radiat* **2001,** *8* (Pt 2), 61-5.

19. George, G. N.; George, S. J.; Pickering, I. J. *EXAFSPAK*, http://www-ssrl.slac.stanford.edu/~george/exafspak/exafs.htm: Menlo Park, CA, 2001.

20. Bencze, K. Z.; Kondapalli, K. C.; Stemmler, T. L., X-Ray Absorption Spectroscopy. In *Applications of Physical Methods in Inorganic and Bioinorganic Chemistry: Handbook, Encyclopedia of Inorganic Chemistry, 2nd Edition*, Scott, R. A.; Lukehart, C. M., Eds. John Wiley & Sons,LTD: Chichester, UK, 2007; pp 513-28.

21. Cotelesage, J. J.; Pushie, M. J.; Grochulski, P.; Pickering, I. J.; George, G. N., Metalloprotein active site structure determination: synergy between X-ray absorption spectroscopy and X-ray crystallography. *J Inorg Biochem* **2012,** *115*, 127-37.

22. Riggs-Gelasco, P. J.; Stemmler, T. L.; Penner-Hahn, J. E., Xafs of Dinuclear Metal Sites in Proteins and Model Compounds. *Coord Chem Rev* **1995,** *144*, 245-286.

23. Miller, J. H., Experiments in Molecular Genetics. In *Experiments in Molecular Genetics* [Online] Cold Spring Harbor Laboratory: Cold Spring Harbor, N.Y., 1972; pp. xvi, 466 p.

24. MicroCal-LLC, VP-ITC MicroCalorimeter User's Manual. In *VP-ITC MicroCalorimeter User's Manual* [Online] Malvern: Northampton, MA., 2002.

25. Golynskiy, M. V.; Gunderson, W. A.; Hendrich, M. P.; Cohen, S. M., Metal binding studies and EPR spectroscopy of the manganese transport regulator MntR. *Biochemistry* **2006,** *45* (51), 15359-72.

26. Kuzmic, P., Program DYNAFIT for the analysis of enzyme kinetic data: application to HIV proteinase. *Anal Biochem* **1996,** *237* (2), 260-73.

27. Riddles, P. W.; Blakeley, R. L.; Zerner, B., Reassessment of Ellman Reagent. *Methods Enzymol* **1983,** *91*, 49-60.

28. Colpas, G. J.; Maroney, M. J.; Bagyinka, C.; Kumar, M.; Willis, W. S.; Suib, S. L.; Baidya, N.; Mascharak, P. K., X-Ray Spectroscopic Studies of Nickel-Complexes, with Application to the Structure of Nickel Sites in Hydrogenases. *Inorg Chem* **1991,** *30* (5), 920-928.

29. Stemmler, T. L.; Sossong, T. M.; Goldstein, J. I.; Ash, D. E.; Elgren, T. E.; Krutz, D. M.; PennerHahn, J. E., EXAFS comparison of the dimanganese core structures of manganese catalase, arginase, and manganese-substituted ribonucleotide reductase and hemerythrin. *Biochemistry* **1997,** *36* (32), 9847-9858.

30. Higgins, K. A.; Chivers, P. T.; Maroney, M. J., Role of the N-terminus in Determining Metal-Specific Responses in the E. coli Ni- and Co-Responsive Metalloregulator, RcnR. *J Am Chem Soc* **2012,** *134* (16), 7081-7093.

31. Allen, F. H., The Cambridge Structural Database: a quarter of a million crystal structures and rising. *Acta Crystallogr B* **2002,** *58*, 380-388.

32. Clark-Baldwin, K.; Tierney, D. L.; Govindaswamy, N.; Gruff, E. S.; Kim, C.; Berg, J.; Koch, S. A.; Penner-Hahn, J. E., The limitations of X-ray absorption spectroscopy for determining the structure of zinc sites in proteins. When is a tetrathiolate not a tetrathiolate? *J Am Chem Soc* **1998,** *120* (33), 8401-8409.

33. Sydor, A. M.; Lebrette, H.; Ariyakumaran, R.; Cavazza, C.; Zamble, D. B., Relationship between Ni(II) and Zn(II) coordination and nucleotide binding by the Helicobacter pylori [NiFe]-hydrogenase and urease maturation factor HypB. *J Biol Chem* **2014,** *289* (7), 3828-41.

34. Pederick, V. G.; Eijkelkamp, B. A.; Begg, S. L.; Ween, M. P.; McAllister, L. J.; Paton, J. C.; McDevitt, C. A., ZnuA and zinc homeostasis in Pseudomonas aeruginosa. *Sci Rep* **2015,** *5*, 13139.

35. Lisher, J. P.; Higgins, K. A.; Maroney, M. J.; Giedroc, D. P., Physical characterization of the manganese-sensing pneumococcal surface antigen repressor from Streptococcus pneumoniae. *Biochemistry* **2013,** *52* (43), 7689-701.

36. Musiani, F.; Zambelli, B.; Bazzani, M.; Mazzei, L.; Ciurli, S., Nickel-responsive transcriptional regulators. *Metallomics* **2015,** *7* (9), 1305-18.

37. Richardson, J. S.; Videau, L. L.; Williams, C. J.; Richardson, D. C., Broad Analysis of Vicinal Disulfides: Occurrences, Conformations with Cis or with Trans Peptides, and Functional Roles Including Sugar Binding. *J Mol Biol* **2017,** *429* (9), 1321-1335.

38. Martino, L.; He, Y.; Hands-Taylor, K. L.; Valentine, E. R.; Kelly, G.; Giancola, C.; Conte, M. R., The interaction of the Escherichia coli protein SlyD with nickel ions illuminates the mechanism of regulation of its peptidyl-prolyl isomerase activity. *FEBS J* **2009,** *276* (16), 4529-44.

39. Grossoehme, N. E.; Mulrooney, S. B.; Hausinger, R. P.; Wilcox, D. E., Thermodynamics of Ni2+, Cu2+, and Zn2+ binding to the urease metallochaperone UreE. *Biochemistry* **2007,** *46* (37), 10506-16.

40. Zambelli, B.; Danielli, A.; Romagnoli, S.; Neyroz, P.; Ciurli, S.; Scarlato, V., High-affinity Ni2+ binding selectively promotes binding of Helicobacter pylori NikR to its target urease promoter. *J Mol Biol* **2008,** *383* (5), 1129-43.

APPENDIX A

FTNB

Table A.1. Strains made in attempt to express FtnB protein

Construct	About	Outcome
DH5α_FtnB_His_p283	C-terminal His-tag, Kn^R	Extremely low expression, no solubility
DH5α_FtnB_pET21a	Amp^R	Extremely low expression, no solubility
DH5α_His_FtnB_p11	N-terminal His-tag, Amp^R	Extremely low expression, no solubility
DH5α_pDB_His_GST_FtnB	N-terminal His-GST fusion, Kn^R	Expression, needs cholate and lysozyme for solubility, minimal TEV cleavage
DH5α_FtnB_Stag_pETDuet	C-terminal S-tag, Amp^R	Extremely low expression, no solubility
DH5α_FtnA_FtnB_Stag_pETDuet	FtnA at site 1, C-terminal S-tag, Amp^R	No FtnB expression
DH5α_His_FtnB_pETDuet	C-terminal His-tag, Amp^R	No FtnB expression
DH5α_FtnB_mycHis_pBAD	AraBAD promoter, C-terminal mycHis tag, Amp^R	No FtnB expression
DH5α_MBP_TEV_pET21a	Amp^R to co-express in vivo with GST/NusA fusion	TEV expresses, but fails to cleave FtnB in vivo
DH5α_His_FtnB_FtnA_pETDuet	His-tag, FtnA at site 2, Amp^R	No FtnB expression
DH5α_pDB_His_NusA_FtnB	N-terminal His-NusA fusion, Kn^R	Expression, needs cholate and lysozyme for solubility, minimal TEV cleavage
DH5α_pColdII_His_TEV_SFtnB	Cold induction vector (15°C) with codon optimized *Salmonella enterica* FtnB	Great expression, but no solubility

DH5α_pColdII_NoHis/TEV/NdeI_SFtnB	*Salmonella* FtnB without His tag or NdeI site	Great expression, but no solubility
DH5α_pColdII_NoHis/TEV_SFtnB	*Salmonella* FtnB without His tag	Great expression, but no solubility

Expression of the FtnB protein proved extremely problematic. The *E. coli* form of the protein has almost no expression without a protein fusion tag. With a fusion tag like GST or NusA, expression is substantial but requires lysis in the presence of 1 mg/mL lysozyme and 0.8% cholic acid to solubilize. Additionally, cleavage with TEV only has minimal impact and obtaining clean FtnB without the fusion tag or TEV is very difficult with the exception of a small amount of the monomeric form of the protein, which I do not feel is the functional form.

As for the codon optimized form of Salmonella typhimurium FtnB, expression levels are very high, but solubility is non-existent. Attempts were made to solubilize the cell pellet after sonication in 50 mM KPI, 2 M urea, pH = 12.0 in order to extract the protein from the pellet. From here, dialysis in 4 liters of 50 mM KPI, pH =8.0 was used but resulted in precipitation. 50 mM Tris, pH = 8.0 worked better, but failed to bind the nickel column despite the His-tag. Additionally, concentration and loading onto the gel filtration column showed multiple species of varying sizes but validating the resulting form as the true in vivo form of this protein was impossible. The protein also showed issues concentrating and was not fully clean. In the future, treating FtnB like a membrane protein might be a better option.

APPENDIX B

PERMISSIONS

Publisher permission (below) for Chapter 2. Additional information can be found at http://www.jbc.org/site/misc/edpolicy.xhtml.

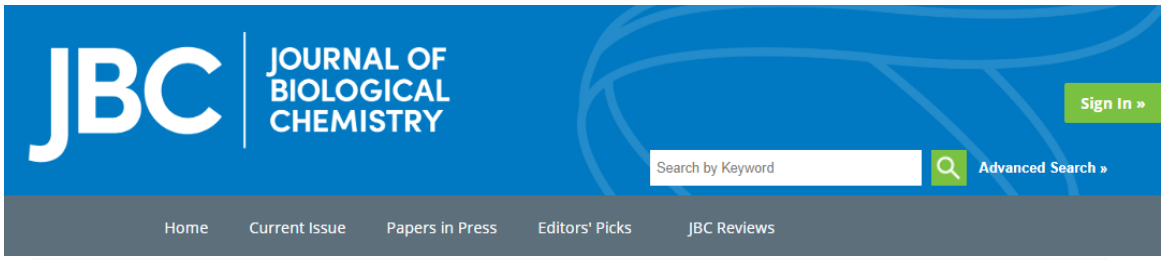

Copyright and license to publish

The text below explains the process for reusing content that was originally published in JBC. If you want to reuse previously published content in a new submission to JBC and need guidance regarding permissions, please click here.

For authors:

Effective with initial submissions from January 1, 2018, authors must agree that if their manuscript is accepted, they will grant ASBMB an exclusive, irrevocable License to Publish their work; the copyright remains with the authors.

Manuscripts initially submitted prior to January 1, 2018 are subject to JBC's former policy whereby, as a condition of publication, authors transfer copyright to ASBMB upon acceptance.

Authors of manuscripts, submitted at any time, need not contact the journal to request permission to reuse their own material. Authors who granted ASBMB exclusive license to publish and authors who transferred copyright to ASBMB, are allowed to do the following:

a. to use all or part of the work in compilations or other publications of the Authors' own commercial and noncommercial works (includes theses/dissertations), to use figures, photos, and tables created by them and contained in the work, to present the work orally in its entirety, and to make copies of all or part of the work for the Authors' use for lectures, classroom instruction or similar uses. If the author is employed by an academic institution, that institution also may reproduce the article for teaching purposes.
b. to post the accepted manuscript version of the work, the "Paper in Press," on the author's personal web page, their personal or institutional repository, or their funding body's archive or designated noncommercial repository, provided that a link to the article in the *Journal of Biological Chemistry* is included.
c. to post a manuscript version of the work on not-for-profit preprint servers provided that the Authors retain distribution rights to the work, that ASBMB formatted final files are not posted, and that a link to the article in the *Journal of Biological Chemistry* is included.
d. to post the final edited PDFs, created by ASBMB, to their own departmental/university websites, provided that the posting does not happen until 12 months after publication of the work in the *Journal of Biological Chemistry*, and that a link to the article in the *Journal of Biological Chemistry* is included.

Reuse of JBC content must include the following: This research was originally published in the Journal of Biological Chemistry. Author(s). Title. J. Biol. Chem. Year; Vol:pp-pp. © the American Society for Biochemistry and Molecular Biology *or* © the Author(s).

Authors may choose to publish their article under the JBC's paid open access publishing option, Author's Choice, which means that for an additional publication fee: 1) the final, edited PDF and full text html of their article will be immediately available on jbc.org and in PubMed Central (PMC) without the usual 12-month embargo period, and 2) the article will be distributed under the CC-BY license which automatically grants all commercial and noncommercial use of the article to all, as long as appropriate attribution is given to the original work.

Publisher permission (below) for Chapter 4. Additional information can be found at https://www.elsevier.com/about/policies/copyright/permissions.